LI
LABORATORY INVESTIGATION
THE BASIC AND TRANSLATIONAL PATHOLOGY RESEARCH JOURNAL
VOLUME 98 | SUPPLEMENT 1 | MARCH 2018

USCAP 2018 ABSTRACTS

TECHNIQUES
(2229-2304)

107TH ANNUAL MEETING
GEARED TO LEARN

MARCH 17-23, 2018
Vancouver Convention Centre
Vancouver, BC, Canada

Published by
SPRINGER NATURE
www.ModernPathology.org

USCAP Creating a Better Pathologist
AN OFFICIAL JOURNAL OF THE UNITED STATES AND CANADIAN ACADEMY OF PATHOLOGY

EDUCATION COMMITTEE

ABSTRACT REVIEW BOARD

To cite abstracts in this publication, please use the following format: **Author A, Author B, Author C, et al. Abstract title (abs#). *Laboratory Investigation* 2018; 98 (suppl 1): page#**

2229 PREVIOUSLY PUBLISHED

2230 Cell-free DNA Analysis of Acellular Pancreatic Cyst Fluid

Joseph F Annunziata[1], *Jan F Silverman*[1], *Christina Narick*[2], *Sydney Finkelstein*[3]. [1]Allegheny General Hospital, Allegheny Health Network, Pittsburgh, PA, [2]Interpace Diagnostics, Pittsburgh, PA, [3]Interpace Diagnostics

Background: Cytologic evaluation of aspirated pancreatic cyst fluid includes level of epithelial atypia and detection of mucin. Acellular status represents an important technical limitation. We addressed this by targeting cell-free DNA and protein (CEA) derived from cyst lining cells. We analyzed a large clinical database (n=10,661) with respect to biochemical (CEA), molecular (KRAS/GNAS oncogene point mutation) and predictive outcome parameters. Acellular cyst fluid correlations were compared with findings from specimens showing cytology adequate cellularity.

Design: Real world cytology interpretation was extracted from original reports. Cytologic atypia from specimens judged adequate (n=7057) was classified into three levels: No atypia, mild and severe. CEA levels were grouped into below and above 192 ng/mL. Presence and extent of cytologic atypia was correlated with molecular parameters consisting of DNA level, oncogene (KRAS, GNAS) point mutation and tumor suppressor gene loss using a panel of 24 markers linked to 10 tumor suppressor genes (1p, 3p, 5q, 9p, 10q, 17p, 17q, 19q, 21q, 22q) predictive of outcome (low/high risk: Endoscopy 47:136;2015).

Results: Elevated CEA level, presence of oncogene mutation and high risk predictor status was observed in 40%, 28% and 9% respectively of aspirated reported as acellular (n=3604). These acellular cyst fluid characteristics were equivalent to that seen in cellular samples reported as no cytologic atypia and significantly lower than specimens with mild and severe atypia (p<.0001 all correlates).

Conclusions: It is reasonable to regard acellular pancreatic cyst fluid specimens to be equivalent to that of cellular samples manifesting no epithelial atypia. At the same time, acellular status does not rule out potentially aggressive underlying disease. Of note, cell free nucleic acid and protein analysis are techniques that can provide diagnostic information in acellular pancreatic specimens.

2231 Nanostring is Very Specific in Identifying ALK Gene Rearrangements Compared to IHC and FISH in Lung Adenocarcinoma

Hanan Armanious[1], *Gilbert Bigras*[2], *Iyare Izevbaye*[3]. [1]Edmonton, AB, [2]Cross Cancer Institute, Edmonton, AB, [3]University of Alberta

Background: *ALK* gene rearrangements are present in 3-5% of lung adenocarcinomas. Its detection provides a predictive approach to select patients eligible for targeted treatment with the ALK inhibitor Crizotinib. IHC and FISH remain the gold standard for ALK rearrangements detection in molecular pathology practice. FISH is especially helpful in cases with equivocal results in IHC testing, however, FISH is costly, time consuming, requires significant manpower and multiple sequential runs because of its limited ability to multiplex different targets. Newer techniques such as Nanostring may provide a superior testing methodology. Here we used a new technology, the Nanostring assay, which detects ALK rearrangements by 5′/3′ positional imbalanced probe gene expression.

Design: RNA was extracted from 49 archival formalin fixed paraffin embedded lung adenocarcinomas with histologic diagnosis by a pathologist and available ALK results by IHC and FISH. The ALK results by IHC and FISH included 15 positive, 25 negative and 9 equivocal cases by IHC. The nanostring based 5′/3′ positional imbalanced probe gene expression was used where 4 probes for 5′ and 4 probes for 3′ were used and the ratio of 5′/3′ that diverges from 1 was indicative of a fusion event. Samples were run on Nanostring ncounter and analyzed by nsolver software. Moreover, this assay has fusion probes to 3 of the common fusion partners with ALK and can detect the exact fusion partner. The results were compared with FISH and IHC to determine assay sensitivity and specificity.

Results: Comparison of ALK nanostring assay vs IHC and FISH showed 100% specificity with all 25 negative cases concordance, while sensitivity was 67% with 10 out of 15 positive cases concordance. Positive and negative predictive values were 100% and 62% respectively. The specificity for equivocal cases by IHC by the nanostring compared to FISH was 89%. Furthermore, in 9 out of 10 positive cases by nanostring the ALK fusion partner could be identified by the specific probe.

Conclusions: These results demonstrate the ability of the nanostring assay to detect ALK rearrangements with comparable specificity to the reference IHC and FISH techniques in lung adenocarcinoma samples. The assay also demonstrated the ability to identify the specific fusion partner of ALK on the same run. This is besides the rapid turnaround time, high throughput and cost effectiveness However, more assay optimization is required especially to improve the assay sensitivity.

2232 Multiplex Immunofluorescence (mIF) and Novel Computational Method Demonstrates Co-expression of B7-H3 in Tumor-associated CD31+ Endothelium of Merkel Cell Carcinoma (MCC)

Phyu Aung[1], *Souptik Barua*[2], *Edwin R Parra*[1], *Barbara Mino*[1], *Jonathan Curry*[1], *Priyadharsini Nagarajan*[1], *Carlos Torres-Cabala*[1], *Alexander Lazar*[1], *Arvind Rao*[1], *Ignacio Wistuba*[1], *Victor Prieto*[1], *Michael Tetzlaff*[1]. [1]The University of Texas MD Anderson Cancer Center, Houston, TX, [2]Rice University, Houston, TX

Background: MCC is an aggressive cutaneous neuroendocrine carcinoma whose pathogenesis and prognosis are closely linked to the integrity of the immune system. Although clinical responses to immune checkpoint blockade have been promising, they remain unpredictable, underscoring a critical need to delineate additional prognostic biomarkers for this disease. B7-H3 (B7RP-2) mostly functions in adaptive immune responses and is expressed on T-cells, antigen presenting cells, some normal epithelia and tumor cells, and rarely, in tumor-associated vasculature. Endothelial expression of B7-H3 in ovarian cancer significantly associates with shorter patient survival. Here, we leveraged mIF with novel computational approaches to precisely quantify a dynamic range of colocalized B7-H3 expression in endothelial cells of MCCs.

Design: mIF was performed on 52 MCCs using the Opal florescence IHC Kit™ (Perkin Elmer) using antibodies for CD31 and B7-H3 with DAPI nuclear stain applied to a single tissue section and scanned (Vectra 3.0.™; Perkin Elemer). Up to 5 individual tumor fields (669x500µm each) were selected using the phenochart 1.0.4 viewer (PerkinElmer), and these fields were scanned at high resolution (x20). Marker expression (B7-H3 and CD31) was tabulated as a series of (X,Y) coordinates in each selected field (InForm 2.1.0™). A spatial colocalization ratio was determined by estimating the distribution of distances of B7-H3+ (X,Y) coordinates around the CD31+ (X,Y) coordinates. A nearest neighbor distribution function calculated, within any given distance (radius), what % of CD31+ cells also had a B7-H3+ cell.

Results: We stained 52 MCCs for CD31 and B7-H3 using mIF and demonstrated B7-H3 expression within CD31+ endothelial cells (Figure). Using a novel computational algorithm, we demonstrated that within a range of minimum distances, there is a dynamic frequency of colocalized CD31 and B7-H3 expression across 52 MCCs. (Table 1)

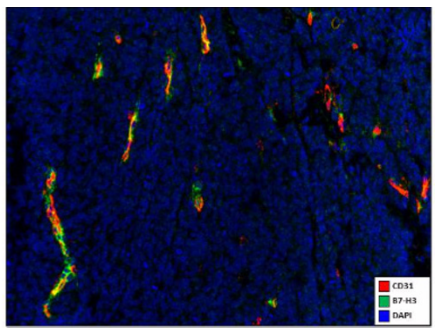

mIF shows colocallized expression of CD31 (red) and B7-H3 in endothelial cells of MCC. Each CD31+ and B7-H3+ pixel was tabulated as a series of (X,Y) coordinates, and the frequency of their respective overlap within a given distance was calculated (Table1).

	Minimum distance of overlapping expression		
	1.57 µm	3.14 µm	6.28 µm
Colocalized expression Median (%)	28.4	42.6	56.9
Colocalized expression Range (%)	6.6-99.1	6.8-99.1	7.1-99.1

Conclusions: B7-H3 shows a dynamic range of colocalized expression in the endothelial cells of MCC. Additional studies will determine associations between B7-H3 endothelial expression and the tumor associated lymphoid infiltrate or measurements of patient outcome.

2233 PREVIOUSLY PUBLISHED

2234 Assessment of Peripheral Blood Contamination in Bone Marrow Aspirate Samples

Jayalakshmi Balakrishna[1], *Elaine K Jordan*[2], *Salman Ahmad*[3], *Katherine Calvo*[4], *Raul Braylan*[1]. [1]Bethesda, MD, [2]Clinical Center/NIH, [3]Clinical Center/NIH, Bethesda, MD, [4]NIH, Bethesda, MD

Background: Determining the extent of peripheral blood (PB) contamination in bone marrow (BM) aspirate samples is important for accurately quantifying BM (non-circulating) cells, particularly when the enumeration of cells is critical (e.g., blasts). Different methods have been proposed to determine hemocontamination in BM aspirates, including those based on ratios of BM and PB hemoglobin, number of non-nucleated red cells (RBC) in PB and BM, and percentage of neutrophils (N) in BM aspirates.

Design: A total of 12 samples of unmodified fresh BM aspirate and corresponding PB, as well as serial dilutions of BM with PB from the same patient (80% BM + 20% PB, 40% BM + 60% PB and 20% BM + 80% PB) were analyzed for complete blood counts (CBC) using the Sysmex XN-3000™ Hematology System (Sysmex America Inc., Lincolnshire, IL). The fraction of PB in BM (FPB) was calculated based on the number of RBC and white blood cells (WBC) in the BM and PB, obtained from the CBC analysis, using the formula: {[(RBC BM/RBC PB)xWBC PBx100]/WBC BM}. Using this dilution factor, a corrected percentage of individual BM cells can be calculated from the observed percentage of the cell type.

Results: The calculated FPB followed the expected values in the serially diluted samples (Figure 1). The calculated and expected FPB values were not similar when N was used in place of RBC, especially when the PB N counts were higher. The serial dilutions of BM with PB showed a progressive increase in non-nucleated RBC count proportional to the FPB. Noticeably this trend was not shown by N (Figure 2). The calculated FPB was consistently slightly lower than the expected FPB in all the samples, suggesting that some of the RBCs reside in the BM. This observation was confirmed by the consistently lower calculated FPB values at the initial dilution (80% BM + 20% PB). However, this apparent difference was small and thus, the effect on the calculated percentage of cells of BM origin should be negligible.

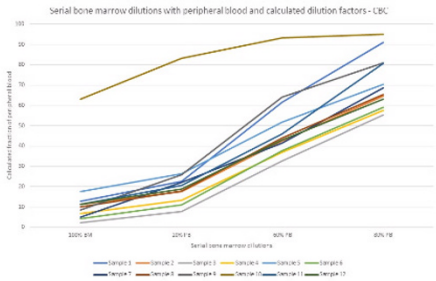

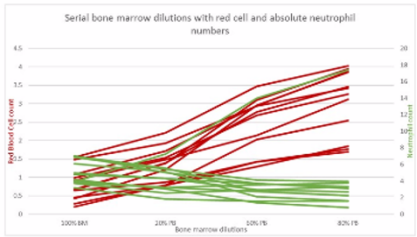

Conclusions: By this experiment, we demonstrated that a hemodilution fraction can be calculated using the number of RBCs and total WBCs in the BM and PB. The calculated FPB were similar to the expected FPB and could be reliably used to assess the correct percentage of individual cell populations in BM aspirates used for flow cytometry or any other quantitative analysis of marrow cells. Our findings also showed that using mat for calculation of PB contamination in BM aspirate samples may not be as accurate as using RBC as demonstrated in this study.

2235 Determination of MLH1 and MGMT Promoter Methylation Status Using The Illumina High-Throughput MethylationEPIC (850k) Platform

Jamal Benhamida[1], *Marc Ladanyi*[1], *Jiajing Wang*[1]. [1]Memorial Sloan Kettering Cancer Center, San Francisco, CA

Background: Methylation of the MLH1 and MGMT promoters are important biomarkers in mismatch repair defective colorectal carcinomas (CRC) and gliomas, respectively. The methylation status for these genes has traditionally been assayed by single gene tests. New high-throughput platforms, however, provide the ability to profile the methylation status across the genome for research and clinical applications. In this study, we explore the feasibility of assaying MLH1 and MGMT promoter methylation status using the Illumina methylationEPIC (850k) bead array platform.

Design: Our cohort consists of 32 cases (N=11 MGMT positive gliomas and N=11 negative samples; N=5 MLH1 positive CRCs and N=5 negative samples). The reference method was pyrosequencing of bisulfite-treated DNA to interrogate five MLH1 promoter CpG loci (in-house assay) or twelve MGMT promoter CpG loci (ARUP test 2009310). Samples were processed on Illumina 850k chips and read on their iScan system. The platform assays 866,836 cytosine loci across the genome, covering loci in >95% of RefSeq genes. Of the five MLH1 promoter CpG loci assayed by the reference method, one locus (cg23658326) overlaps with the 850k platform. Because the methylation status of neighboring loci are highly correlated, we looked at this locus as a surrogate marker (0.3 beta-value threshold). Of the twelve MGMT promoter CpG loci, none are represented on the array. Instead, we use a previously validated logistic regression model (MGMT-STP27) that predicts methylation status using two nearby loci (cg12434587 and cg12981137) in the MGMT promoter region. Data analysis was performed with R using Illumina normalization with background correction using the Minfi package.

Results: For MGMT, the predictive model showed 100% sensitivity (11 positive cases correctly predicted) and 82% specificity (9 out of 11 negative cases correctly predicted). For MLH1, CpG locus cg23658326 showed clear methylation in all five positive cases (beta-values all greater than 0.45). All negative samples showed no methylation (beta-values all less than 0.10).

Conclusions: The findings support the ability of the methylationEPIC (850k) platform to assay MLH1 and MGMT promoter methylation and suggests that its implementation could replace other single gene methylation assay. Based on this exploratory data, we are pursuing validation of the platform for clinical diagnostic purposes.

2236 Quantification & Qualification of Cell-Free Circulating Tumor DNA (cfctDNA)

Daniel Bergeron[1], *Melissa Soucy*[1], *Shelbi Burns*[1], *Jasmina Uvalic*[1], *Michael Peracchio*[1], *Kevin Kelly*[2], *Guruprasad Ananda*[3], *Honey V Reddi*[1]. [1]The Jackson Laboratory for Genomic Medicine, [2]The Jackson Laboratory for Genomic Medicine, Farmington, CT, [3]The Jackson Laboratory, Farmington, CT

Background: Small molecules of DNA released from tumors into the bloodstream, termed cell-free circulating tumor DNA (cfctDNA), has emerged as a promising candidate to provide clinicians with a non-invasive cancer biomarker. The utility of cfctDNA in the realm of clinical oncology is predicated on the notion that these molecules can be detected from a patient's plasma and used to monitor tumor progression and evaluate treatment. Utilizing a simple blood draw to determine oncological status is advantageous when in most cases a traditional biopsy often times invasive or impossible. Current cfctDNA extraction methods yield modest quantities of nucleic acid content, emphasizing the importance of sensitive and accurate quantification and qualification of cfctDNA in the molecular sequencing process.

Design: Plasma from 91 patients were processed using Bioo Scientific NEXTprep-Mag™ cfDNA Isolation Kit. Purified cfctDNA was quantified using the KAPA Human Genomic DNA (hgDNA) assay. Customized parameters were used with the hgDNA kit; of which included using primers specifically targeting the 129 and 305 base pair fragments, therein identifying DNA content of a desired size (140bp to 180bp). Additional qualification was provided by a DNA integrity score, an in-house metric derived from the average Cq values for the 129bp and 305bp amplicons, which is indicative of possible genomic DNA contamination. Of the 91 samples, 12 were prepared for sequencing based on the resultant quantification and qualification data from this custom approach.

Results: Comparative analysis with Qubit fluorometric assay revealed that the custom approach was superior when characterizing cfctDNA quantity and quality. Further, the custom PCR-based assay provided an essential quality metric based on intrinsic Cq values. Finally, next generation sequencing data from the samples prepared based on their quantification and qualification values from the method (inclusion cut-offs of ≥0.5 ng/uL and ≤0.8 respectively) surpassed all JAX bioinformatic QC cutoffs (MTC >20,000x).

Qubit (ng/uL)	hgDNA (ng/uL)	DNA Integrity Score	Mean Target Coverag
1.25	3.87	0.513	72,640

Conclusions: The analysis presented here effectively determined that using a custom assay provides more robust quantification data in comparison with the Qubit assay. The method is also capable of generating a quality metric absent from the Qubit approach. When used to prepare a subset of samples for NGS these quantity and quality measures produced libraries that passed clinical quality sequencing metrics.

2237 Histopathologic Evaluation of Endometrial Ablation Failure: A Proposal for Enhanced Uterine Dissection

Brooke E Bertus[1], *Carie J Boykin*[1], *Haydon E Bennett*[1], *Colin Winkie*[1], *Ragheb Rezko*[1], *James Coad*[1]. [1]West Virginia University, Morgantown, WV

Background: Abnormal uterine bleeding occurs in up to 30% of reproductive age women. For these patients, global endometrial ablation is an effective, minimally invasive therapeutic option. Endometrial ablation failures, however, can occur and result in a hysterectomy for a variety of reasons. Well-suited for most diagnostic assessments, uteri are traditionally bivalved in the frontal/coronal plane for pathologic evaluation. This approach disrupts the regional intrauterine cavity architecture and hence limits the gross evaluation of post-ablation uteri. This study's purpose was to assess the utility of a modified dissection method to better detect uterine changes associated with endometrial ablation failure, including residual/regenerated functional endometrium, intrauterine adhesions (*syncytia*), hematomata, retained necrotic tissue, adenomyosis, fibroids and others.

Design: A novel cutting technique was used on ten post-endometrial ablation uteri (*Figures 1 and 2; red lines represent tissue sectioning*). The uteri were first transversely sectioned through the lower uterine corpus. The lower uterine segment/cervix was then midline sagittally sectioned into right and left sides. The upper uterine half was then trisected sagittally into right cornu, fundus and left cornu tissue blocks. Finally, the bilateral cornua were tangentially sectioned from the corpus up across the inner tubal os to the external uterotubal junction. The uteri were macroscopically evaluated with microscopic correlation at 14 locations around the intrauterine cavity (*Figure 2 - designations A-N*). Tissue blocks were submitted from these 14 locations for formalin fixation, routine processing and hematoxylin and eosin staining.

Results: At the time of hysterectomy, the specimens were 14 ± 10 months post-treatment. The uteri weighed 144 ± 59 g and were 10 ± 2 cm in length, 5 ± 1 cm in thickness and 6 ± 2 cm in width. Variable degrees of residual functional (*n=8*) versus entirely atrophic (*n=2*) endometrium were identified without polyps. Focally, two (*n=2*) uteri had retained necrotic surface tissue. Six (*n=6*) uteri had mild to moderate adenomyosis with one having fibroids over 1 cm. Two (*n=2*) uteri had intrauterine cavity adhesions. No hematometra was identified.

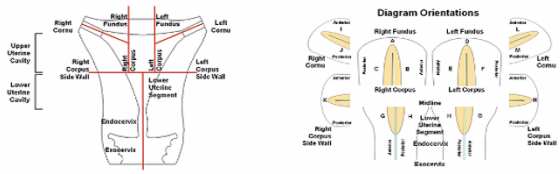

Figure 1. Uterine sectioning with anatomic location correlations.

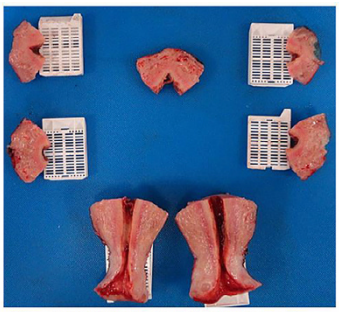

Figure 2. Modified dissection of a post-endometrial ablation uterus.

Conclusions: Using this enhanced cutting method over the classic bivalve approach, the multifactorial nature behind endometrial ablation failures should be better elucidated, especially changes in intrauterine cavity architecture, adhesions and surface necrotic tissue.

2238 Diagnostic Application of CyTOF in Hodgkin Lymphoma

David Cantu[1], *Yuan Yuan Chen*[2], *Young Kim*[3]. [1]City of Hope National Medical Center, Monrovia, CA, [2]City of Hope, Duarte, CA, [3]City of Hope Medical Center, Duarte, CA

- Paraffin embedded tissue sections are stained with antibodies attached to metal-chelating polymers. The tissue is ablated and the metals isotopes are measured by the mass cytometer and images are reconstructed.
- Forty markers per cell can be used simultaneously allowing a complete characterization of malignant cells and the surrounding microenvironment in one image.
- The resolution of the images generated is comparable to light microscopy.
- The amount of antigen present can also be measured by using this technique.
- The diagnosis of Hodgkin lymphoma can be challenging in core biopsies and multiple sections might be needed if conventional immunohistochemistry is used. One of the advantages of CyTOF is that only one slide is needed.
- Conventional techniques, such as immunohistochemistry are much more limited in the number of markers that can be evaluated per slide, meaning that multiple slides may be needed to fully characterize the sample, which may exhaust the material.

Design: A tissue microarray section with 10 cases diagnosed with Hodgkin lymphoma was used. The slide was stained with CD3, CD4, CD8, CD15, CD20, CD30, CD45, PAX-5 and FoxP1 according to the protocol dictated by fluidigm. The slide was placed in the Helios CyTOF and the images were generated using the Helios Software v6.5.358.

Results: The images generated by the software highlight the Reed-Sternberg cells and characterize the cells around them confirming the utility of this method. In addition, the images show the distribution of the antigen and can be separated into individual subsets or coupled with other images to compare the results.

Conclusions: The study shows that time-of-flight mass cytometry is a reliable diagnostic method that allows the characterization of disease processes by using up to forty markers per cell and measuring the amount of antigen present. The images generated using CyTOF are very useful in mapping a tumor and can have diagnostic, prognostic and therapeutic implications.

2239 Measuring Tumor Microenvironment in Classical Hodgkin Lymphoma using CyTOF

David Cantu[1], *Yuan Yuan Chen*[2], *Young Kim*[3]. [1]City of Hope National Medical Center, Monrovia, CA, [2]City of Hope, Duarte, CA, [3]City of Hope Medical Center, Duarte, CA

- Paraffin embedded tissue sections are stained with antibodies attached to metal-chelating polymers. The tissue is ablated and the metals isotopes are measured by the mass cytometer and images are reconstructed.
- Forty markers per cell can be used simultaneously allowing a complete characterization of malignant cells and the surrounding microenvironment in one image.
- The resolution of the images generated is comparable to light microscopy.
- The amount of antigen present can also be measured by using this technique.
- Traditional methods used to study the microenvironment, such as immunohistochemistry, are much more limited in the number of antibodies that can be simultaneously analyzed on a slide, reducing the number of markers that can be used to characterize the microenvironment.
- The malignant cells in classical Hodgkin lymphoma represent less than 1% of the tumor cellularity. A complete characterization of the microenvironment is extremely important to understand the pathology of this entity.
- The number of tumor-associated macrophages in Hodgkin lymphoma can predict treatment outcomes.

Design: A tissue microarray section with 10 cases diagnosed with Hodgkin lymphoma was used. The slide was stained with CD3, CD4, CD8, CD15, CD20, CD30, CD45, CD68, CD163, PD L1, PAX-5 and FoxP1 according to the protocol dictated by Fluidigm. The slide was placed in the Helios CyTOF and the images were generated using the Helios Software v6.5.358.

Results: The images generated by the software highlight the Reed-Sternberg cells and characterize the cells around them confirming the utility of this method. In addition, the images show the distribution of each antigen and can be separated into individual subsets or coupled with other images to compare the results and map the presence of every cell type.

Conclusions: The study shows that time-of-flight mass cytometry is a reliable diagnostic method that allows the characterization of disease processes by using up to forty markers per cell and measuring the amount of antigen present. The images generated using CyTOF are very useful in mapping a tumor and can have diagnostic, prognostic and therapeutic implications. In times like these where individualized medicine is becoming a preferred approach for patient care, CyTOF can provide a lot of useful information regarding a tumor. In addition, it can also generate invaluable data in research studies allowing a better understanding of the pathophysiology of tumors which can be of therapeutic signifi

2240 Ultra-Rapid Colocalized 4-plex Staining Thanks to Microfluidic Technology

Giulia Cappi[1], *Diego G Dupouy*[2], *Ata Tuna CIFTLIK*[3]. [1]Lunaphore Technologies SA, [2]Lunaphore Technologies SA, Lausanne, Vaud, [3]Lunaphore Technologies SA, Lausanne, VD

Disclosures:
Giulia Cappi: *Employee*, Lunaphore Technologies SA
Diego Dupouy: *Stock*, Lunaphore Technologies SA
Ata Tuna CIFTLIK: *Employee*, Lunaphore Technologies SA

Background: Multiplexing holds great promise to advance tissue cancer diagnostics and enable personalized cancer treatments. Semi-automated protocols have been demonstrated on commercial machines using tyramide signal amplification (TSA), being, however, time consuming. We recently presented an automated microfluidic tissue processor (MTP) based on fast fluid exchange that allows uniform spatial distribution and precise control of delivery of reagents, allowing for the reduction of incubation time.

Design: FFPE samples of breast carcinomas were manually pre-treated: 10 min baking at 60 °C, 10 min deparaffinization, rehydration in ethanol (100%, 95%, 70% and 40%) and HIER treatment at 95 °C for 40 min with Tris/EDTA pH9 followed by 20 min cooling at room temperature. Sections were then loaded on the MTP for staining. Target markers were pan-cytokeratins (CK, clone: AE1/AE3, Dako), progesterone receptor (PR, clone: 16, Novocastra) and Her2 (polyclonal, Dako). HRP-labeled antibodies (ImmPRESS VectorLab) and Alexa Fluor-labeled TSA (AF488, AF546, AF647, Life Tech.) were employed to detect the signal. Primary and secondary antibodies were incubated 4 min for PR and 2 min for CK and Her2. Antibodies were removed in between staining cycles by eluting during 4 to 6 min at 65°C (Figure 1).

Results: Tissue sections were stained in less than 20 minutes per marker and a 4-plex assay was achieved in 54 min. Results indicate that the detection is specific to CK (red), PR (green), Her2 (yellow) and DAPI (blue). Figure 2A shows the colocalized staining in the 4 channels, while Figure 2 B, C, D and E show the signals corresponding to DAPI, PR, Her2 and CK, respectively. Primary and secondary antibodies were removed from the tissue surface, while the fluorescently-labelled TSA remained unaffected by this step.

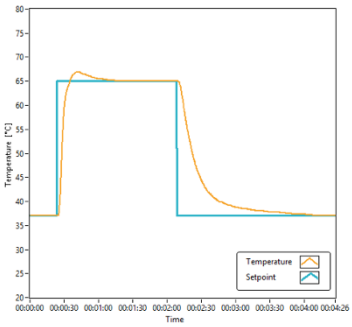

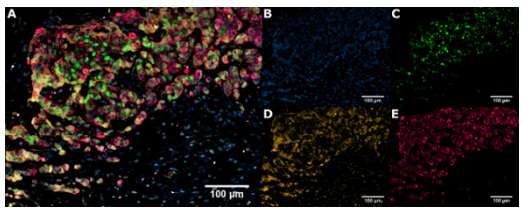

Conclusions: This work demonstrated an automated 4-plex staining in 54 min thanks to the MTP. The rapidity and flexibility of the staining allowed by the technology is particularly suitable for assay development, as it offers the possibility to tune parameters, such as concentration, incubation time and temperature, in incomparable times. The possibility of multiplexing several markers on the same tissue section could be beneficial to improve the precision of the diagnosis and eventually to allow personalized targeted therapies. We believe that our technology could be a powerful tool for reducing turn-around times in diagnostic settings and could help in the definition of subclasses of tumours.

2241 CellSolutions Non-Gynecologic Cytologic Preparations: An Acceptable Alternative to ThinPrep Technique

Tiffany N Caza[1], *Melissa Stemmer*[2], *Cheri J Wegerski*[2], *Kamal Khurana*[3]. [1]SUNY Upstate Medical University, Clay, NY, [2]SUNY Upstate Medical University, [3]SUNY Health Sci. Ctr., Syracuse, NY

Background: CellSolutions is a relatively newly developed low cost thin layer cell preparation method. In this study, the performance of CellSolutions was compared with ThinPrep Liquid based cytology method for evaluation of non-gynecological cytology specimens.

Design: Residual cellular material was used from 74 nongynecologic specimens obtained from 74 patients. Each sample was initially centrifuged and the cell pellet obtained was evenly split for preparation using ThinPrep and CellSolutions reagents. Thin layer slides were prepared using conventional ThinPrep methodology and CellSolutions F50 processor. Both ThinPrep and CellSolutions slides were evaluated for cellularity, distortion of cells, and number of diagnostic cells using a score of 1) minimal cellularity or very distorted, 2) moderate cellularity or slightly distorted, and 3) high cellularity or no distortion. These components were averaged to make a mean performance score (MPS). Student's t-tests were used to determine if the scores for two methods were significantly different.

Results: Table 1 shows the scores comparing the CellSolutions method to the ThinPrep method. The mean performance scores for CellSolutions was higher for for body fluids and slightly lower for fine needle aspiration specimens and urine specimens (body fluids - MPS CellSolutions 7.67, ThinPrep 7.24, $p > 0.05$, fine needle aspiration specimens- MPS CellSolutions-6.84, ThinPrep 7.11, $p > 0.05$), Urine specimens- MPS CellSolutions 7.1, ThinPrep 7.3, $p > 0.05$). However the differences in scores were not statistically significant. There was also no difference in diagnostic discrepancies between the two methods (discordance rate = 2.7% for both methods).

	Body fluids	Fine needle aspiration	Urine	Total
Cellularity, ThinPrep	2.27 (0.75)	2.21 (0.79)	2.4 (0.70)	2.27 (0.75)
Cellularity, CellSolutions	2.56 (0.69)	2.26 (0.81)	2.3 (0.67)	2.45 (0.72)
Distortion, ThinPrep	2.91 (0.29)	2.79 (0.42)	2.8 (0.42)	2.86 (0.34)
Distortion, CellSolutions	2.69 (0.56)	2.37 (0.60)	2.9 (0.32)	2.64 (0.56)
Diagnostic cells, ThinPrep	2.07 (0.84)	2.11 (0.81)	2.1 (0.74)	2.08 (0.81)
Diagnostic cells, CellSolutions	2.42 (0.78)	2.21 (0.85)	1.9 (0.74)	2.29 (0.81)
Total score, ThinPrep	7.24 (1.51)	7.11 (1.52)	7.3 (1.49)	7.22 (1.49)
Total score, CellSolutions	7.67 (1.58)	6.84 (1.61)	7.1 (1.20)	7.38 (1.57)

Conclusions: CellSolutions thin layer cytologic preparation performs similarly to the ThinPrep method, with comparable cellularity, resolution, and numbers of diagnostic cells for non-gynecological cytology specimens. It can serve as an acceptable alternative low cost method for slide preparation.

2242 Computer-Assisted Analysis of Tumor Budding in Colorectal Cancer- The Development of a de novo Computer Algorithm

Wei Chen[1], *Mohammad F Fauzi*[2], *Metin Gurcan*[1], *Debbie Knight*[1], *Heather Hampel*[1], *Wendy L Frankel*[1]. [1]The Ohio State University Wexner Medical Center, Columbus, OH, [2]Multimedia University, Cyberjaya, Selangor

Background: Tumor budding has emerged as an important adverse prognostic factor for many different cancer types. It is defined as the presence of single tumor cells or small tumor clusters (up to five cells) that 'bud' from the invasive front of the main tumor. In colorectal carcinoma (CRC), tumor budding has been independently associated with lymph node metastasis and poor outcome. Pathologic assessment of tumor budding by light microscopy requires close evaluation of tumor invasive front on intermediate/high power magnification, entailing locating the 'hotspot' of tumor buds, counting all buds in one 20x field, and generating a tumor bud score. By automating this time-consuming task, computer-assisted image analysis tools can be helpful for daily pathology practice, since tumor budding reporting is now recommended on select cases. In this study, we focus on the development of a de novo computer algorithm that automates morphometric analysis of tumor budding in CRC.

Design: 15 cases with varying number of tumor buds (0 to 20 per 20x field) were identified from archives, stained with H&E and cytokeratin AE1/3, and scanned at 40x. Mucinous and poorly differentiated

adenocarcinomas were excluded. Computer algorithms were trained to recognized tumor buds, first using cytokeratin slides then H&E slides. Color features were used to identify tumor bud candidate regions, by first segmenting the tissue regions, followed by detection of nucleated carcinoma cells. Next, the candidate regions were further refined by analyzing the area and distance to the tumor front, and the number of nucleated carcinoma cells within the region. All cases were marked by pathologists as the gold standard for comparison.

Results: We developed computer algorithms to automatically detect tumor invasive front and tumor budding hot spots. The initial set of 15 high power field cytokeratin images revealed an overall sensitivity of 92% and specificity of 89% in tumor bud detection by the computer algorithm. Detection on 5 whole slide cytokeratin images showed comparable sensitivity and specificity.

Conclusions: To the best of our knowledge, this is the first *de novo* systematic development of computer algorithm to detect and quantify tumor budding from the histopathological slides of CRC. The relative high sensitivity and specificity of tumor bud detection by our computer algorithm demonstrates the promise of the proposed automated system, and lays the foundation to developing algorithms using H&E slides.

2243 Detection of Large Chromosomal Abnormalities in Tumors through Analysis of Off-Target Next-Generation Sequencing (NGS) Read Data

Simon B Chen[1], *Henning Stehr*[2], *James L Zehnder*[3], *Jonathan C Dudley*[3]. [1]Stanford University, Stanford, CA, [2]Stanford University, [3]Stanford University School of Medicine

Background: Targeted next-generation sequencing (NGS) using hybrid-capture target enrichment methods are now routinely used for identifying aberrations in targeted genes in solid tumors, including mutations and translocations. Gene-level copy number changes within the targeted region can also be inferred by normalized fold-depth of coverage relative to other genetic regions and control samples. In addition to reads from targeted genes, NGS panels also produce off-target reads from genetic sequences that are not among the targeted genes. Off-target reads are a by-product of hybrid capture-based targeted NGS and usually comprise 30-40% of sequenced material. Off-target reads are scattered in a relatively unbiased fashion across the genome, providing low-coverage whole-genome sequencing. Our study investigates the feasibility of using off-target reads to characterize large chromosomal abnormalities in tumors, a role that has been traditionally performed by cytogenetics techniques, including array comparative genomic hybridization (aCGH), fluorescence in-situ hybridization (FISH), and conventional karyotyping.

Design: A pilot cohort of solid tumor cases for which cytogenetics analysis had shown chromosomal aneuploidy, and a control cohort of cases for which aCGH had shown no chromosomal abnormality, were identified. Sequencing using hybrid capture-based targeted NGS was performed on formalin-fixed, paraffin-embedded tissue block for each case. Using a novel bioinformatics pipeline, off-target read data was analyzed for chromosomal-level copy number changes to determine chromosomal aneuploidy status. The results from off-target NGS analysis were compared to those from cytogenetics.

Results: For the pilot cohort, 5 cases with chromosomal aneuploidy on cytogenetics were identified (1 aCGH, 2 FISH, and 2 karyotyping). For cases with prior aCGH or FISH, NGS revealed identical chromosomal arm gains/losses as cytogenetics. For each case with prior karyotyping, NGS confirmed one of two chromosomal-level copy number changes identified by karyotyping. For the control cohort, 9 cases with prior normal aCGH were identified, and NGS revealed no chromosomal abnormality.

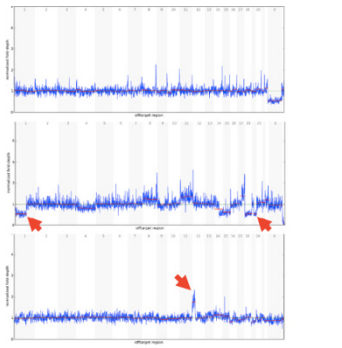

Figure. Off-target read plots from NGS showing the normalized fold-depth across each chromosome. Within a given chromosome column, the two horizontal red bars correspond to the normalized fold-depths across the p and q chromosomal arms, respectively. Top: a desmoplastic nevus that also had an aCGH assay performed to assess for global genomic instability, finding a normal XY karyotype. Middle: an anaplastic oligodendroglioma with 1p/19q loss detected by FISH. Bottom: a pineal germ cell tumor with isochromosome 12p detected by FISH. In each case, there is concordance between the off-target read plot and the orthogonal cytogenetic method (arrows). The off-target read plot for the oligodendroglioma also shows additional genomic instability missed by the targeted FISH assay.

Conclusions: Analysis of off-targeted reads from hybrid capture-based NGS sequencing appears to be a feasible approach for identifying large chromosomal abnormalities in solid tumors. Off-target read analysis appears to yield comparable chromosomal-level findings as FISH and aCGH for tumors harboring chromosomal aneuploidies.

2244 Hyperspectral Cell Sociology Tools for the Study of Tumour-Immune Cell Interactions in Lung Adenocarcinoma

Katey S Enfield[1], *Spencer D Martin*[1], *Victor D Martinez*[1], *Sonia H Kung*[1], *Paul Gallagher*[1], *BC Cancer Agency - Deeley R Centre*[2], *Zhaoyang Chen*[1], *Stephen Lam*[1], *John C English*[3], *Wan L Lam*[1], *Calum MacAulay*[1], *Martial D Guillaud*[1]. [1]British Columbia Cancer Research Centre, Vancouver, BC, [2]Trev and Joyce Deeley Research Centre, Victoria, BC, [3]Vancouver General Hospital, Vancouver, BC

Background: The immune compartment of the tumour microenvironment (TME) has emerged as a critical mediator of patient outcome that is therapeutically targetable. Immune deconvolution algorithms and flow cytometry are important tools for the characterization of the TME, but these fail to capture the spatio-regional information that is critical to understanding immune-tumour cell interactions. We have developed a platform for the analysis of multicolour immunohistochemistry (IHC) stains for the quantification of cell-cell spatial relationships within the TME.

Design: Whole tissue sections from 20 lung adenocarcinomas with at least 5 years follow-up were stained for CD3 (pan-T cell), CD8 (cytotoxic T cell), and CD79a (B cell and plasma cell) and counterstained with haematoxylin. Multispectral images were acquired for five fields of view and analyzed to quantify cell types. Regions of Interest ROIs were then identified and analyzed in order to quantify cell-cell spatial relationships. Non-random patterns of immune cell distributions were identified using the Monte Carlo re-sampling method 500 iterations . Cell counts, densities, spatial relationships, and significant immune cell distributions were associated with clinical features Kruskal-Wallis $p<0.001$.

Results: Our analysis generated 234 image files for analysis, with an average of 16,400 cells per file. The densities of intra-tumoural CD8+ cytotoxic T cells were significantly higher in non-recurrent cases, agreeing with literature reports. Similarly, cell sociology results identified relationships associated with metastasis: tumour cells in non-metastatic cases had increased numbers of CD8+ cytotoxic T cell neighbours. Following Monte Carlo analysis, non-random cell-cell spatial proximities emerged that were not identified at a cell density level.

Conclusions: We have developed a hyperspectral imaging platform that builds upon traditional IHC analysis methods by further quantifying cell spatial relationships. Additionally, data can be iteratively re-sampled using our methodology allowing for the identification of non-random patterns that could hold prognostic or predictive power. These automated quantification methods could be used to enhance our understanding of complex TME relationships.

2245 Analytical Concordance Between Pre-Treatment Instrument Models for Two PD-L1 CDx Assays

Hayley Finkelstein[1], *Charlotte Roach*[2], *Malinka Jansson*[2], *Josette William Ragheb*[3], *Gary Ponto*[2], *Karina Kulangara*[2], *Emin Oroudjev*[2]. [1]Agilent Technologies, Carpinteria, CA, [2]Agilent Technologies, [3]NeoGenomics, Aliso Viejo, CA

Disclosures:

Hayley Finkelstein: *Employee*, Agilent Technologies
Gary Ponto: *Consultant*, Agilent Technologies
Karina Kulangara: *Employee*, Agilent Technologies

Background: Clinical pathology depends on advanced and reliable instrumentation for correct patient diagnosis. The PT Link instrument is designed to perform deparaffinization, rehydration, target retrieval on formalin-fixed, paraffin-embedded (FFPE) tissue sections prior to immunohistochemical (IHC) staining. An updated PT Link instrument model, PT200, has been developed as a replacement to the previous model PT100. While the two PT Link models both meet specifications for parameters critical for the pre-treatment procedure and reagent performance, the PT200 contains several hardware and usability improvements. Two commercially available CDx assays, PD-L1 IHC 22C3 pharmDx and PD-L1 IHC 28-8 pharmDx, were initially validated using only PT Link model PT100. To expand the assays' labeling for use with the next generation PT200 model, a concordance study of PT100 vs. PT200 was conducted.

Design: The following method was used to demonstrate PT Link instrument model concordance for two commercial CDx assays. For the PD-L1 IHC 22C3 pharmDx assay, 119 non-small cell lung carcinoma (NSCLC) FFPE specimens were stained using the PT100 PT Link instrument and compared to replicate slides stained using the PT200 instrument. The same approach was followed for 110 non-squamous NSCLC (nsNSCLC) and 90 melanoma FFPE specimens using the PD-

L1 IHC 28-8 pharmDx assay. Slides were blinded and randomized and then evaluated by a pathologist per each assay's interpretation guidelines and were given a diagnostic status for the relevant clinical cut-offs. PT Link instrument concordance was determined for each assay.

Results: Data for each assay and cut-off was analyzed separately. Confidence intervals were calculated using the Wilson Score method. Results are shown in the table below.

PT100 vs PT200 Diagnostic Agreement	Point Estimate Agreement (95% Wilson confidence interval lower bound)				
	PD-L1 IHC 22C3		PD-L1 IHC 28-8		
	≥1% NSCLC	≥50% NSCLC	≥1% nsNSCLC & melanoma	≥5% nsNSCLC	≥10% nsNSCLC
Negative	94.1% (84.1%)	94.7% (87.1%)	97.3% (92.3%)	96.6% (88.5%)	100% (94.3%)
Positive	98.5% (92.1%)	93.2% (81.8%)	97.6% (91.8%)	98.0% (89.7%)	100% (92.3%)
Overall	96.6% (91.7%)	94.1% (88.4%)	97.4% (94.1%)	97.3% (92.3%)	100% (96.6%)

Conclusions: The high agreement between PT Link PT100 and PT200 indicate the two instrument models are functionally comparable when used with both PD-L1 IHC diagnostic assays. The data was used to obtain approval from the FDA for the addition of the new PT Link model to the assays' labeling.

2246 Development and Assessment of a Droplet Digital RT-PCR Method for BCR-ABL1 Monitoring

Joel France[1], *Hou-sung Jung*[1], *Gregory Tsongalis*[1], *Eric Y Loo*[1], *Joel Lefferts*[2]. [1]Dartmouth-Hitchcock Medical Center, Lebanon, NH, [2]Lebanon, NH

Background: Monitoring BCR-ABL1 fusion transcript levels by qRT-PCR is standard of care for patients with chronic myeloid leukemia (CML) being treated with tyrosine kinase inhibitors. Assays providing a higher degree of standardization, accuracy, precision, and sensitivity are becoming more important for patient management. Droplet digital PCR (ddPCR) is a new technique with several potential advantages over traditional qRT-PCR, including absolute quantitiation of molecular targets and greater sensitivity. Our molecular laboratory developed a ddPCR assay to detect the BCR-ABL1 fusion mRNA transcript. Here, we compare its performance against our current cartridge-based qRT-PCR assay.

Design: RNA extraction and quantification was performed on 52 samples immediately after BCR-ABL1 testing using a cartridge-based qRT-PCR assay on the GeneXpert platform (Cepheid, Sunnyvale, CA, USA). Extraction was performed with the QIAamp RNA Blood Mini Kit and quantification was done by Nanodrop. RNA samples were assessed with our lab-developed RT-ddPCR assay, targeting the BCR-ABL1 fusion and GUSB (internal control) transcripts. Absolute quantitation of these transcripts was used to calculate % BCR-ABL1 and molecular response (MR or log reduction) values.

Results: Of 52 specimens, seven contained RNA concentrations <20 ng/µL and were deemed inadequate for evaluation. Out of the remaining 45 specimens, nine had qualitatively discordant results, with six positive by ddPCR only, and three positive by q-RT-PCR only. All nine discordant cases were low-level positives (MR^4-MR^5). Linear regression modelling of the remaining 36 concordant sample results showed an R^2 of 0.8545.

Conclusions: Results of this comparison study show good correlation (R^2 = 0.8545) between results from samples with >20ng/µL RNA analyzed by both RT-ddPCR and cartridge-based qRT-PCR. While additional validation studies are still required, our lab-developed ddPCR assay may have greater analytical sensitivity than the cartridge-based assay as six samples were identified as positive by ddPCR only, and only three samples were positive by cartridge-based assay only. These initial results show support for using ddPCR for disease monitoring and possible evaluation of deep molecular response in patients with CML.

2247 Comparison of Histologic and Magnetic Resonance Methodologies for the Estimation of Hepatic Steatosis

C. Eric Freitag[1], *Irma Andersson*[1], *Wei Chen*[1], *Alice Hinton*[1], *Douglas Levin*[1], *Martha M Yearsley*[1], *Zarine Shah*[1]. [1]The Ohio State University Wexner Medical Center, Columbus, OH

Background: Liver biopsy followed by histologic evaluation is considered the gold standard for assessing hepatic steatosis. However, this technique is subject to clinical complications, sampling error, and intra-/inter-observer variability. Therefore, non-invasive techniques for the estimation of liver steatosis have been the subject of various investigations. In this study, we evaluated different methods for the histologic evaluation of hepatic steatosis and compared this to new magnetic resonance imaging (MRI) based radiologic techniques.

Design: This was an IRB approved HIPPA compliant prospective study of 38 patients with NAFLD. Liver fat content and stiffness were estimated by two radiologists using MRI-derived proton density fat fraction (MRI-PDFF) and magnetic resonance elastography (MRE), respectively. Then, liver biopsies were performed, as standard of care, with subsequent histologic estimation of steatosis assessed separately by two pathologists in increments of 5% by two methods: (1) whole slide estimation at 40x and (2) field-by-field evaluation at 200x with an overall average calculated. Areas showing artefactual distortion were omitted. Concordance correlation coefficients (CCC), Pearson's correlation and linear regression models were utilized.

Results: There was good interobserver agreement among pathologist estimation of hepatic steatosis at 40x and 200x, and among radiologist assessment using MRI-PDFF (Table 1). Additionally, there was significant association between radiologic and histologic estimations of liver steatosis ($p<0.001$), although histologic estimations were comparatively higher with mean differences of 14.71% at 40x ($p<0.001$; 95% CI 9.15, 20.27) and 12.26% at 200x ($p<0.001$; 95% CI 7.10, 17.43). Liver stiffness measured by MRE was not correlated with fat content estimated histologically ($r=0.174$, $r=0.135$) or by MRI-PDFF ($r=0.176$).

Table 1. Concordance Correlation Coefficients (CCC) Assessing Interobserver Agreement

Method	CCC	95% Confidence Interval
Pathologists - 40x	0.836	(0.709, 0.911)
Pathologists - 200x	0.907	(0.830, 0.950)
Radiologists - MRI-PDFF	0.993	(0.987, 0.996)

Conclusions: In our study, estimation of liver steatosis by histologic methods and MRI-PDFF were relatively similar and reproducible. There was good interobserver agreement among pathologists for histologic evaluation of hepatic steatosis and among radiologists using MRI-PDFF. There was also statistically significant association between these methodologies, although histologic estimations of hepatic steatosis were consistently higher. Field-by-field assessment of steatosis at 200x showed a higher CCC among pathologists compared to low power whole-slide evaluation. MRE evaluation of liver stiffness was not predictive of liver fat content.

2248 Application of a Novel Ex-Vivo Microscopy, MUSE (Microscopy with UV Surface Excitation) in Surgical Pathology

Amir Ghorbani-Aghbolaghi[1], *Maxwell Fung*[1], *Austin Todd*[1], *Maija Kiuru*[2], *Morgan A Darrow*[2], *Tao Wang*[2], *Nicholas B Coley*[2], *Yasmine Sana Lahoubi*[3], *Farzad Fereidouni*[2], *Richard Levenson*[4]. [1]University of California, Davis, Sacramento, CA, [2]UC Davis, [3]Annaba, [4]Sacramento, CA

Disclosures: Richard Levenson: *Ownership Interest,* MUSE Microscopy Inc.

Background: MUSE is a novel ex-vivo microscopy method that employs 280-nm UV excitation and oblique cis-illumination to generate high-quality images from cut surfaces of the fresh or fixed tissue in approximately 2 minutes without requiring thin-sectioning via cryomicrotomy or standard histological processing. MUSE staining and imaging does not impair the tissue for future use in traditional H&E preparation or molecular testing. The aim of this study was to evaluate the MUSE in assessing a wide range of surgical pathology cases.

Design: 25 samples of 10 different tissues (kidney, thyroid, colon, rectum, small intestine, breast, prostate, lung, liver and skin) were examined by two surgical pathologists and two dermatopathologists with a few minutes of training as well as two pathology residents with at least two months of experience on MUSE. The MUSE diagnostic score was calculated by the percentage of correct diagnosis of MUSE images. MUSE comparison score was assessed by the concordance between paired images captured by MUSE and correlated H&E images generated by whole slide scanner (Score 0: MUSE was not useful/ Score 1: useful but not diagnostic/ Score 2: diagnostic but weaker than H&E / Score 3: Equal to H&E / Score 4: Stronger than H&E).

Results: Preliminary results indicate that the MUSE method is a strong asset on diagnosing surgical specimens by achieving a total diagnostic score of 82.5%. It was most diagnostic on Thyroid, skin, GI, and breast samples; by diagnostic score of 100%, 89%, 79% and 75%

respectively. MUSE also received the average comparison score of 2.22 which shows that it is a useful diagnostic tool, but slightly weaker than H&E on providing all the histologic details.

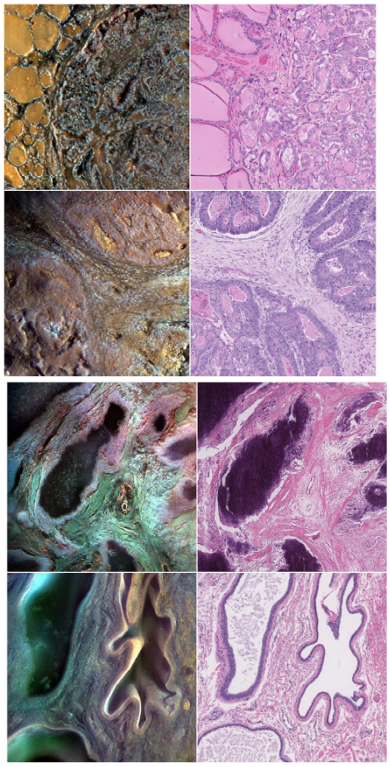

Conclusions: MUSE can be a fast, reliable and inexpensive approach for evaluating surgical specimens. The utility of MUSE in intraoperative consultation, especially will be a focus of future work.

2249 Eight-Color Multiplex Immunohistochemistry for Simultaneous Detection of Multiple Immune Checkpoint Molecules within the Tumor Microenvironment

Mark Gorris[1], *Altuna Halilovic*[2], *Katrin Rabold*[2], *Anne van Duffelen*[3], *Iresha Wickramasinghe*[3], *Dagmar Verweij*[3], *Inge Wortel*[3], *Johannes Textor*[3], *Jolanda de Vries*[3], *Carl Figdor*[3]. [1]RIMLS, [2]Radboudumc, Nijmegen, Gelderland, [3]Radboudumc

Background: Therapies targeting immune checkpoint molecules CTLA-4 and PD-1/PD-L1 have advanced the field of cancer immunotherapy. New monoclonal antibodies targeting different immune checkpoint molecules, such as TIM3, CD27 and OX40, are being developed and tested in clinical trials. In order to make educated decisions and/or design new combination treatment strategies, it is vital to learn more about co-expression of immune checkpoints, both of inhibitory and stimulatory nature, on individual cells within the tumor microenvironment. Recent advances in multiple immunolabeling and multispectral imaging enables simultaneous analysis of more than three markers within a single formalin-fixed paraffin embedded tissue section, with accurate cell discrimination and spatial information. However, multiplex immunohistochemistry with a maximized number of markers presents multiple difficulties. These include the primary antibody concentrations and order within the multiplex panel, which are of major importance for the staining result.

Design: Here we report on the development, optimization and application of an eight-color multiplex immunohistochemistry panel, consisting of PD-1, PD-L1, OX40, CD27, TIM3, CD3, a tumor marker and DAPI.

Results: This multiplex panel allows for simultaneous quantification of five different immune checkpoint molecules on individual cells within different tumor types. This analysis revealed major differences in the immune checkpoint expression patterns, both between tumor types and between patients.

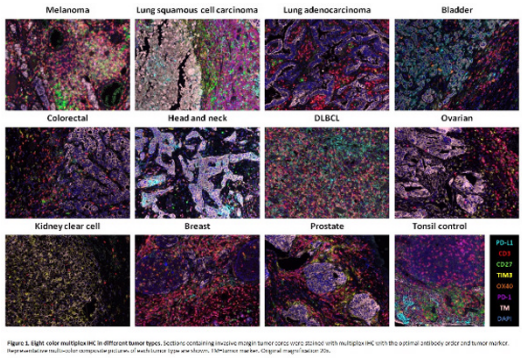

Conclusions: This multiplex immunohistochemistry method could ultimately, by characterizing the tumor microenvironment of various malignancies of patients that have been treated with different immune checkpoint modulators, form the rationale for the design of immune checkpoint based immunotherapy.

2250 Absence of Tubuloreticular Inclusions In a Transgenic Mice Model of Lupus-like Nephritis

Alia Gupta[1], *Bei Liu*[2], *Zihai Li*[2], *Ping Zhang*[3]. [1]Troy, MI, [2]Medical University of South Carolina, [3]William Beaumont Hospital, Birmingham, MI

Background: Tubuloreticular inclusion bodies (TRI), often located in the endoplasmic reticulum of glomerular endothelium, are considered relatively specific for lupus nephritis types 2 to 5, except HIV associated nephropathy. The etiology of TRI in lupus nephritis remains unclear. Our previous studies have demonstrated that gp96 transgenic (96tm) mice model were characteristic for lupus-like nephritis, similar to human types 2 and 3 lupus nephritis; they were associated with high serum levels of ANA and double-stranded DNA, immunofluorescent deposition of immunoreactants and immune complex deposits as seen in 96tm (J of Immunology 2006; 177: 6880-6888). The aim of this study was to scrutinize TRI by electron microscopy (EM) in 96tm mice for potential etiology of TRI.

Design: 30 genetically engineered mice were divided into two broad groups: Group 1: wild-type (WT)/ negative control mice (n=15) and Group 2: transgenic mice (n=15). Negative control mice did not express functional Toll-like receptor (TLR-/- mice) or Toll-IL-1R domain-containing adapter protein (TIRAP-/- mice), whereas the transgenic mice expressed surface gp96. These were further divided into pure 96tm mice, TLR-/- 96tm mice and TIRAP-/- 96tm mice. They were examined using EM. Location of electron dense deposits was graded as 0 (no deposit), 1+ (minimal deposits in mesangium), 2+ (mesangial expansion by deposits) and 3+ (with subendothelial deposits). TRIs were carefully searched for, in glomerular subendothelial and epithelial cells.

Results: Controls were either negative for deposits or showed minimal deposits. Type II and type III lupus nephritis demonstrated mesangial and subendothelial deposits (Table 1). Additional modification of TLR or TIRAP in transgenic mice showed partial reduction in deposits. However, none of the control or transgenic mice kidneys presented with any TRI in the glomerular endothelial or epithelial cells.

GROUP	SUB-GROUP	MICE MODELS (n=30)	ELECTRON DENSE DEPOSIT SCORES	TUBULORETICULAR INCLUSIONS
1	1	WT mice, n=5	0.00 ± 0.00	ABSENT
1	2	TLR-/- mice, n=5	0.40 ± 0.25	ABSENT
1	3	TIRAP-/- mice, n=5	1.00 ± 0.00	ABSENT
2	4	96tm Tg mice, n=5	2.33 ±0.33	ABSENT
2	5	TLR-/- 96tm mice, n=5	1.40 ± 0.25	ABSENT
2	6	TIRAP-/- 96tm mice, n=5	1.60 ±0.25	ABSENT

Table 1: Deposits and TRI in Wild Type Mice (subgroups 1-3), Lupus Nephritis Subgroup 4 and Partially Treated Subgroups 5-6

Conclusions: We failed to identify TRI in this model of lupus-like nephritis, raising 2 possibilities:

1. Transgenic mice model does not fulfill all the criteria and might not be entirely representative of human lupus nephritis.

2. In our experience TRI are more common with type 3 and 4 lupus nephritis. Hence, we propose that type 2 and 3 lupus nephritis in 20 weeks old mice might not have reached a level of renal damage yet.

2251 Transmission Electron Microscopy of Succinate Dehydrogenase Deficient Neoplasms: Cytoplasmic Vacuolization Seen By Light Microscopy is Compatible with Intracellular Lipid

Christina M Gutierrez[1], *Alton B Farris*[1], *Sean R Williamson*[2], *Carla L Ellis*[1]. [1]Emory University, Atlanta, GA, [2]Henry Ford Health System, Detroit, MI

Background: Succinate Dehydrogenase Deficient Neoplasms (SDHN) are a recognized subtype of tumors associated with very characteristic histopathologic features, including flocculent cytoplasmic inclusions that are identifiable by light microscopy. The true nature of the finding has yet to be confirmed (limited data suggesting abnormal mitochondria exists). Succinate dehydrogenase has the chief role of oxidizing succinate to fumarate in step 6 of the citric acid cycle. A lack of succinate dehydrogenase leads to increased levels of intracellular succinate, a known inhibitor of lipid peroxidation. Our study seeks to use transmission electron microscopy (TEM) to provide more insight on the nature of these structures.

Design: TEM (retrieval from the paraffin embedded block) was performed on 4 SDHN (3 RCC and one adrenal lesion) from four patients. The diagnosis of SDH deficient carcinoma was confirmed on all lesions by molecular sequencing studies and by demonstration of the loss of SDHB staining with immunohistochemistry (IHC). Light microscopy revealed the presence of abundant intracytoplasmic inclusions. Digital images of each tumor were obtained and analyzed. See Figure 1.

Results: Although retrieval of tissue from a formalin fixed, paraffin embedded block can lead to processing artifact, digital images on all cases revealed the presence of multiple, well circumscribed electron lucent vacuoles that were morphologically compatible with intracellular lipid droplets. Normal appearing mitochondria were clearly visible in kidney cases 2 and 3 (arrows).

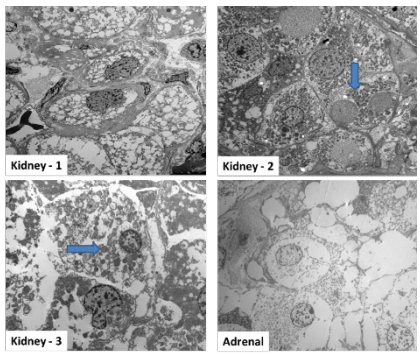

Conclusions: Unfortunately, many of the techniques utilized to identify cellular lipid (i.e. Oil red – O, Sudan Black B) require fresh tissue preparations and the pathologic diagnosis of SDHN is commonly made after formalin fixation has already taken place. Our findings suggest that the size, morphology and biochemical background of the inclusions identified by ultrastructural examination on all cases is compatible with intracellular lipid, thus offering an alternative approach for lipid identification in situations where the only tissue available has been formalin fixed and embedded in paraffin. Further study (potentially in concert with the above described techniques) is required for confirmation.

2252 Evaluation of the Tumor Microenvironment Using Multiplex Immunohistochemistry

Evan Himchak[1], *David Muirhead*[2], *Michael Lewallen*[2], *Joo Song*[3], *Young Kim*[4], *Bharat Nathwani*[3], *Dennis D Weisenburger*, *Alex F Herrera*[5], *Raju K Pillai*[4]. [1]City of Hope, Duarte, CA, [2]City of Hope, [3]City of Hope National Medical Center, Duarte, CA, [4]City of Hope Medical Center, Duarte, CA, [5]COH

Background: The tumor microenvironment is the benign cellular environment that dynamically interacts with malignant cells. In lymphomas such as FL and classical Hodgkin lymphoma, the microenvironment plays a critical role in tumor cell survival, proliferation, and treatment resistance. Gene expression profiling of tumor-infiltrating lymphocytes in FL revealed two immune response signatures associated with disparate clinical outcomes. Increased tumor associated macrophages, PD1 positive T cells, and regulatory T cells are described as prognostic relevance. Immunohistochemistry (IHC) is currently limited by the number of antigens that can be simultaneously examined. In this study, a 5 color multiplex IHC assay was developed and validated for characterization of the tumor microenvironment and defining the spatial relationship between the malignant cells and the immune cell infiltrate.

Design: After deparaffinization and antigen retrieval with CC1, sequential staining for PAX5, CD68, CD8, CD4 and CD21 were performed using the following clones – SP34, KP-1, SP57, SP35, EP3093 respectively - in 17 FL cases. The extent of the follicular compartment was assessed semiquantitatively using the PAX5 stain (50%, 50-75%, or >75%). The interfollicular CD4:CD8 ratio and the average of CD68 positive follicular macrophages per 10 high-power fields (hpf) were also estimated.

Results: Chromogenic substrates for CD4 (teal), CD8 (purple), PAX5 (brown), CD21 (black), and CD68 (red) were visualized with light microscopy. Images from control tonsil and an FL case are shown in Fig 1 and 2 respectively. In FL cases, a spectrum of immune responses to the malignant cells were observed. 4/17 FL cases had a disease extent <50%, 5/17 cases had 50-75%, and 8/17 cases had >75% disease involvement. The average number of follicular macrophages per hpf was 9 (range 3 – 23). The interfollicular CD4:CD8 ratios was 2:1 or greater in 9/17 cases and 1:1 in 2/17 cases. 6/17 cases had predominance of CD8 T-cells.Correlation between extent of disease and CD4:CD8 ratio and macrophages are seen (p=0.04 and 0.005 respectively).

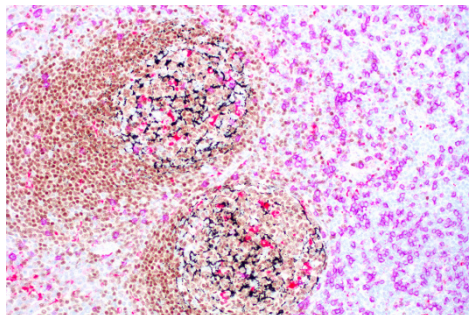

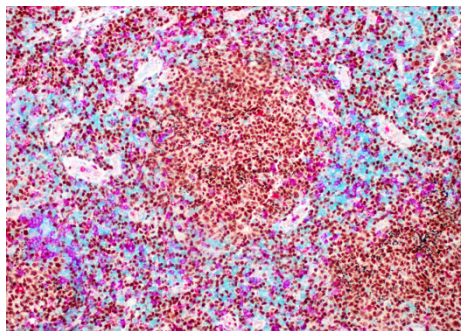

Conclusions: We describe the development of 5 color multiplex IHC assay that can be used in routine clinical labs for evaluation of the tumor microenvironment. In FL, these observations will help with stratification of patient prognosis. An understanding the interactions between tumor cells and micro-environment will lead to development of accurate prognostic indices and personalized therapy.

2253 Mobile Whole Slide Scanner for Digital Pathology

Hanyang Huang[1], *Anil Parwani*[1], *Yi Zhao*[1]. [1]The Ohio State University, Columbus, OH

Background: Pathologists request peer consultation/second opinions, and prepare for tumor board presentations on a regular base. Traditional optical microscopes is being replaced by digital pathology, where pathological slides are scanned automatically. The sequentially scanned images are stitched to show the entire FOV with high resolution. The digitalized WSIs that are analyzed using computer algorithms reduce human error and improve efficiency and accuracy of diagnoses. A major barrier to prevent widespread adoption of digital pathology is unaffordable equipment purchase and maintenance. This paper reports a smartphone based whole slide scanner (WSS) using liquid lens technologies to reduce system dimension and cost.

Design: The device is based on an adaptive zoom microscope design using elastomer-liquid lenses with tunable optical powers. The system comprises an objective lens, two elastomer-liquid lenses, a tube lens, mirrors, an eyepiece lens, and smartphone camera lens and image sensor. The optical power of liquid lenses can be tuned by changing the pressure. The two liquid lenses are tuned synchronously to maintain an afocal configuration and change the optical magnification of the system from 20X to 40X. In the design, all components including slides are kept stationary. This allows the miniaturization and low cost of the system. Furthermore, the thickness profiles of the lens membranes are made inhomogeneous to reduce the optical aberrations. This allows the optical resolution to reach WSI requirement. The slide is placed in a miniaturized motorized stage and translated in x and y directions. The sequentially captured images are stitched using panorama algorithm in Matlab. Two adjacent images have at least a 15% overlap.

Results: In the experiment, all the images are acquired using iPhone

SE camera. The resolution test using USAF 1951 resolution target indicates that the resolution can reach 0.275 um/pixel at 40X and 0.55 um/pixel at 20X. The imaging test using H&E stained renal, cardiac and blood smear slide indicat

Conclusions: In conclusion, we report a mobile WSS with reduced dimension and cost using liquid lens technologies. The system can reach magnifications from 20X to 40X with sufficient resolutions. This system addresses the imperative need for an affordable WSS with sufficiently high resolution to allow mobile and tele pathology. This study greatly improves quality of healthcare, increases efficiency for pathologists, and reduces burden of slide archiving management.

2254 Digital Image Analysis of MYC Immunohistochemical Stain May Better Predict MYC Gene Rearrangement than Manual Analysis

Meghan M Hupp[1], *Monna Marolt*[2], *Tessier Katelyn*[3], *Brian Dunnette*[4], *Elizabeth Courville*[5]. [1]University of Minnesota, Minneapolis, MN, [2]Wyoming, MN, [3]Masonic Cancer Center Bioinformatics Core, Minneapolis, MN, [4]University of Minnesota, [5]Minneapolis, MN

Background: Translocation of the *c-MYC* gene is well-described in aggressive B cell lymphomas including Burkitt lymphoma and diffuse large B-cell lymphoma (DLBCL). MYC protein expression is detected in a higher proportion of DLBCL than *MYC* gene translocation. It is tempting to use immunohistochemical (IHC) staining for MYC protein expression to triage which B-cell lymphomas require genetic studies, or to classify the B cell lymphoma by protein expression. Unfortunately, determination of IHC positivity can have wide inter-observer variability. Digital image analysis is an emerging reproducible method of quantifying nuclear positivity. This study investigates the correlation of MYC IHC interpretation by manual analysis and digital analysis.

Design: In this retrospective study, all aggressive B cell lymphoma cases on which a MYC stain was performed as part of routine clinical care from March 2015 to December 31, 2016 were selected for review. Slides were scanned at 40x using an Aperio ScanScope XT (Leica Biosystems) whole slide scanner and converted to digital images. Each MYC IHC slide was annotated using Aperio ImageScope viewing software, selecting up to ten 1x1mm areas with the best quality tissue. The annotations were analyzed using the Aperio Nuclear algorithm, with no manipulations made to the algorithm. A hematopathologist reviewer independently graded the percent positivity for each of the marked areas on the MYC slide.

Results: Our cohort consisted of 87 cases, including 72 (82.8%) diffuse large B cell lymphoma, 12 (13.8%) post-transplant lymphoproliferative disorder (PTLD), and 3 (3.4%) Burkitt lymphoma. Fourteen (16.1%) of the cases had a *MYC* translocation by FISH analysis. There was a strong positive correlation between manual and digital determination of MYC positivity (Figure). Using a cutoff value for positivity of 40%, the sensitivity and specificity for a MYC gene rearrangement by the digital method were 0.857 and 0.66, respectively, and by the manual method were 0.857 and 0.362, respectively.

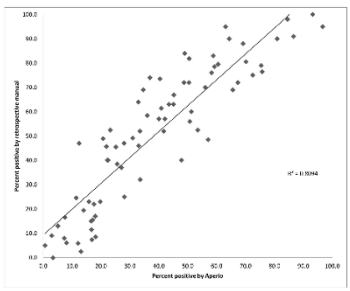

Conclusions: Digital image analysis is a viable alternative to manual estimation of MYC IHC positivity with a similar sensitivity and higher specificity for MYC gene rearrangement. The utility of this tool is amplified by the pre-loaded nuclear algorithm, which requires no manipulation. Digital analysis may be especially useful when the manual interpretation is equivocal or near the cutoff value.

2255 Intelligent Nanorockets With Targeted, Propulsive And Continuous Sensing Capacity

Bincy Jose[1], *Sharon O'Toole*[2], *Robert Forster*[3], *John O'Leary*[2]. [1]Trinity College Dublin, Dublin, [2]Trinity College Dublin, Dublin, Ireland, [3]Dublin City University

Background: Nanoparticles with nanomotors are an exciting new field of biotechnology research, with a multitude of potential industrial applications for selective delivery.

Design: The aim of the project is to develop innovative nanomachines (nanorockets) that can be deployed to actively seek a target, deliver cargo and report on microenvironment. The design of an effective targeted, nanomotor driven system is challenging. It is essential to control the shape and structure of the motor, the nature of the catalyst, fuel concentration and type, as well as the speed and directionality of motion which requires technical advances in material science.

Results: Origami DNA nanoboxes with an aptamer based lock is functionalised onto one end of nanorockets and that recognises the target of interest, e.g., MCMs, PI3KAP1, DSG3, Mybl-2 or SSB-1 for cellular targets. The presence of the target specifically triggers the opening of the DNA nanobox to expose the enzyme glucose oxidase (Gox) on the inside of the nanorocket. Once exposed, this enzyme uses endogenous glucose to produce hydrogen peroxide. Decomposition of the peroxide on the electro-catalytic region of the nanoparticle creates bubbles to propel the nanobot towards the site of target release.

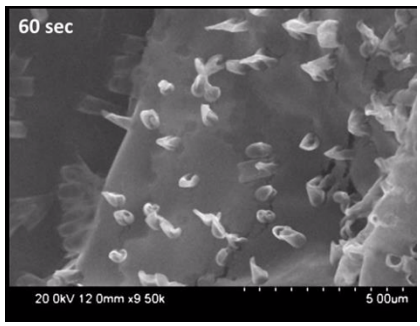

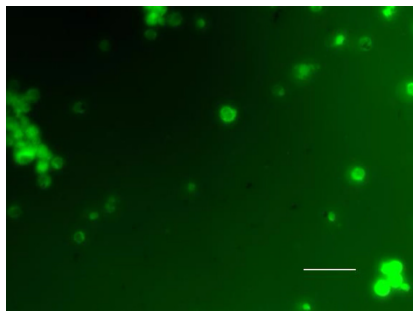

Conclusions: Coupling of nanotechnology and protein engineering will allow extremely efficient finely targeted delivery of bioactive molecules. This science will take us closer to the goal of self-propelled nanomotors for extra efficient cargo delivery applications that will have profound impacts on our lives.

2256 Digital PCR (Polymerase Chain Reaction): A Novel Technique for C-MYC Detection in Vascular Lesions

Ipshita Kak[1], *Snezana Vukmirovic-Popovic*[2], *Guillaume Pare*[3]. [1]University of Toronto, Toronto, ON, [2]Hamiton, ON, [3]McMaster University

Background: ***Introduction:*** C-MYC amplification has been found to be a major differentiating factor between angiosarcoma and atypical vascular lesions (AVL), however, digital Polymerase Chain Reaction (PCR) which is a novel technique gaining momentum in hematological and a few solid malignancies hasn't been previously studied in this cohort.

Objectives: To evaluate the diagnostic accuracy of digital PCR for assessing c-MYC expression in comparison to immunohistochemistry (IHC), fluorescent in situ hybridization (FISH) and gene expression.

Funding: Ontario Institute for Cancer Research(OICR)

Design: ***Methods:*** A total of 42 samples and 7 controls were stained by Abcam primary antibody (ab32072) and interpreted by 2 independent readers. The study samples were extracted using Qiagen's AllPrep DNA/RNA FFPE Kit. Extracted DNA was processed on QuantStudio 3D Digital PCR using RNAase P as housekeeping gene. Results generated were analyzed using Thermofisher Analysis Suite and R statistical software. RNA sequencing utilized Ion AmpliSeq™ Transcriptome Human Gene Expression Kit. FISH used dual color c-MYC+ copy number probe set.

Results: ***Results:*** C-MYC demonstrated 100% specificity (sp) and 41.2% sensitivity(sn) in differentiating atypical vascular lesions and angiosarcoma (p=0.024, AUC=0.709) compared to IHC (sn:90.9% , sp:82.6% , p<0.0001) and FISH (sn:72.7%, sp:91.3% , p<0.0001, AUC=0.866). In delineating primary from secondary angiosarcoma, digital PCR emerged as an extremely strong diagnostic parameter with a sensitivity of 83.3% and specificity of 100% (p<0.0001, AUC=0.967) with respect to IHC (sn:100% , sp:25%, p=0.05) and FISH

(sn:85.7%, sp:75%, p=0.001, AUC=0.795). The coefficient of variation was 7.4% demonstrating the robustness of the assay. The inter-rater reliability for c-MYC IHC was 0.98 indicating the high degree of concordance among the readings. RNA sequencing demonstrated a total of 91 significant genes among which PCDHB16, ZFPM2 and FKBP7 were up-regulated in the angiosarcoma group and LRRC15, ZBTB7C and RAB38 were down-regulated compared with the AVL group.

Cost-benefit analysis reflects that digital PCR at 29 CAD$/slide is the most cost-effective alternative when compared to IHC at 53 CAD$/slide, FISH (226 CAD$/case) and RNA sequencing at 270 CAD$/case.

Conclusions: In summary, the results of this novel study demonstrate that digital PCR serves as a cost-effective and specific diagnostic tool in assessing c-MYC expression in the vascular cohort.

2257 A Complex Four-Break Rearrangement Involving Chromosomes 9, 15, 17 and 22-Integration of Multiple Techniques to Resolve a Leukemia Diagnosis

Jeremiah Karrs[1], *Andrea Ferreira-Gonzalez*[2], *Christopher Vlangos*[1], *Roger Riley*[1], *David Wilkinson*[3], *Michael Idowu*[1], *Justin Dalton*[1], *Colleen Jackson-Cook*[1]. [1]Virginia Commonwealth University Health System, Richmond, VA, [2]VCU Health, [3]Virginia Commonwealth Univ, Richmond, VA

Background: Karyotypic analysis, as a sole diagnostic test, recognizes many pathognomic translocations for patients with leukemia, but interpretation of these findings can be aided by correlation with higher resolution molecular methods. We present a complex, 4-break rearrangement that resulted in a single BCR-ABL1 fusion gene, along with the juxtapositioning, but not true "fusion", of the PML-RARA loci. This case demonstrates the strength of using complementary molecular and cytogenetic techniques to arrive at the correct diagnosis.

Design: We present the genetic and histopathologic findings used to rule out acute promyelocytic leukemia in this unusual case.

Results: The patient (65y, M) was found to have a white blood cell count of 127K at an outside hospital, and his workup revealed a myelogenous leukemia reported by another lab to have a single fusion signal for both the BCR-ABL1 and PML-RARA genes. He was transferred to our hospital, where his peripheral blood had a myeloid left shift with rare blasts (1%) and thrombocytosis. A bone marrow study demonstrated hypercellularity (100%) with myeloid hyperplasia and our cytogenetic testing revealed the presence of a four-break, complex rearrangement. A break on chromosome 9 (at band 9q34) resulted in the segment distal to this break being translocated to a chromosome 22 (at band 22q11.2), thereby forming the Philadelphia chromosome [der(22)]. Chromatin from chromosome 22 (22q11.2 to 22qter) was translocated to chromosome 17 (at band 17q12), the 17q12 to 17qter segment was translocated to chromosome 15 (at band 15q24 [der(15)]), and finally, the 15q24 to 15qter segment was translocated to the aberrant chromosome 9. FISH testing confirmed a BCR-ABL1 fusion gene on the der(22), but careful inspection of the chromosomes 15 and 17 showed the close proximity, but not true "fusion", of the PML and RARA loci on the der(15). This was consistent with RT-qPCR, which demonstrated a BCR-ABL Major break point fusion product, but no evidence of a PML-RARA fusion product, affirming the histopathologic impression of chronic myeloid leukemia.

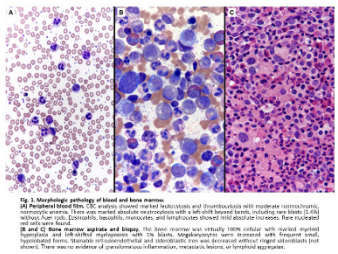

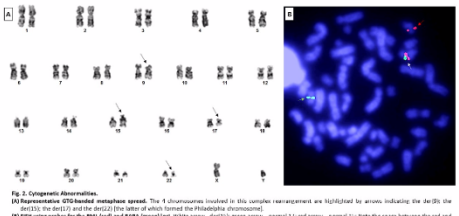

Conclusions: Cytogenetics remains the standard in investigating leukemia for balanced translocations, but as molecular oncology evolves, an increased role will be placed on integrating different tests to provide the correct diagnosis for patients. This case illustrates expert utilization of different genetic techniques, in conjunction with histopathology, to provide clinicians with the correct diagnosis.

2258 Immediate Bedside Adequacy Assessment of Bone Marrow Core Biopsies: Early Identification of Sub-Optimal Evaluations Through Evaluable Marrow Length and Inter-Trabecular Areas by X-Ray Imaging

Amanda Kitson[1], *Srikanth Ragothaman*[1], *Rajan Dewar*[1]. [1]University of Michigan, Ann Arbor, MI

Background: Adequate bone marrow (BM) evaluation is crucial to the diagnosis of hematolymphoid disorders, providing information on the overall cellularity, lineage proportion and morphology, and allowing for immunohistochemical staining. The 2008 World Health Organization (WHO) defines an adequate BM core biopsy as 1.5 cm in length with at least 10 morphologically preserved inter-trabecular areas (ITA). However, gross examination of the core biopsy can be misleading due to attached clot, thick periosteum and bone, or tangential biopsies, resulting in a long biopsy fragment without adequate evaluable marrow or ITAs by microscopy. Suboptimal BM biopsies hinder appropriate diagnosis, delay patient care, and may require the patient to undergo additional BM biopsies. Image analysis via a cabinet x-ray system can be utilized as a point-of-care tool to assess the amount of evaluable marrow and ensure an adequate core biopsy at the bedside, permitting the collection of additional tissue at time of the procedure if necessary.

Design: 53 consecutively obtained BM biopsies were obtained and analyzed with a cabinet x-ray system (Faxitron) soon after biopsy, then subjected to routine histology and processing. High resolution images of the core biopsy were obtained (Fig. 1). Length of the biopsies and number of ITAs were calculated from the x-ray images. Gross measurement of biopsy length and microscopic assessment of evaluable marrow were compared to the measurements obtained by x-ray imaging. Adequate BM biopsies were defined as at least 1.5 cm of evaluable marrow with at least 10 ITAs.

Results: Only 13/53 core biopsies exceeded the WHO standard of 1.5 cm by microscopy, while 34/53 were grossly estimated to be >1.5 cm (mean overestimation of 0.43 cm/biopsy by gross measurement, Fig. 2). There was general concordance between the number of ITAs and length of core biopsies. 10/53 biopsies were <1 cm. Utilizing x-ray image measurements, core biopsy fragment length was shown to be in great agreement with microscopic estimation of BM core biopsy length and number of ITAs. X-ray imaging readily identified clot sections (non-radiopaque), sclerotic cortical bone (absence of trabeculae), and periosteum (soft tissue shadow) in all 10 sub-1 cm biopsies.

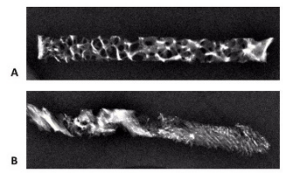

Figure 1. Examples of x-ray images of bone marrow core biopsies. An adequate biopsy that is both >1.5 cm in length and demonstrates >10 ITAs (A). A suboptimal biopsy, which grossly appears adequate in length, showing predominantly periosteum and cortical bone with no true ITAs (B).

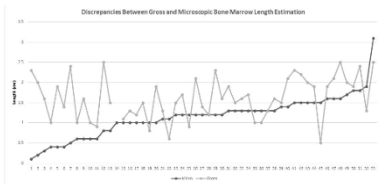

Figure 2: Comparison of the gross bone marrow biopsy measurement and the microscopic bone marrow length estimation, demonstrating a mean overestimation of 0.43 cm/biopsy by gross measurement. X axis reports biopsy case number and Y axis reports length estimation in centimeters.

Conclusions: We conclude that core biopsy length and number of ITAs can easily be estimated using bedside point-of-care x-ray analysis to ensure adequate BM evaluations. We propose the routine use of this technology for immediate assessment of BM core biopsies.

2259 Unusual Parietal Epithelium Associated Bowman's Capsule and other Extraglomerular Immune Complex Deposits on Electron Microscopy in Various Glomerulonephritides

Kyungmin Ko[1], *DongHyang Kwon*[2], *Eileen Rusnock*[3], *Bhaskar Kallakury*[1]. [1]MedStar Georgetown University Hospital, Washington, DC, [2]MedStar Georgetown University Hospital, Washington, DC, [3]MedStar Georgetown University Hospital, Washington, DC

Background: Extraglomerular immune complex deposits are relatively frequently identified in tubular basement membranes, interstitium and blood vessel walls in lupus, IgA and other nephritides. In 2 recent cases we incidentally observed parietal epithelium associated Bowman's capsule deposits with striking resemblance to subepithelial glomerular tuft immune deposits. This prompted us to retrospectively reexamine cases of different immune complex mediated glomerulonephritis to determine the frequency of parietal epithelium associated and other extraglomerular deposits.

Design: Adult and pediatric renal biopsies from Medstar Georgetown University Hospital received between 2005 and 2017 were categorized into 'non lupus membranous, ', 'postinfectious , membranoproliferative, crescentic, ', diffuse proliferative lupus ', 'IgA/HSP' glomerulonephritides, amongst other categories. Four to five cases were randomly selected from each category for a total of 50 cases and electron microscopic examination was performed to determine the frequency and distribution of Bowman's capsule and other extra glomerular immune complex deposits.

Results: We found a total of eight out of 50 (16%) cases with extraglomerular immune complex deposits in various locations including Bowman's capsule, tubular basement membranes, interstitium and blood vessel walls. In three of the eight cases, Bowman's capsule deposits associated with parietal epithelium similar to those in the subepithelial location of glomerular basement membranes were observed (figures 1 and 2). All Bowman's capsule subparietal epithelial deposits were found in cases of membranous-type glomerulonephritis (2 cases of lupus membranous and 1 case of primary membranous glomerulonephritis) compared to groups of all other immune complex glomerulonephritis($p = 0.03$ by Fisher's exact test). The presence of tubular basement membrane deposits showed a trend towards cases of lupus nephritis ($p = 0.06$).

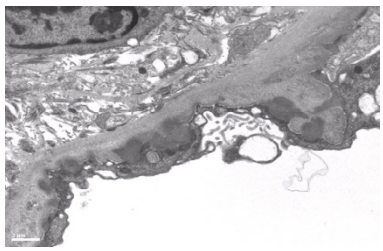

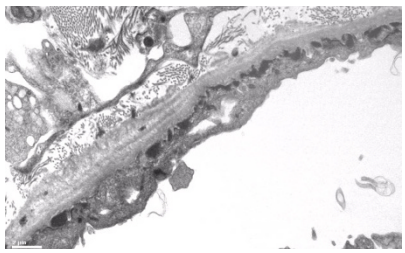

Conclusions: Bowman's capsule associated subparietal epithelial deposits similar to glomerular tuft deposits are relatively infrequent and associated with membranous glomerulonephritis. The possibility of parietal epithelium expressing in situ antigens similar to visceral epithelium with formation of in situ immune complexes appears to be a possible explanation. A larger survey of the entire spectrum of immune complex glomerulonephritis is required to verify the association and assess specificity of the various extraglomerular immune complex type deposits.

2260 Profiling the Tumor Microenvironment: Characterization of Immune Checkpoint Marker Expression and Infiltrating Immune cells by Dual ISH-IHC in FFPE Tissue

Annelies Laeremans[1], *Courtney Anderson*[2], *Jeffrey Kim*[1], *Ming-Xiao He*[3], *Bingqing Zhang*[3], *Emily Park*[2], *Xiao-Jun Ma*[4]. [1]Advanced Cell Diagnostics, Newark, CA, [2]Advanced Cell Diagnostics, Hayward, CA, [3]Advanced Cell Diagnostics, [4]Advanced Cell Diagnostics, Inc., Hayward, CA

Disclosures:
Courtney Anderson: *Employee*, Advanced Cell Diagnostics
Bingqing Zhang: *Employee*, Advanced Cell Diagnostics
Emily Park: *Employee*, Advanced Cell Diagnostics
Xiao-Jun Ma: *Employee*, Advanced Cell Diagnostics

Background: Cancer immunotherapy has advanced to the forefront of molecular medicine. Characterizing the tumor microenvironment (TME) for immune response and checkpoint function with single-cell and spatial resolution can provide critical insight into new immunotherapeutic strategies and identify new predictive biomarkers for identifying patients most likely to benefit from immunotherapeutic strategies including PD-1/PD-L1 immune checkpoint blockade. While biomarker analysis technologies are available, most do not provide spatial and cell type-specific information critical to assess specific cell types with lineage and functional information in the evolving microenvironment of each tumor. Also, multiplexing capabilities are highly desirable to obtain comprehensive single cell-level co-expression information and maximize the use of limited biopsied material.

Design: We evaluated the infiltration of immune cells and the expression profiles of immune checkpoint markers (PD1, PD-L1 and TIM3) in the TME of 60 NSCLC and 30 ovarian cancer archived FFPE biopsies. By applying RNAscope® in situ hybridization (ISH) assay, combined with immunohistochemistry (IHC) for CD8 or CD45 protein, specific markers expressed in tumor and immune cells were visualized and quantified.

Results: This dual ISH-IHC approach enabled the visualization of IFNg transcripts, frequently expressed within CD8 IHC (+) cells. Infiltrating Treg (FOXP3+CD4+) and CTL (INFg+CD8+) immune cells are quantified in selected tumors. Expression profiling of the immune checkpoint markers in the TME presented a unique and heterogeneous pattern of PD-L1 and PD1 expression. In addition, co-expression of multiple checkpoint molecules, including PD1 and TIM3, is revealed at single cell level.

Conclusions: The RNAscope® assay is a highly specific and sensitive RNA ISH technology that identifies gene expression at the single cell level while maintaining an intact environment to provide morphological context. Here, the expression profiles of immune checkpoint markers and infiltrated immune subsets were evaluated in the TME of lung and ovarian cancer FFPE tissues by dual ISH-IHC to understand the expression of key functional markers and complex spatial relationships among the different cell types. The expression and co-expression profiles may reveal insights into combinatorial therapies targeting multiple checkpoint pathways.

2261 Ultra Efficient Quantitative T cell Receptor Repertoire Sequencing

Harry B Larman[1], *Janelle Montagne*[2]. [1]Johns Hopkins University, Baltimore, MD, [2]Johns Hopkins University

Background: Sequencing-based analysis of the T cell receptor (TCR) repertoire is a powerful new approach for enhancing our understanding of adaptive immune responses. However, current methods for quantitative TCR repertoire analysis are complex and expensive. This can largely be attributed to the sequence diversity of the TCRß chain variable domain, which necessitates the use of a highly multiplexed pool of primers for amplification. Primer competition and inherently differential amplification efficiencies introduce strong biases that confound clonal quantification by high throughput DNA sequencing. The complementarity determining region 3 (CDR3) of the TCRß chain harbors the greatest amount of sequence diversity, primarily confers the antigen specificity to a T cell, and can be used to uniquely identify T cell clonal identity. We have therefore developed an efficient approach to specifically analyze CDR3 sequences of the TCRß chain using short read Illumina sequencing.

Design: We have addressed primer competition and amplification bias by maximally reducing the number and sequence complexity of our primers. This was achieved by placement of primers in a region of relatively low sequence diversity. We designed three sets of primers in this region: one set encompassing all sequences, one set allowing for one mismatch between primer and sequence, and one set with one mismatch and parsimonious incorporation of the "universal" base inosine. We automated design of the latter two primer sets with an algorithm that incorporates these considerations.

Results: To assess the performance of our approach, we analyzed peripheral blood mononuclear cells (PBMCs) from two different donors. We have directly compared our results to those from Adaptive Biotechnologies, currently considered the gold standard for TCR repertoire analysis. We observed that all three primer sets generate quantitative repertoire data sets, with results very similar to Adaptive Biotechnologies at about 100-fold reduced cost.

Conclusions: We anticipate that our approach will be efficient and cost-effective for better understanding post-infection/vaccine T cell responses, analysis of tumor infiltrating lymphocytes, the tracking of minimal residual disease in T cell leukemias and lymphomas, along with numerous additional applications.

2262 FLI1 is Frequently Expressed by Hematolymphoid Neoplasms, Carcinomas, and Melanoma: A Significant Diagnostic Pitfall

John Lee[1], *Angela Wu*[2], *Andrew Bellizzi*[1]. [1]University of Iowa Hospitals and Clinics, Iowa City, IA, [2]Univ. of Iowa General Hospital, Iowa City, IA

Background: Immunohistochemistry (IHC) for the ETS family transcription factor FLI1 is frequently used to support a diagnosis of Ewing sarcoma (ES) or as evidence of vascular differentiation. We recently encountered a case in which diffuse, strong expression in a round cell neoplasm led to a favored interpretation of ES; subsequent workup confirmed a diagnosis of diffuse large B-cell lymphoma. We performed this study to examine the extent of FLI1 expression in hematolymphoid neoplasms, carcinomas, and melanoma.

Design: IHC using a mouse monoclonal antibody to FLI1 (clone G146-222) at a dilution of 1:125 was performed on tissue microarray slides (tumors arrayed as triplicate 1 mm cores) from 417 hematolymphoid neoplasms, 65 adenocarcinomas, and 27 melanomas. Tumors were assessed for intensity (0, 1+, 2+, 3+) and extent (0-100%) of expression with an H-score calculated (intensity*extent).

Results: When positivity is defined as any H-score >/=1, FLI1 is expressed by 100% of lymphomas, 80% of carcinomas, and 96% of melanomas. When only diffuse, strong staining (i.e., H-score >/= 200) is considered, 61% of lymphomas, 100% of renal cell carcinomas, and 19% of melanomas remain positive (see Table).

Tumor (n)	% with H-score >/=200	Mean H-score (if positive)
Hematolymphoid neoplasms (417):		
Diffuse large B-cell lymphoma, germinal center (65)	83	215
Diffuse large B-cell lymphoma, activated B-cell (48)	85	246
Burkitt lymphoma (33)	39	172
Follicular lymphoma (47)	49	196
Chronic lymphocytic leukemia/small lymphocytic lymphoma (33)	73	226
Marginal zone lymphoma (35)	71	235
Mantle cell lymphoma (12)	92	256
Multiple myeloma (13)	15	148
T-cell lymphoma (28)	61	223
Anaplastic large cell lymphoma (18)	61	222
Lymphoblastic lymphoma (15)	60	233
Granulocytic sarcoma (21)	76	247
Classical Hodgkin lymphoma (49)	20	135
Adenocarcinomas (65):		
Lung (36)	8	96
Breast (10)	0	66
Colon (7)	0	13
Esophagus (5)	0	14
Kidney (7)	100	260
Melanoma (27)	19	97

Conclusions: Diffuse, strong FLI1 expression **does not** confirm a diagnosis of ES or the presence of vascular differentiation, as it is frequently strongly expressed by lymphoma and renal cell carcinoma and occasionally strongly expressed by melanoma.

2263 Ciliary Ultrastructural Features in a Cyclin O-Deficient Murine Model of the Reduced Generation of Multiple Motile Cilia Syndrome

Josep Lloreta-Trull[1], *Mercedes Simon-Grimaldos*[2], *Marta Garrido*[3], *Silvia Hernández-Llodrà*[4], *Nuria Juanpere*[5], *Gabriel Gil-Gomez*[6]. [1]Hospital del Mar-UPF, Barcelona, Spain, [2]Hospital del Mar, [3]Hospital del Mar Research Institute, [4]Pompeu Fabra University, [5]Hospital del Mar-Parc de Salut Mar, Barcelona, Spain, [6]Hospital del Mar Research Institute, Barcelona

Background: Recently, Cyclin O (*CCNO)* mutations were identified in a subset of Primary Ciliary Dyskinesia (PCD) patients affected by recurrent upper and lower airway infections, bronchiectasis, hydrocephalus (~10%), and reduced fertility. This PCD subset has been termed Reduced Generation of Multiple Motile Cilia (RGMC) and is also caused by mutations in the *MCIDAS* gene, that is adjacent to *CCNO* on chromosome 5q. There are few reports on this syndrome, some of them based on animal models.Our laboratory has developed a constitutive loss-of-function mouse model with complete *CCNO* deficiency. There are very few data on the electron microscopic changes in cases of RGMC or on its murine counterparts. The aim of the present study has been to characterize the ultrastructural features of cilia and related structures in our *CCNO* deficiency murine model.

Design: This is a descriptive study of fine structural changes in two experimental groups, consisting respectively of three wild-type and three *CCNO* deficient mice. Transmission electron microscopy was performed on perfusion-fixed samples of brain periventricular ependymal cells, uterine tubal epithelium and tracheal mucosa. Uranyl acetate and lead citrate stained thin sections were examined in a Phillips-FEI CM100 electron microscope. The Ethics Guidelines for Laboratory Animal Research from the PSMAR Consortium (Parc de Salut Mar - Hospital del Mar Research Institute) were strictly followed.

Results: The most striking ultrastructural findings were detected in the ependymal and respiratory tract cilia. In addition to a marked reduction in number of cilia compared to controls, there was a very defective basal body formation, with disassembled microtubules resulting in a meandering, spread-out or annular shape (figures 1 and 2). In the vicinity of these abnormal basal bodies, rounded structures similar to deuterosomes were rarely seen. The axial symmetry of cilia was partially lost. The axoneme was normal, without significant abnormalities of the doublets, dynein arms or nexin links. Radial spokes were partially lost in some of the cilia.

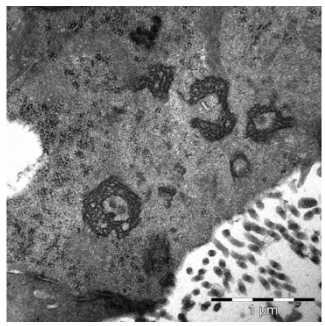

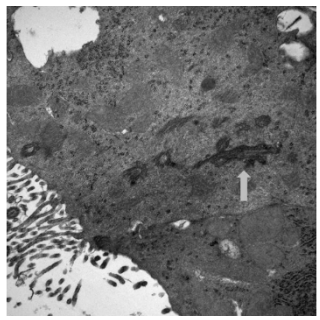

Conclusions: The constitutive *CCNO*-deficient mouse model is characterized by abnormalities related to early ciliogenesis, basal body formation and ciliary polarity. This may explain the more severe abnormalities, mostly hydrocephalus, that affect these mice and to a lesser degree patients with *CCNO* deficiency. This animal model can be useful in the investigation of the increasingly complex field of ciliary dyskinesia.

2264 Raising the Dead: The Presence of Extensive Tumor Necrosis Does Not Significantly Impair Targeted Next-Generation Sequencing

Navin Mahadevan[1], *David Hwang*[1], *Elizabeth Garcia*[1], *Neal Lindeman*[1], *Lynette Sholl*[1]. [1]Brigham and Women's Hospital, Boston, MA

Background: Tumor genomic sequencing, particularly using next-generation sequencing (NGS), has become part of modern pathology practice, and often yields diagnostic and therapeutic information. The presence of significant necrosis in tissue samples is thought to be deleterious for sequencing assays due to possible release of PCR inhibitors, paucity of viable cells, and fragmentation of DNA, a problem that is compounded in FFPE tissue. Indeed, tumor adequacy guidelines often call for the selection of non-necrotic tumor cells; however, selection of adequately cellular, viable tumor tissue can be challenging in a small biopsy, which may often be the only diagnostic sample for a patient's tumor. We now recognize that dying tumor cells release fragmented DNA into plasma that can be successfully sequenced using NGS. Most FFPE tissue-based NGS library preparation methods include a DNA fragmentation step; thus, we hypothesized that the presence of even significant necrosis would not impede high quality NGS results from tumor tissue.

Design: Tumors that had undergone targeted NGS at our institution (2015-2017) were selected (n=63) for the presence of tumor necrosis (0-95%), based on percent necrosis reported by the reviewing pathologist and visual review of digital slide images. Quality metrics, including input DNA concentration, total reads, % passed-filter reads,

% selected bases, mean read depth, and % duplication were gathered for all cases, and stratified by quartiles of necrosis. Estimated tumor percent based on pathologist review and by analysis of variant allele fraction (VAF) were compared to determine whether the presence of extensive necrosis (>50%) may alter estimation of tumor content. In addition, results for a single tumor sequenced without and with extensive necrosis were compared.

Results: All quality metric data did not significantly differ between non-necrotic tumor or between quartiles of tumor necrosis ($p > 0.05$). Estimates of tumor percent by pathology review and by VAF did not significantly differ in the presence of significant necrosis. Comparison of a tumor sequenced without and with extensive necrosis showed similar CNV and SNV profiles.

Conclusions: FFPE tumor tissue, even if it contains extensive tumor necrosis, can still be successfully sequenced using NGS without significant reduction in sequence quality. From this work, we propose that even tumor samples with majority necrosis will yield high-quality NGS results and should not be excluded from consideration for routine testing.

2265 Amplicon-Enriched Next Generation Sequencing of Low-Input DNA Specimens Shows Reduced Library Complexity and Decreased Detection Sensitivity

Patrick R Mann[1], *Eric J Duncavage*[1], *John Pfeifer*[1]. [1]Washington University, St Louis, MO

Background: In massively parallel sequencing of solid tumors, samples are commonly enriched for genes of interest through PCR amplicon-based methods. An advantage of amplicon-based methods is the ability to generate sequencing data from small biopsy specimens with minimal DNA input amounts in the range of 2-10ng. The potential disadvantage with this enrichment is the inability to track duplicate reads and estimate library complexity (number of unique DNA molecules). We performed amplicon-enriched NGS on a series low DNA input cases and incorporated unique molecular indexes (UMIs) to determine library complexity.

Design: To ascertain library complexity in a controlled setting we used a series of cell lines diluted to variant allele fractions (VAFs) between 40% and ~1% with DNA inputs including 50,10, 5, and 2ng (n= 32 cases). We further selected a series of 3 clinical FFPE samples with known variants <5% VAF using 2, 5, 10, and 50ng of DNA (n=12 cases). All cases were enriched for the AmpliSeq cancer panel (Thermo Fisher) coordinates using an UMI-based amplicon assay (Agilent HaloplexHS). Cases were sequenced on an Illumina NextSeq using 2x150bp reads.

Results: Cell line dilutions were sequenced to a mean of greater than 20,000x total coverage. At the lowest dilution (VAF ~1%) all mutations were detected with higher input DNA samples (50ng and 10ng) but only 33% of variants were detected with 5ng of input DNA and 0% were detected with 2ng of DNA despite similar total coverage. For cell line samples with 50ng of DNA, unique reads represented 12% of total reads compared to only 1.2% for cases with 2ng of DNA, consistent with low library complexity. For FFPE samples with VAFs <5%, while all mutations were detected with 50ng and 10ng of input DNA, only 2 of 3 mutations were detected with 2ng and 5ng of DNA, despite high total coverage depths (>3,000x).

Conclusions: Using UMIs to track individual reads in amplicon-based enrichment panels, we demonstrate that while high coverage sequencing data can be generated using low DNA inputs, sequencing complexity (unique reads) is significantly reduced, resulting in the inability to detect lower frequency variants despite adequate sequencing QC metrics (depth). These data suggest that amplicon-based cancer assays may have compromised sensitivities when sequenced using low input FFPE samples.

2266 Pathology Beyond 2D: Imaging and Analysis of Cells and the Tumor Microenvironment in Three Dimensions

James Mansfield[1], *James Wainright*[2], *Christopher Bagnall*[3], *Geraint Wilde*[2], *Meredith Price*[2], *Mark Browne*[2], *Benjamin Willcox*[3]. [1]Andor Technology, Belfast, Ulster, [2]Andor Technology, [3]University of Birmingham

Background: The success of cancer immunotherapy treatments and the development of immuno-oncology into the "fifth pillar" of cancer treatment has fueled a rapid growth in interest into methodologies that investigate immune cells in the context of the tumor microenvironment. However, nearly all technologies that investigate the immune contexture of tumors either rely on homogenization or disaggregation of the sample and the concomitant loss of spatial relationships, or rely on a thin section (5 um or less), two-dimensional sample of a biopsy, which is a poor representation of an inherently three-dimensional structure.

Design: An image of a thin section will tend to over-estimate the numbers of proximal cells and underestimate the numbers of more distant cells due to sampling error. To address this, we have implemented an imaging system capable of 3D confocal and super-resolution imaging, tiling of large sample areas and imaging samples over time along with software for the visualization and analysis of the datasets.

Results: We present here a series of examples showing the utility of 3D fluorescence imaging of labeled cells in thick (ca. 100 micron) FFPE tissue sections. By using a multimarker immunostaining scheme, this enables the phenotyping of cells within the tumor microenvironment and the calculation of distance metrics between cells in three dimensions.

Conclusions: This methodology is an inherently better means of assessing cellular distributions in the tumor microenvironment and can give a much better representation of the complicated 3D structure of a tumor than imaging of thin sections.

2267 Use of a Multiplex Targeted Sequencing Assay to Detect Disease-Defining Fusion Genes in Bone and Soft Tissue Neoplasms

Jose Mantilla[1], *Robert Ricciott*[2], *Eleanor Chen*[1], *Yajuan Liu*[1], *Benjamin Hoch*[2]. [1]University of Washington, Seattle, WA, [2]Seattle, WA

Background: The discovery of disease-defining chromosomal alterations has facilitated and expanded the classification of bone and soft tissue neoplasms. Due to differential diagnosis of similar-appearing lesions multiple FISH probes and immunohistochemical stains, which can be costly and time-consuming, are often required for definitive diagnosis. In this study, we evaluate the utility of an Anchored Multiplex PCR and next generation sequencing (NGS) assay to target captured mRNA (ArcherDX FusionPlex Sarcoma Panel) and simultaneously detect multiple gene fusions associated with sarcomas.

Design: 44 tumors from our institution were retrospectively reviewed by 4 pathologists and their morphologic, immunohistochemical and cytogenetic features recorded. These included mesenchymal neoplasms with disease-defining gene fusions and previously unclassified sarcomas. RNA was extracted from tissue, reverse-transcribed and processed for the FusionPlex Sarcoma panel. The presence of specific gene fusions was identified by NGS and compared with the prior diagnosis. Negative controls (non-neoplastic tissue) were used.

Results: The 44 tumors were initially classified as 8 synovial sarcomas (SS), 11 myxoid/round cell liposarcomas (M/RCLS), 6 low grade fibromyxoid sarcomas (LGFMS), 5 epithelioid hemangioendotheliomas (EHE), 4 solitary fibrous tumors (SFT), 3 undifferentiated round cell sarcomas, 3 aneurysmal bone cysts (ABC), 1 Ewing sarcoma, 1 extraskeletal myxoid chondrosarcoma (EMC), 1 nodular fasciitis, and 1 angiomatoid fibrous histiocytoma (AFH). A novel fusion of EWSR1 and PBX3 was identified in the AFH. One case initially diagnosed as SS was found to harbor a *BCOR-CCNB3* fusion and reclassified accordingly. All undifferentiated round cell sarcomas showed disease-defining fusions, including *BCOR-CCNB3*, *CIC-DUX4*, and *CIC-NUTM2A*. There were no discrepancies with FISH results of cases with previously detected fusions [See Table].

Original diagnosis	n	Gene fusions detected	New diagnosis
SS	8	SS18-SSX1 (6) SS18-SSX2 (1) BCOR-CCNB3 (1)	SS (7) BCOR-CCNB3 sarcoma(1)
M/RCLS	11	FUS-DDIT3 (11)	M/RCLS (11)
AFH	1	EWSR1-PBX3 (1)	AFH
LGFMS	6	FUS-CREB3L2 (6)	LGFMS (6)
Ewing sarcoma	1	EWSR1-FLI1 (1)	Ewing sarcoma (1)
EMC	1	TAF15-NR4A3 (1)	EMC (1)
Nodular fasciitis	1	COL1A1-USP6 (1)	Nodular fasciitis (1)
ABC	3	RUNX2-USP6 (1) COL1A1-USP6 (1) No fusions detected (1)	ABC (3)
EHE	5	YAP1-TFE3 (1) WWTR1-CAMTA1 (4)	EHE (5)
SFT	4	NAB2-STAT6 (4)	SFT (4)
Undifferentiated RCS	3	BCOR-CCNB3 (1) CIC-NUTM2A (1) CIC-DUX4 (1)	BCOR-CCNB3 sarcoma (1) CIC-NUTM2A sarcoma (1) CIC-DUX4 sarcoma (1)

Conclusions: Use of FusionPlex Sarcoma panel provides a novel cost-effective methodology to detect gene fusions, aiding in the diagnosis of neoplasms with recurrent cytogenetic alterations. Advantages over FISH include the ability to simultaneously test for multiple rearrangements as well as detect novel fusion partners that would not be otherwise identified. FusionPlex can be routinely utilized

in diagnosing sarcomas, especially those with round cell morphology, unusual features or morphology suggestive of a translocation sarcoma.

2268 Development of Functional Requirements for Ex-Vivo Applications of In-Vivo Microscopy Systems: A Proposal from the In-Vivo Microscopy Committee of the College of American Pathologists (CAP)

Sharad Mathur[1], *Maryann Fitzmaurice*[2], *Nicholas Reder*[3], *Savitri Krishnamurthy*[4], *Mary Kennedy*[5], *Gary Tearney*[6], *Maria Shevchuk*[7]. [1]Overland Park, KS, [2]Case Western Reserve University School of Medicine, Cleveland, OH, [3]University of Washington Medical Center, Seattle, WA, [4]M. D. Anderson Cancer Center, Houston, TX, [5]College of American Pathologists, [6]Harvard University, Boston, MA, [7]Weill Cornell Medical College, New York, NY

Background: In-Vivo Microscopy (IVM) systems, many of which are FDA-approved for clinical practice, allow direct, real-time visualization of tissue histology in patients for biopsy guidance, screening, and diagnosis without the need for tissue removal, processing, or staining. IVM technologies in use and in clinical research include confocal microscopy, optical coherence tomography, multiphoton microscopy, and spectroscopic imaging. These technologies show great promise for a variety of applications on resection and biopsy specimens (ex-vivo microscopy, EVM) for use by Pathologists; however, systems designed for EVM are much less available commercially, at least in part due to lack of adequate market research and defined minimal functional requirements (FR).

Design: The IVM Committee of the College of American Pathologists (CAP) identified potential EVM pathology applications based on the published literature. A subcommittee of IVM and EVM early adopters and experts developed FR and defined these for the most likely initial applications of EVM.

Results: Potential EVM applications include:

- Assessment of margins
- Tissue adequacy of needle biopsies and aspirates for diagnosis
- Selection of tissue for molecular studies or biobanking
- Transplant tissue assessment
- Guidance in block selection from gross specimens.

The first three applications were selected for development of FR. FR were identified based on existing laboratory practices and guidelines (e.g. CAP Laboratory Accreditation checklists) and input from experts in the field, and were categorized as:

- Size of device – footprint, portability
- Cost – capital equipment cost, cost per reportable result, cost of data storage
- Specimen preparation requirements, if any
- Total time per specimen – specimen preparation, image acquisition, interpretation
- Field of view/resolution – area of tissue to be imaged, required magnification
- Morphologic diagnostic capability – disease discrimination
- Yield – proportion of cases successfully imaged and interpreted
- Accuracy – positive and negative predictive values as compared to current gold standard
- Ease of use
- Safety

A summary of selected FR is presented in the Table.

Minimum Functional Requirement	Size		Specimen Preparation	Total Time				Field of View/ Resolution	
EVM Application	Footprint	Portability		Specimen Preparation	Image Acquisition	Interpretation	Comment	Area of Tissue to be Imaged	Required Magnification
Assessment of margins	Up to 3' x 2' (similar to cryostat); countertop or freestanding	Fixed, portable, or handheld	<5 min; simple (1-step), minimal training required, no adverse effects on FFPE histology, IHC, ISH, genomic testing.	1-5 min, maximum	<20 min, preferably <10 min	5-10 min, maximum	Total <20 min for uncomplicated specimens (comparable to frozen section)	100 sq cm, maximum	10-20x
Assessment of aspirate or core biopsy adequacy for diagnosis	Up to 1' x 1' (fit on Cytology or specimen cart)	Portable (handheld preferred)	<5 min; simple (1-step), minimal training required, no adverse effects on FFPE histology, IHC, ISH, genomic testing.	1-5 min, maximum	<5 min	<5 min	Total <10 min (comparable to touch imprints)	1-5 sq cm, maximum	10-20x
Identification of lesional tissue for genomic studies or biobanking	Up to 1' x 1' (fit on Cytology or specimen cart)	Portable (handheld preferred)	<5 min; simple (1-step), minimal training required, no adverse effects on FFPE histology, IHC, ISH, genomic testing.	1-5 min, maximum	<5 min	<5 min	Total <10 min (comparable to touch imprints)	1-5 sq cm, maximum	10-20x

Conclusions: There was consensus (or a limited range of options) for each FR that would accommodate the selected EVM applications. Publication and dissemination of these FR will provide guidance to engineers, researchers, and vendors on how to optimally adapt IVM technologies for EVM for widespread adoption by Pathologists.

2269 Developing an Efficient Approach For the Assessment of Tumor Extension by Ex Vivo Imaging of Breast Specimens. A Pilot Study Using X-Ray Tomosynthesis with Histopathologic Correlation

Kant M Matsuda[1], *Andrea Phillips*[1], *Matthew G Hanna*[1], *Anne Grabenstetter*[1], *Edi Brogi*[1]. [1]Memorial Sloan-Kettering Cancer Center, New York, NY

Background: The assessment of the extent of invasive carcinoma and ductal carcinoma in situ (DCIS) in surgical excision specimens can be challenging, and has substantial implications for tissue sampling and margin evaluation. Advanced imaging techniques such as tomosytethesis are now readily available and suitable for use in the laboratory.

Design: The aim of our study is to develop an *ex vivo* tissue imaging approach to improve the macroscopic evaluation and sampling of breast excision specimens. Fresh breast excision specimens (7 cases), were examined with a commercially available Tomosynthesis X-ray (T-xray) system (Kubtec Medical Imaging, Stratford, CT, USA). After routine sectioning of the specimen, each tissue slice was examined by T-xray, and a gross photograph was obtained (Fig. 1). The T-Xray images were processed using Image J software (available at NIH/gov) by segmentation using *k*-means clustering after background subtraction This method has been successfully applied for the evaluation of mammographic density (Carri K. Glide-Hurst, *et al.* Med Physics. 34(11), 2007.p4491-8). The findings in each processed image were carefully paired with macroscopic and histopathologic findings in the corresponding tissue section. Image analysis was validated by the pathologic correlation of the extent of invasive carcinoma and DCIS.

Results: The processed images of the fresh tissue slices matched the histopathologic findings. Benign breast stroma showed higher and brighter signal intensity compared to the areas involved by carcinoma (invasive carcinoma or DCIS). While some areas of invasive carcinoma (Fig 2, red line) and DCIS (Fig 2, green line) were delineated with segmentation, not all foci of carcinoma showed definite separation from the benign adjacent fibrous tissue by image segmentation (Fig 2, yellow line). In a case subject to detailed quantitative study, image analysis of the histopathology-based region of interest demonstrated significantly decreased signal intensity in areas of invasive carcinoma or DCIS (5.82+/-0.48) compared to the signal intensity of the uninvolved fibrous tissue (9.58+/- 0.67) (unpaired t-test; p=0.0014).

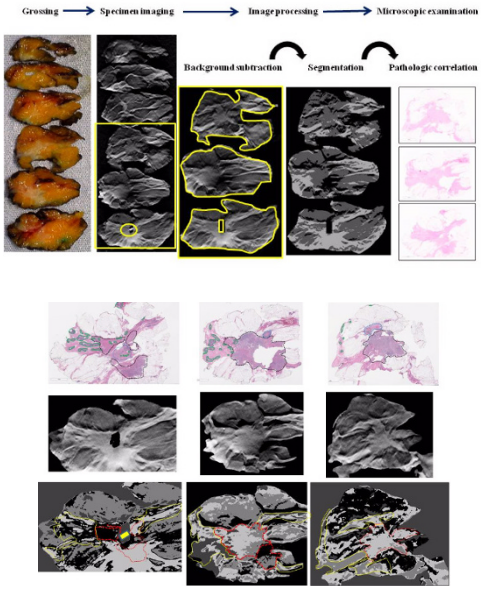

Conclusions: Our pilot study highlights a novel approach to the macroscopic evaluation of breast specimens in the pathology laboratory that could enhance the *ex-vivo* detection of breast carcinoma and targeted sampling of tumor-rich areas, increasing the efficiency of pathologic examination, and reducing the costs of tissue processing and histologic review.

2270 Fast and Molecular Friendly Heat and Mechanical Agitation Based EDTA Decalcification of Bone Marrow Trephine Biopsies Provides High Quality DNA with Preserved Histology and Immunohistochemistry

Madhu Menon[1], *Lisa Whiteley*[2], *Joanne Beher*[3], *Natalie Karmo*, *Faith Fletcher*[2], *Kelly Adamczyk*[2], *Juan Gomez-Gelvez*[2], *Kedar Inamdar*[4], *Milena Cankovic*[1], *Dhananjay A Chitale*, *Richard Zarbo*[1]. [1]Henry Ford Hospital, Detroit, MI, [2]Henry Ford Hospital, [3]Henry Ford Hospital, Detroit, MI, [4]Henry Ford Health System, Detroit, MI

Background: Modern hematopathology relies heavily on molecular studies as diagnostic, prognostic and predictive ancillary studies, especially with the advent of next generation sequencing (NGS). While bone marrow (BM) aspirate smears continue to be used as the primary DNA source, hemodilution and BM fibrosis might make them non-representative of native BM including lack of potential sub clones. Traditional Hydrochloric acid (HCL) based decalcification (HD) makes bone marrow trephine biopsy non-amenable to DNA studies. We demonstrate a temperature and magnetic stirring based EDTA decal (ED) method that preserves DNA and provides a reasonable turnaround time.

Design: BM biopsies were received in formalin and treated with HCL (RDO rapid decal, Apex, Aurora, IL) or 10% EDTA (Mol-Delcalcifier and BoneStation, Milestone Medical, Kalamazoo, MI) (at 37 and 50 °C) followed by regular processor vs. rapid processor (Tissue Tek VIP 300E vs. Tissue-Tex Xpress x50, Sakura, Torrance, CA). Immunohistochemistry (IHC) was performed for CD20, CD3, CD34, TdT, CD138 and Tryptase. DNA was evaluated by spectrophotometry and amplification of control size ladder mix generating amplicons of 100, 200, 300, and 400 base pairs (bp) (Invivoscribe, San Diego, CA). Student T test was used for statistical analyses.

Results: BM histology and IHC was unaltered by ED (37 °C or 50 °C) or use of regular vs. rapid processor. When comparing ED method across all conditions, best results were obtained with ED at 50 °C + regular tissue processor with reliable amplification up to 300 bps. For 400 bp, this method reliably generated amplicons albeit at lower peak heights (as compared to 100-300 bp) while other conditions mostly failed to generate any 400 bp amplicons. In contrast, HD amplified DNA only up to 100 bp although mean peak amplicon height for 100 bp was substantially less than ED method (13732 vs. 24275). Surprisingly, DNA quality of ED was superior to clot section. ED (50 °C) with regular processor demonstrated statistically significant superiority over use of rapid processor at either 37 or 50 °C for 100-300 bp ($p<0.05$).

Conclusions: We demonstrate that increasing temperature to 50 °C (with magnetic stirring) during ED does not alter histology or immunohistochemistry and yields good quality DNA with reasonable turnaround time (approximately 5 hours decalcification) as compared to the historically long decalcification periods (up to 24 hours) of EDTA based methods. NGS studies are in progress to further validate this process.

2271 Impact of the Prosigna (PAM50) Assay on Adjuvant Clinical Decision-making in Early-stage Postmenopausal Breast Cancer (PMBC) Patients

Sambit K Mohanty[1], *Dinesh Pradhan*[2], *Tarini P Sahoo*[3], *Dilip Kar*[4], *Manas Baisakh*[5], *Ushashree Das*[4], *Chinmaya Pani*[4]. [1]Advanced Medical Research Institute and Hospital and Metropolis India Heath Care, Cuttack, Odisha, [2]University of Pittsburgh Medical Center, [3]Chirayu Medical College and Hospital, [4]Advanced Medical Research Institute and Hospital, [5]Apollo Hospitals

Background: Gene expression profiling determines the risk of recurrence (ROR) in hormone positive, early stage, post-menopausal breast cancer (PMBC) patients, which helps in better clinical patient management. This study was undertaken to examine the influence of Prosigna assay on adjuvant treatment decisions in these PMBC patients.

Design: This is a prospective multicenter study on PMBC patients from India. Nanostring's Prosigna assay, based on the PAM50 gene signature, was performed to identify the risk of distant recurrence score; low (0-40), intermediate (41 to 60) or high (61-100). The participating oncologists completed questionnaires based on the clinico-pathologic and immunohistochemical parameters, about their treatment recommendations, before and after the assay results.

Results: Thirty-five patients were enrolled in the study between July 2014 and August 2016. The patients were postmenopausal, hormone receptor positive, HER2 negative, and lymph node negative, and were either stage 1 or stage 2 tumors. After receiving the ROR score, treatment recommendations were changed for 3 (18.7%) patients in the high and intermediate risk category and for 14 (87.5%) in the low risk category (Figure 1). The confidence of medical oncologists in their treatment recommendations increased in 18/35 (51.42%) patients. Grouping high- or intermediate- vs. low-risk categories, we find that there was a significant (McNemar's test; $p=0.013$) net upward shift of risk category (14 up vs. 3 down) due to the Prosigna assay results; the upward shift of assessed risk is even more pronounced in the high- vs. intermediate/low risk ($p=0.077$). There was no significant net shift to or from intermediate categories. Overall, the Prosigna test results led to a change in adjuvant treatment decisions in 17/35 (48.58%) patients. Interestingly, the correlation of the ROR scores (high and intermediate vs. low) based on the clinical parameters and the Prosigna score showed a significant difference ($p=0.013$, McNemar's test). There was significant correlation among Prosigna ROR score(low & intermediate vs high risk), histologic grade & Ki-67 proliferation index (Figure 2)

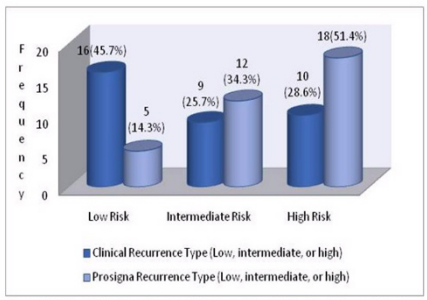

Figure 1. Risk of distant recurrence at 10 years: determination by clinicopathologic factors (dark blue) vs. Prosigna risk of recurrence score (light blue).

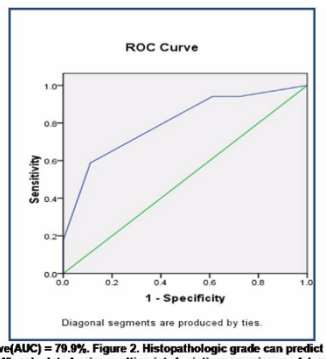

Area under the curve(AUC) = 79.9%. Figure 2. Histopathologic grade can predict of Prosigna result with a p value = 0.043, calculated using multivariate logistic regression model, adjusted with Ki-67 proliferation index and has area under the curve 79.9% in ROC analysis (Area under the curve, AUC = 79.9%).

Conclusions: Risk of recurrence score assessed by the Prosigna assay showed significant difference from clinicopathologic assessment, thereby influencing the treatment decisions. Further studies with a larger cohort of patients with clinical follow-up information are warranted to evaluate the impact of GEP on long-term outcomes and to substantiate the current findings.

2272 Evolving Companion Diagnostic Paradigm for Immunohistochemistry: Individualized Immunoprofiles in the Emerging Era of Antibody Drug Conjugate Based Therapies

W. D. Mojica[1], *Elizabeth Okundaye*[2], *P Mojica*[3], *S Kandel-Amataya*[4], *B Song*[5], *Elizabeth Korangy*[6]. [1]University at Buffalo, Williamsville, NY, [2]St. Mary's College, [3]Wayne State University, [4]Univer, [5]UB, [6]University at Buffalo

Background: The intent of adjuvant therapies (AdjTx) is to combat progression of disease. Novel types of AdjTx, like antibody drug conjugates (ADC), have the potential to maximize targeted therapy and reduce rates of recurrence. However, a major barrier exists because identification of which cells to target, i.e., which cell have metastatic potential within a tumor, cannot be determined at this time. Creation of an immunoprofile characterizing every malignant cell in a tumor with targetable plasma membrane proteins (PMbP) may serve as a novel means in guiding currently available ADC based therapies and the development of additional promising ADC's. This approach affords new opportunities for companion diagnostic development using established techniques like immunohistochemistry (IHC). A model and the findings of this concept, using triple negative breast cancer (TNBC) as the target malignancy, are herein presented.

Design: Cases of TNBC were identified from archival files. Six PMbP, 5 (AXL, DLL-3, L1CAM, PTK-7, Trop-2) with ADC's target ready and currently in clinical trials for several different tumors, and 1 (CDH2) currently undergoing pre-clinical evaluation, were included in the panel. Antibodies (Abs) to these PMbP's were purchased from commercial sources (AXL:Cell Signaling; CDH2, L1CAM, DLL-3: Thermo Scientific; PTK-7: ProteinTech; Trop-2: Santa Cruz) and IHC performed using conventional methods. The stained slides for each case were scanned for each Ab and the images overlain relative to each other to create a composite. The composite image was evaluated for percent coverage of tumor by the panel of Abs.

Results: 34 cases of TNBC were available for evaluation in this study. None of the tumors were found to express all 6 proteins or have 100% coverage by the panel of Abs. 18 (53%) were found to be expressed in greater than 50% of the tumor cells by either one, or a combination of, 2 or more Abs. Only 3 cases (9%) of the tumor cases had no expression of any of the targetable PMbP's.

Conclusions: The use of a panel of Abs to characterize the target landscape of a tumor revealed 1) the heterogeneity in expression of targetable PMbP between tumors of the same morphologic subcategory; 2) absence of expression in every malignant cell in the tumors by any single Ab, therefore necessitating the need to test using a panel approach; and 3) limitations of the current panel. Continued exploration through the addition of more Abs to the panel are needed to maximize this approach for clinical use.

2273 Quantification and Viability Assessment of Cytopathologist-Performed Ultrasound-Guided Fine Needle Aspiration Biopsy (USFNA) of Nonpalpable Inguinal Lymph Nodes (LNs) in HIV-infected Adults

Dianna Ng[1], *Stephen Nishimura*[1], *Steven Deeks*[1], *Jeanette Ruiz*[2], *Rita Ung*[1], *Rebecca Hoh*[1], *Viva Tai*[1], *Poonam Vohra*[2]. [1]UCSF Medical Center, San Francisco, CA, [2]University of California San Francisco, San Francisco, CA

Background: Despite effective antiretroviral therapy, HIV persists indefinitely, with the vast majority of the virus in difficult-to-access lymphoid tissues, particularly LNs. USFNA may allow for safe and minimally invasive access to this tissue. The aim of this study is to assess the utility of USFNA of non-palpable inguinal LNs to characterize the HIV reservoir and immune function in LNs from HIV-infected adults.

Design: After obtaining informed consent, inguinal LNs were identified by ultrasound (US) in 16 individuals (age 41-76, average 58 years old; 15 males, 1 male-to-female transgender) from HIV+ patients (range since diagnosis: 8-38 years) . Using a 23 gauge, 1/½ inch needle, 3-6 passes were made under local anaesthesia for each lymph node. One LN was sampled in 14 subjects, while bilateral inguinal LNs were sampled in 2 subjects. A portion of each pass was taken for rapid on-site evaluation (ROSE). The remaining sample was transferred into Roswell Park Memorial Institute (RPMI) medium. Cell count was assessed using an automated cell counter by trypan blue. Viability was measured using LIVE/DEAD™ by flow cytometry. Aliquots were then distributed to multiple research groups for various studies, including Tat/rev induced limiting dilution assay (TILDA), mass cytometry, and HLA tetramer staining of CD8+ T cells.

Results: LN size was recorded in 4 individuals and ranged from 1.0 to 1.7 cm. The procedure was well tolerated and there were no adverse events. The median cell count was 1.2 million cells (range 128,000-7.7 million). Cell viability was available in 5 cases with a median of 86% (range 64-92%). CD4 yield was calculated from 5 LN samples and ranged from 47% to 89%. The CD4 yield was least in the sample with abundant red blood cells. Sufficient tissue was obtained to measure the size and genetic characteristics of the reservoir, using a number of assays. Sufficient tissue was also obtained to isolate and characterize HIV-specific CD8+ T cells.

Conclusions: 1. Cytopathologist performed USFNA of non-palpable inguinal LNs in HIV-infected adults is a well-tolerated and safe procedure.

2. USFNA of LNs provided sufficient and viable samples for various HIV-1 reservoir and pathogenesis studies.

3. USFNA provides the capacity to study the same site longitudinally over time, which will allow for more precise assessment of how a variety of potentially HIV curative interventions affect immune function and the reservoir.

2274 A Novel Image Analysis Algorithm to Classify Bladder Wall Layers: A Step Towards Automated Sub-Staging Of T1 Bladder Cancer

Muhammad Khalid Khan K Niazi[1], *Thomas Tavolara*[1], *Vidya Arole*[1], *Cheryl Lee*[1], *Anil Parwani*[1], *Metin Gurcan*[1]. [1]The Ohio State University, Columbus, OH

Background: Clinicians need better tools to accurately stage and risk stratify patients with T1 bladder cancer in order to appropriately direct curative therapies and minimize treatment-related complications. This abstract is a part of a large study where we are attempting to develop an automated system to sub-stage T1 bladder cancer. One of the prerequisites of this large study is develop an automated system to recognize different layers of bladder wall (LBW) from images of H&E bladder biopsies

Design: Humans have cells in visual cortex that are known to respond to simple shapes like lines and curves. As visual stimuli move through the ventral stream, more complex cells respond to more complex recognition tasks. Deep learning tries to provide this ability to computers by autonomously learning discernable features from a huge number of training samples. Unfortunately, the limited availability of labeled bladder samples makes the use of deep learning impractical for automated recognition of LBW. Hence, a deep learning system trained using limited samples is deemed to undermine the reliability of the pathology findings. Humans appear to have intrinsic ways to transfer knowledge between recognition tasks. That is, we recognize and apply relevant knowledge from previous learning experiences when we encounter new tasks. We present a similar approach – instead of completely relying on labeled bladder biopsies, we use deep learning to extract discernable knowledge from non-pathology images, and then use the limited labeled images to fine tune it to recognition of LBW.

Results: Our dataset consists of 37 images of de-identified H&E bladder biopsies scanned at 40x magnification. We created an interface that allows the pathologist to view side-by-side the original whole slide image and its respective heat-map (representing the probability of being either one of the LBW) on a computer screen (See Figure 1). The pathologist was provided with a zoom-in and out functionality to carefully review all the 37 images. The pathologist opted to score each image between zero (being the worse) and five (being the best) with a step size of 0.5. The proposed method resulted in an average accuracy of 92.7 (+/- 6%)

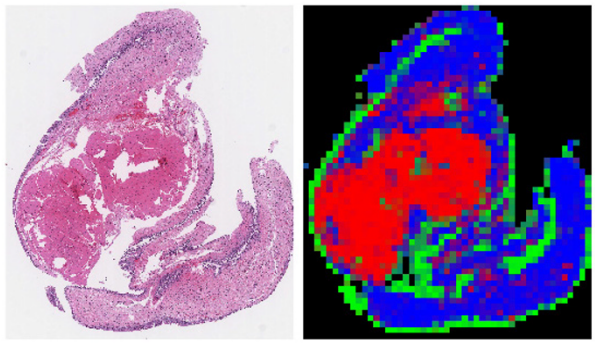

Figure 1: Example image. Left: Example image of a bladder biopsy scanned at 40x magnification. The image has a size of 10K X 10K pixels. b) The result of proposed automated bladder layers recognition system. The green color corresponds to urothelium, blue color represents lamina propria while the red color stands for deep muscle.

Conclusions: We showed that it is possible to transfer knowledge between recognition tasks, i.e. use discernable features learnt from non-pathology images to recognize LBW. Overall, the proposed system resulted in a reasonable accuracy. However, it struggled to classify LBW in cauterized tissue.

2275 3D Imaging of Cleared Surgically Resected Human Pancreatic Tissue

Michaël Noë[1], *Neda Rezaee*[2], *Kaushal Asrani*[2], *Michael Skaro*[3], *Vincent P Groot*[4], *Pei-Hsun Wu*[3], *Matthew Olson*[5], *Seung-Mo Hong*[6], *Sung Joo Kim*[7], *Matthew J Weiss*[8], *Christopher L Wolfgang*[8], *Martin A Makary*[8], *Jin He*[8], *John L Cameron*[8], *Denis Wirtz*[9], *Laura Wood*[10], *Ralph Hruban*[1]. [1]Johns Hopkins Medical Institutions, Baltimore, MD, [2]Johns Hopkins Medical Institutions, [3]Johns Hopkins University, Baltimore, MD, [4]Johns Hopkins Medical Institutions, Baltimore, MD, [5]Dundalk, MD, [6]Asan Medical Center, Seoul, [7]Asan Medical Center, Seoul, [8]Johns Hopkins University School of Medicine, [9]Johns Hopkins University, [10]Johns Hopkins Hospital, Baltimore, MD

Background: Since the days of Rudolph Virchow, pathologists have studied diseases in two dimensions (2D). Visualizing pathologies in three dimensions (3D), however, can provide unique insights into the biology of human diseases. We cleared and immunolabeled thick (~0.5cm) sections of surgically resected human pancreata and visualized normal pancreas, pancreatic intraductal neoplasms and invasive carcinomas in 3D.

Design: A rapid and easy to implement DiBenzyl Ether (DBE) based technique was used to clear thick sections of surgically resected human pancreatic parenchyma. Protocols were optimized for both fresh and formalin-fixed, paraffin-embedded (FFPE) tissue (see Figure 1). The penetration of antibodies for immunolabeling, such as antibodies to CK19, into the dense tissue was optimized by applying centrifugal and convection flow. Immunolabeling was visualized in 3D using the LaVision Ultramicroscope II (Light Sheet Microscopy) and the Zeiss LSM800 (Laser Scanning Microscope). 3D reconstruction and animations were prepared with Bitplane Imaris software.

Results: The technique was successfully applied to 26 sections of pancreas, providing visually stunning 3D images of normal pancreatic tissue, pancreatic intraepithelial neoplasia (PanIN; https://youtu.be/o4hJrit2x7o), intraductal papillary mucinous neoplasms (IPMNs) and infiltrating pancreatic ductal adenocarcinomas (PDACs). The visualization of disease in 3D highlighted processes, such as invasive carcinoma growing into pre-existing pancreatic ducts (https://youtu.be/06MI6ICxB0E), which are hard to conceptualize in 2D.

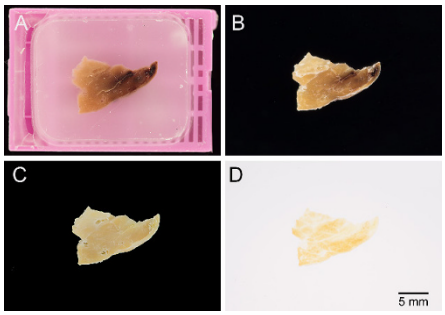

Conclusions: Three dimensional visualization of cleared human solid organs provides an extraordinary opportunity to understand the true complexity of human disease. Expanding this technique to FFPE tissue opens pathology archives to 3D visualization of unique biosamples and rare diseases. The application of immmunolabeling and clearing to human pancreatic parenchyma, as we present here, provides detailed visualization of normal pancreatic anatomy, and can be used to characterize the three dimensional architecture of disease processes ranging from PanIN and IPMN to PDAC.

2276 Objective Discrimination of Breast Cancer Cells (MCF-7) from Normal Human Mammary Epithelial Cells (HMEpC) by Raman Microspectroscopy (RM): Molecular Basis for Application of RM in Cancer Diagnosis

Hemanth Noothalapati[1], *Yui Suzuki*[2], *Asuka Asuka*[3], *Riruke Maruyama*[4], *Tatsuyuki Yamamoto*[1]. [1]Raman Center for Medical and Biological Applications, Shimane University, [2]Shimane University of Life and Environmental Science/Graduate School, [3]Shimane University Faculty of Medicine, Izumo, Shimane, [4]Shimane University Faculty of Medicine, Izumo, Shimane

Background: Conventional cytology is easy to perform and relatively non-invasive. However, there are a certain number of indeterminate cases even when it is expected to play a critical role in making a therapeutic decision. Application of RM in cytology as an adjunct to morphology is anticipated to solve such a problem, particularly because it is a non-invasive, label-free method that provides rich chemical information. It has been reported that RM could be used to improve accuracy of cytological and even histopathological diagnosis, but to our knowledge, this novel technique tends to be employed without concrete knowledge of molecular changes in cells.

Design: Raman spectra were obtained from 30 independent HMEpC and MCF-7 cells. Each spectrum is an average of 5 random points in a cell. Data from all 60 cells were then analyzed together. Change in the ratios of biomolecules can be potential indicators of cancer. However, the main difficulty in RM is to extract pure biochemical components from complex cellular data. First, conventional univariate approach (analyzing one band at a time) was applied. Then, we utilized multivariate curve resolution analysis (MCR) to analyze full region and separate physically meaningful spectra from hyperspectral cube, find their relative abundances and elucidate the underlying molecular changes in cancer cells.

Results: Average Raman spectra of 30 HMEpC and MCF-7 cells each is shown in Fig. 1A. Raman bands at 1440 (Lipid), 1003 (protein) and 786 (DNA) were used to calculate ratios such as DNA / Lipid (Fig. 1B) and Protein / Lipid (Fig. 1C) by univariate method. Though there are differences, it is not reliable as multiple components contribute to each band. Then, by employing MCR analysis with non-negative constraints, we extracted 5 reliable and physically meaningful pure biochemical spectra comprising of DNA, proteins and surprisingly 3 independent lipid components (Fig. 2A). Lipid 1 is assigned to polyunsaturated fatty acids (PUFA) while other 2 components correspond to low unsaturated lipids. Intriguingly, PUFA is more abundant in HMEpC than MCF-7 though scientific literature tells otherwise. Moreover, ratio of total DNA / PUFA (Fig. 2B) and Protein / PUFA (Fig. 2C) are strictly regulated (HMEpC << MCF-7) and has been used objectively to discriminate cancer cells from normal cells.

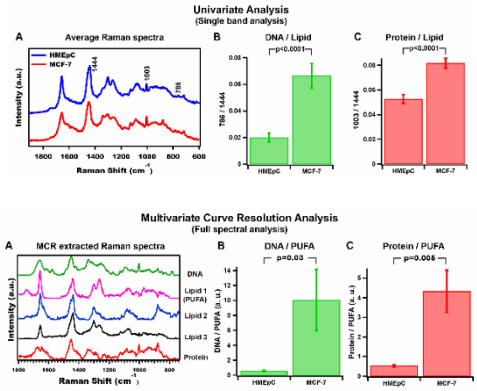

Conclusions: RM has the potential to become an excellent cytodiagnostic tool that can both accurately and objectively discriminate cancer cells from normal cells.

2277 A Next Generation Sequencing Approach for Direct and Definitive Determination of Biallelic CEBPA Mutations

Arantza Onaindia[1], *Roberto Ruiz-Cordero*[2], *Wei Chen*[2], *Bedia A Barkoh*[2], *Kristen Floyd*[2], *Meenakshi Mehrotra*[2], *Naveed R Farhana*[2], *Mark Routbort*[3], *L. Jeffrey Medeiros*[2], *Rajyalakshmi Luthra*[2], *Keyur Patel*[4]. [1]Instituto de Investigacion Marques de Valdecilla (IDIVAL)/UT-MD Anderson, Houston, TX, [2]The University of Texas MD Anderson Cancer Center, Houston, TX, [3]Bellaire, TX, [4]UT-MD Anderson Cancer Center, Sugar Land, TX

Background: Acute myeloid leukemia (AML) with biallelic mutations of *CEBPA* represents a new entity in the 2016 update of the World Health Organization classification. However, determination of monoallelic versus biallelic nature in routine clinical testing can be challenging due to the distance between the N-terminal and C-terminal mutations. We developed a simple and clinical workflow-ready assay for direct and definitive determination of biallelic *CEBPA* mutations.

Design: Genomic DNA from 13 patients in which *CEBPA* double mutations in the N- and C-terminal domains as shown by Sanger sequencing formed the study group. The entire coding region of the *CEBPA* gene was amplified with two custom designed primers. NGS Library preparation was performed using the Nextera XT DNA Sample Preparation Kit (Illumina, San Diego, CA). Libraries were size selected (600-1100bp) using the Blue Pippin automated gel system (Sage Science, Beverly, MA). Paired-end sequencing was performed on MiSeq Nano flow cell for paired-end sequencing using the MiSeq 500 Cycles version 2 kit (Illumina). A custom bioinformatics workflow was developed for the detection and review of the mutations.

Results: Adequate sequencing coverage (>250x) was obtained for 88.3% of the coding sequence of *CEBPA* (codons 42 to 358) with 97.3% passing filter and sequencing quality score ≥Q30 84.1% of sequencing data. In 9 patients with adequate NGS coverage, all mutations identified previously by Sanger sequencing were confirmed in the N- and C- terminal loci, of which 8 were biallelic and 1 showed a combination of monoallelic and biallelic mutant reads. Poor coverage was observed for the region from codons 1 through 41 (average 155x, 59-180) affecting determination of biallelic mutations in 4 (30%)

patients that showed mutation in codon 23 (position: c.68).

FOR TABLE DATA, SEE PAGE 827, FIG. 2277

Conclusions: We describe the first-ever clinical workflow-friendly NGS based assay allowing definitive determination of *CEBPA* biallelic mutations in 70% of double-mutant *CEBPA* cases in our dataset. The assay is predicted to cover 86% of reported mutations in key publications representing 50 AML cases with *CEBPA* double mutants. Additional refinement of the protocol is in progress to improve coverage for codons 1 to 138.

2278 Liver Iron Quantitation Via Image Analysis: Correlation with Biochemical Analysis, Pathologist Assessment, and Clinical Status

Adam J Perricone[1], *Alton B Farris*[1]. [1]Emory University, Atlanta, GA

Background: Quantitation of liver iron (Fe) content is an important assay in the workup and diagnosis of hereditary hemochromatosis (HH). A current putative gold standard of liver iron content is biochemical analysis (BA) of sampled tissue, a specialized assay not available at all institutions. Moreover, as iron deposition may be heterogeneous, the sampled tissue may not be reflective of the overall disease process, hindering diagnosis. Other visual methods of grading severity of iron deposition via pathologist assessment are limited by subjectivity and time. Whole slide imaging (WSI) is a burgeoning technology in anatomic pathology. While the performance of imaging techniques other than WSI for quantifying liver iron has been previously examined, in this study we assess the ability of WSI to accurately quantify liver iron by comparing it to BA, as well as pathologist visual methodologies. In addition, we correlate the results of these various iron quantitation methods with HH mutational status.

Design: Liver biopsies were identified through a computer search targeted at identifying cases subjected to BA for work-up of possible HH. Using WSI of Prussian blue slides, %iron was quantitated via a positive pixel count (PPC) algorithm adjusted to detect iron staining (Figure 1). WSI %iron was then correlated to pathologist assessment grading schemes, including Scheuer Score (SS), granule detection score, and Total Iron Score (TIS), as well as HH mutational status (i.e., H63D and C282Y mutations).

Results: Thirty cases were included in the study. A wide range of iron content, as quantitated via BA (10 – 44,282 µg/g dry weight), was present among included cases. Using linear regression, statistically significant correlations were detected between BA and %iron, SS, granule detection, and TIS ($r = 0.39 – 0.60$, $p < 0.05$ for each comparison) with the strongest correlation being between BA and PPC %iron ($r = 0.60$, $p < 0.001$) (Figure 2). In addition, each of the methods demonstrated statistically significant correlations with HH mutational status (t-test $p < 0.05$).

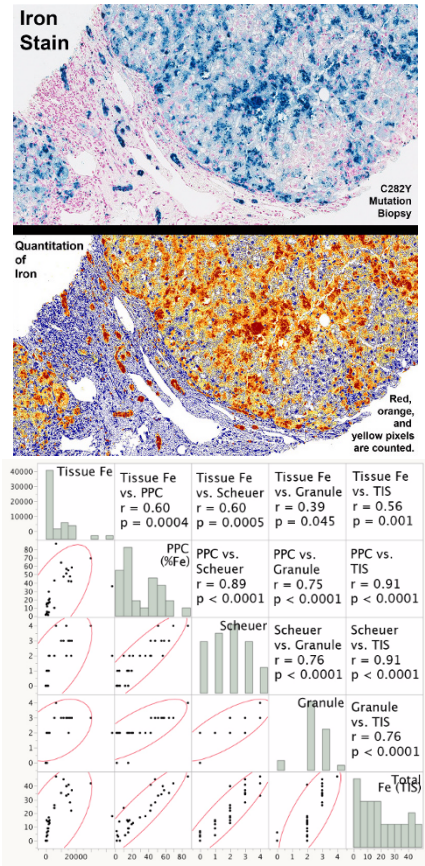

Conclusions: WSI was able to quantitate %iron across a wide range of iron content, and these results correlated with the gold standard of iron quantitation, BA, as well as visual iron quantitation grading schemes. Iron content calculated via WSI also correlated with HH mutational status. These data suggest that, in the work-up of HH, WSI can potentially generate an objective analysis of liver iron deposition.

2279 Deep Image Stacking for High Depth of Focus (DOF) and Resolution

Vishnu Reddy, Birmingham, AL

Background: Depth of focus or field (DOF) in a typical macro / photomicroscopy imaging is very short, typically 1-10 microns depending on the magnification levels. One solution to increase the DOF is through shooting multiple images focused at different depth of planes, and combine all sharp areas into single image though software utility. This involves performing a deep image stack of 50 – 150 images at 1 or 2-micron increments, and use focus stacking software to produce a single high resolution image with very high DOF.

Design: Material and Methods: Digital camera (16-mega pixel) connected to macro bellows, which is attached to relay lens (150 mm zoom lens). Microscope plan achromatic objective lenses (20x and 40x) are mounted on to the front of relay lens through series of adapter rings. The entire setup is mounted on electronically controlled stepper motor macro rail system that coordinates the movement of macro rail and triggering of camera (Fig.1). Cognnisys® stacking rails and Wemacro® rails are used with above setup (Fig.2) for collecting image stack. Individual images with narrow depth of focus are combined into single extended DOF through Zerene Stacker® or Helicon Focus® image stacking software. Thick lymph node sections (10-20 microns) are cut from formalin fixed paraffin tissue blocks and standard with H&E stains, immunohistochemical stains (kappa/lambda), CD138, CD20 and BCL2. Deep image stack of 40 images are obtained at 1-micron intervals using 20x microscope objectives, the deep stack is repeated using 40x objective. Image stacking software is used for generating extended DOF high-resolution image of each slides.

Results: Extended DOF images of H&E sections and immunohistochemical stains showed more details and cellular architecture compared to routine single frame images, especially staining of plasma cells with kappa/lambda stains showed more contextual details in relation to macrophages, lymphoid cells and endothelial cells.

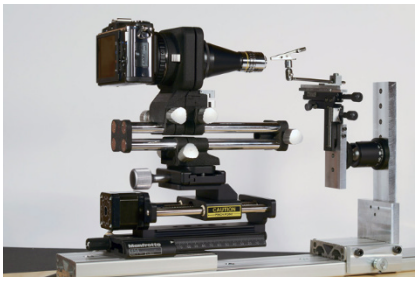

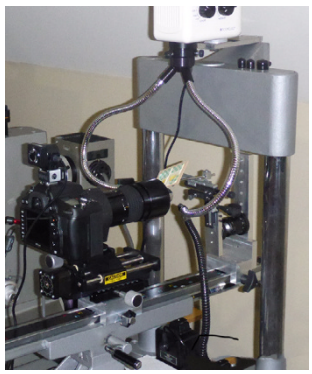

Conclusions: Deep image stacking methodology is an inexpensive alternate to confocal microscopy, and existing microscope lenses can be easily adapted for generating very high-resolution extended DOF images.

2280 Potential Role of Desorption Electrospray Ionization (DESI) Mass Spectrometry Imaging (MSI) for Intraoperative Margin Assessment in Basal Cell Carcinoma

Kevin Yi Mi Ren[1], *Martin Kaufmann*[2], *Shuo Amanda Xu*, *David Berman*[1], *John Rudan*[2], *Douglas MacKay*[2], *Ami Wang*[3], *Sonal Varma*. [1]Queen's University, Kingston, ON, [2]Queen's University, [3]Kingston General Hospital, Kingston, ON

Background: Basal cell carcinoma (BCC) is the most common type of skin cancer. It often occurs in cosmetically important areas such as face, head and neck region, and can cause significant morbidity from local invasion and destruction. Obtaining negative margins with minimal sacrifice of benign tissue in BCC resection is critical in achieving aesthetic outcome and preventing potentially disfiguring recurrences. Recurrence rate can reach 26% in margin positive cases. Mohs surgery improves margin control but is highly resource intensive. DESI MSI is an emerging technique capable of tissue characterization based on metabolite profiling. It can be applied to unstained frozen section slides to create tissue images based on the relative abundance of metabolites that topographically match the histology sections. We present a pilot study assessing DESI's ability to assess BCC resection margins.

Design: Fresh tissue samples from 7 BCC resection cases with well defined tumour and non-neoplastic junction were collected. Unstained frozen section slides incorporating the complete cross section containing deep and peripheral resection margins were subjected to DESI MSI, and subsequently stained by hematoxylin and eosin (H&E) for histology correlation.

Results: Metabolomic profiles from DESI MSI effectively distinguished regions with BCC tumor nests from adjacent non-neoplastic skin. Selected lipids with mass to charge ratio (m/z) 722.51 and 858.52 show increased relative abundance in BCC tumor regions in all 7 cases with good histologic correlation. [Figure 1] In addition, lipids with m/z 748.51, 883.53, 750.54 also exhibit characteristic increased relative abundance in regions containing tumor in most cases. The relative abundance of these metabolites was consistently low in the non-neoplastic tissue margins in all cases, thus appropriately classifying the margins as negative. We are actively analyzing more cases to further confirm the ability of DESI MSI to assess resection margin status.

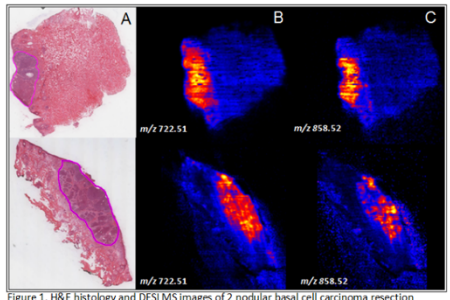

Figure 1. H&E histology and DESI MS images of 2 nodular basal cell carcinoma resection specimens. Tumor nests are outlined in purple on H&E micrograph (A). DESI MSI shows high relative abundance of metabolites with mass to charge ratio (m/z) 722.51 and 858.52 (B&C) in the tumor regions with good histology correlation. The peripheral and deep margins are appropriately marked as negative by DESI MSI.

Conclusions: These findings support the use of DESI MSI to supplement histology in identifying and delineating BCC from adjacent non-neoplastic skin. As real time mass spectrometry techniques are being developed for intraoperative metabolomic based tissue classification. The metabolic signatures obtained from this study may help build a library to guide intra-operative tissue identification and margin assessment.

2281 Metabolomic Assessment of Prostate Adenocarcinoma Biopsy Using Desorption Electrospray Ionization (DESI) Mass Spectrometry Imaging (MSI) with Histologic Correlation

Kevin Yi Mi Ren[1], *Nicole Morse*[2], *Palak Patel*[2], *Jenny Wang*[2], *Tamara Jamaspishvili*[1], *John Rudan*[2], *Robert Gooding*[2], *Martin Kaufmann*[2], *David Berman*[1]. [1]Queen's University, Kingston, ON, [2]Queen's University

Background: Accurate identification of aggressive histologic patterns of adenocarcinoma in prostate needle biopsies can be challenging due to sampling limitations, tumour heterogeneity and subjective interpretation. Variations in histologic risk stratification can lead to inappropriate treatment and unnecessary surgery that can be associated with significant morbidity and health economic burden. Recent studies in prostate cancer metabolomics have identified potential prognostic biomarkers associated with aggressive disease and poor clinical outcome. We present a pilot study using desorption electrospray ionization (DESI) mass spectrometry imaging (MSI) technique to investigate and compare metabolite profiles of benign and malignant prostate tissue with histologic correlation.

Design: To replicate the clinical diagnostic protocol, standard 20-core needle biopsy were obtained from 19 fresh radical prostatectomy specimens using a standard template. Frozen sections from each core were subjected to DESI MSI analysis and subsequently stained by hematoxylin and eosin (H&E) for routine histologic assessment. Mass spectra of benign and malignant regions of interest were compared using qualitative approaches and multivariate statistical analysis.

Results: Using principal component analysis, metabolomic profiles from DESI MSI effectively distinguished benign prostate from adenocarcinoma. Metabolites with mass to charge ratio (m/z) 700 and 863 show high relative abundance in regions with adenocarcinoma, whereas metabolites with m/z 452 and 480 show high relative abundance in benign glandular regions. Direct comparison of DESI MSI with histology shows good topographic correlation of both adenocarcinoma and benign glandular regions. [Figure 1]

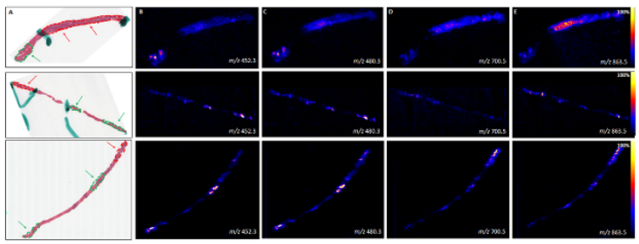

Figure 1. H&E histology and DESI MS images of three prostate cores with adenocarcinoma. On H&E histology micrograph (A), benign glandular regions are outlined in red, and adenocarcinoma regions are outlined in green. DESI MSI shows high relative abundance of metabolites with m/z 452 and 480 (B&C) in benign glandular regions, and high relative abundance of metabolites with m/z 700 and 863 (D&E) in adenocarcinoma regions with good histology correlation.

Conclusions: DESI MSI can be used to supplement histology in differentiating benign and malignant prostatic tissue in needle biopsies. In ongoing validation studies, we are evaluating the potential clinical utility of DESI MSI in the diagnosis and risk stratification of prostatic adenocarcinoma.

2282 Characterization of Microsatellite Instability in Colorectal Cancer Specimens by Next-Generation Sequencing

Navid Sadri[1], *Joseph Willis*[2], *James J Morrow*[3], *David J Alouani*[4], *Maureen Atchley*[5]. [1]Cleveland Medical Center/ Case Western Reserve University, [2]Cleveland Medical Center/ Case Western Reserve University, Cleveland, OH, [3]Case Western Reserve University, Cleveland, OH, [4]Univeristy Hospitals Cleveland Medical Center, Cleveland, OH, [5]University Hospitals Cleveland Medical Center

Background: Microsatellite instability (MSI) is a strong predictor of tumor response to immune checkpoint inhibition with PD-1 inhibitors. This finding resulted in the first FDA approval for a cancer therapy based on a molecular biomarker, agnostic of histologic diagnosis. Accurate and cost-effective clinical assays to assess MSI status are therefore paramount. Here we describe an assay that can be easily performed alone or as an add-on to cancer-associated mutation assessment by NGS.

Design: An amplicon-based sequencing approach was used to assess MSI at monomorphic homopolymer regions selected based on literature review. A cohort of 56 MSS and 35 MSI-positive FFPE colorectal cancer (CRC) specimens were used. MSI status of specimens was established by IHC of mismatch repair (MMR) proteins per standard protocol. We developed a novel, multi-modal analytic pipeline to detect MSI at these loci without the need for matched patient normal tissue. The ten loci that served as significant independent MSI discriminators are shown in Table 1.

Results: We demonstrate that sequencing data from these loci effectively identified 97% of MSI-positive CRC (34/35) and 95% of MSS CRC (53/56) as identified by IHC for MMR proteins. Additionally, we find unique homopolymer characteristics in tumors exclusively lacking MSH-2 and MSH-6 expression relative to other MMR-deficient tumors.

Table 1: Most Significant Loci Associated with MSI-CRC

Marker	Locus coordinates	Marker significantly different (p <.05) between MSS and MSI-CRC for each analytic modality		
		Length	Nucleotide	Skewness
MSI-02	chr2:62063033-62063155	yes	yes	yes
MSI-03	chr5:172421728-172421846	no	yes	yes
MSI-06	chr16:18882608-18882732	yes	yes	no
MSI-08	chr13:31722567-31722688	yes	yes	yes
MSI-12	chr2:148683681-148683698	yes	yes	no
MSI-14	chr17:56435156-56435172	yes	yes	no
MSI-15	chr3:51417599-51417615	yes	yes	yes
MSI-17	chr1:151196698-151196722	yes	yes	yes
MSI-18	chr1:200594037-200594054	yes	yes	yes
NR21	chr14:23652286-23652397	yes	no	yes

Conclusions: This method represents an easy, cost-effective strategy to identify patients with MSI-positive CRC who may benefit from immune checkpoint inhibition that can easily be added to other NGS assays for cancer-associated mutations.

2283 Fourier Transform Infrared (FT-IR) Spectroscopic Imaging: An Insight to its Diagnostic Utility for Evaluation of Pancreatic Ductal Adenocarcinoma (DAC), Intraductal Papillary Mucinous Neoplasm (IPMN), and Pancreatic Intraepithelial Neoplasia (PanIN)

Christine J Salibay[1], *Khin Su Mon*[1], *Shaiju S. Nazeer*[1], *Hari Sreedhar*[1], *Oluwatobi Adelaja*[1], *Asma Sharif*[1], *Frederick Behm*[1], *Michael J Walsh*[1], *Grace Guzman*[1]. [1]University of Illinois at Chicago, Chicago, IL

Background: Pancreatic ductal adenocarcinoma (DAC) is among one of the most aggressive cancers with a dismal prognosis worldwide. The current standard for diagnosis is histopathology, whereby morphologic criteria is the basis of distinguishing infiltrating glands from reactive. At times, subjectivity in pathologic diagnosis can be observed. Therefore, investigation of novel imaging techniques for histopathologic recognition is of great interest. Fourier transform infrared (FT-IR) spectroscopy is an emerging technique which has proven capable of tissue characterization based on biomolecular signatures. However, in review of the literature, there is only one FT-IR case study using human pancreatic tissue that has been conducted. We therefore employed a proof-of-concept study to demonstrate the diagnostic utility of FT-IR in identifying pancreatic intraepithelial neoplasia (PanIN), intraductal papillary mucinous neoplasm (IPMN), and DAC.

Design: Samples were identified through a retrospective search of our pathology database. We selected FFPE whole-tissue sections of pancreatic tissue representing 3 normal, 4 pancreatic intraepithelial neoplasia, 4 IPMN, and 2 DAC from 9 subjects. Diagnoses were verified using published histopathological criteria. H&E slides were mapped for diagnostic regions. All infrared spectra were acquired using an infrared spectroscopic imaging system. Regions of interest were identified and the spectral data were subjected to principal component analysis (PCA) followed by linear discriminant analysis (LDA) to differentiate tissue groups.

Results: Preliminary FT-IR average absorbance spectra (Figure 1) visually highlight the chemical differences between DAC, PanIN, IPMN, and normal pancreatic tissue. Furthermore, pair-wise PCA-LDA (Figure 2) is suggestive that pancreatic tissue groups of normal in comparison to IPMN and PanIN and PanIN in comparison to DAC are spectrally distinct from each other.

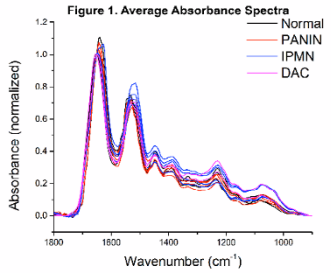

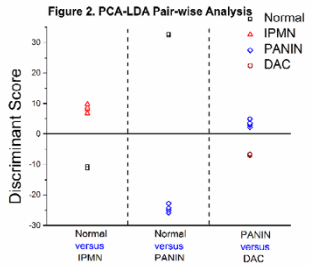

Conclusions: These preliminary findings suggest that biochemical differences within pancreatic tissue groups are detectable by this novel spectral technique. Our results provide a starting point of a diagnostic library to guide subsequent studies of spectroscopic pancreatic tumor imaging techniques. Future studies, including more selective spatial features for extraction of chemical information, judicious selection of spectral features, and a larger cohort, are necessary to further determine FT-IR's diagnostic utility in separating disease categories of pancreatic pathology.

2284 Effects of Different Decalcification Agents on Common Immunohistochemical Markers

Sasan Setoodeh[1], *Rahman Chaudri*[2], *Kyle Molberg*[3], *Stacy Hinson*[2], *Sara Blacketer*[4], *Karen Price*, *Elena Lucas*[2]. [1]UT Southwestern, Dallas, TX, [2]UT Southwestern, [3]University of Texas Southwestern, Dallas, TX, [4]Parkland Hospital, Dallas, TX

Background: Decalcification may affect immunohistochemical (IHC) stains, which are critical in the work-up of metastatic carcinoma to bone. The aim of our study was to evaluate the effects of widely used decalcifying agents on common immunostains.

Design: Small fragments of tissue from normal and neoplastic surgical specimens fixed in 10% formalin for 24-48 hrs were selected including breast, uterus, kidney, lung, thyroid, ovary, colon, small bowel, pancreas, liver, prostate, placenta, and skin. They were subjected to 3 decalcifying solutions EDTA (ACID FREE)™, formic acid (FA)-based decalcifier MasterCal™IM Plus (FA/MC), or 12% hydrochloric acid (HCl) for 1, 2, 6, or 24 hrs. For all specimens, a separate tissue microarray (TMA) was constructed. Each TMA consisted of 12 cores from sections decalcified for the different lengths of time and one reference non-treated section. H&E sections and immunostains using antibodies against 21 antigens characteristically expressed in the respective tissue types were performed on each microarray. The expression of each antibody was reported from 0 to 4+ staining (absent to strong). Change in the staining intensity between the decalcified sections and the reference section was categorized as decreased or increased (mild, moderate, marked or complete).

Results: 1339 immunostains performed on 103 tissue sections from 37 specimens were reviewed. No change in staining with any decalcifying agent was observed for AE1/AE3, CAM5.2, CK20, HepPar-1, PSA, PSAP, and S100. No significant change was observed in any tissues subjected to EDTA with the exception of a mild decrease in PAX8 at 6 and 24 hrs. Of tissues decalcified with FA/MC, a mild decrease of PAX8 was observed at 6 and 24 hrs and a mild to moderate decrease of TTF1 at 6 and 24 hrs. Of tissues decalcified with HCl, PAX8, CDX2, TTF-1, p40, p63, ER, PR, CK7, CK5/6, Synaptophysin, CD56, SALL4 and PD-L1 demonstrated variably decreased staining, most notable at 6 and 24 hrs. Chromogranin demonstrated mildly increased staining with EDTA at 24 hrs, with FA/MC at 2, 6, and 24 hrs, and with HCl at 1, 2, 6, and 24 hrs. Table 1 summarizes the results of IHC change at various time lengths.

Table 1. Changes in IHC intensity

Immunostain (No. of cases)	EDTA				FA/MC				HCl			
	1hr	2hr	6hr	24hr	1hr	2hr	6hr	24hr	1hr	2hr	6hr	24hr
AE1/AE3 (10)												
CAM 5.2 (7)												
CK7 (13)												
CK20 (7)												
CK5/6 (3)												
PAX8 (8)												
TTF1 (7)												
CDX2 (7)												
ER (8)												
PR (8)												
p63 (4)												
p40 (4)												
Chromogranin (2)												
Synaptophysin (2)												
CD56 (2)												
SALL4 (2)												
PSA (2)												
PSAP (2)												
S100 (2)												
HepPar1 (2)												
PD-L1 (1)												

Reference | Mild decrease | Moderate decrease | Marked decrease | Complete loss | Increase

EDTA: EDTA (Acid Free)™, FA/MC: MasterCal™ IM Plus, HCl: 12% hydrochloric acid

Conclusions: With our IHC protocols, EDTA and FA/MC do not affect the results of common IHC stains with the exception of PAX8 and TTF1. HCl reduces intensity of multiple immunostains, especially at 6 and 24 hrs. Decalcification mildly increased Chromogranin reactivity with all agents, possibly due to enhanced antigen unmasking.

2285 Stimulated Raman Histology - a Novel Label-Free Technique to Image Fresh Tissue

Kseniya S Shin[1], *Andrew Francis*[2], *Laligam N Sekhar*[2], *Gordana Juric-Sekhar*[42] *Dan Fu*[2]. [1]University of Washington, School of Medicine, Seattle, WA, [2]University of Washington, Seattle, WA

Background: Rapid intraoperative histologic assessment has major benefits in maximizing tumor removal, reducing recurrence, and improving outcome. The use of frozen sections is common. Yet, the challenge is in sampling error and artifact. In this study, we evaluate a new technique employing stimulated Raman scattering (SRS) phenomena to image fresh intact tissue and generate H&E equivalents as well as elucidate chemical information about the specimen.

Design: The tissue from skull base tumors were obtained from 7 patients undergoing neurosurgical craniotomies. The freshly excised skull base tumors were imaged at 50-100 μm below the tissue surface. By acquiring SRS images of lipids and proteins at 2850 cm^{-1} and 2940 cm^{-1} respectively, a two-color image showing chemical distribution was obtained (see Fig. 1 for setup details). The acquired two-channel data was converted to a pseudo-H&E color map with ImageJ. To validate two-color SRS based tumor detection, we compared two-color SRS images directly with H&E histopathology of paired tissue samples. Finer chemical differences were determined by scanning the high wavenumber region (2800-3100 cm^{-1}) with high spectral resolution (~12 cm^{-1}).

Results: SRS color maps were compared to the H&E stained tissue slides showing consistent features between methods (see Fig. 2). At the same time, additional information was present, as lipids were identified when compared to lipid-deficient conventional histopathology. Because cell nuclei were mostly devoid of lipids while cytoplasm has many membrane structures abundant in lipids, the two-color image provided clear morphology contrasts of cell nuclei. Also, the tissue was not disrupted with processing artifacts. More importantly, SRS imaging can provide 3D subcellular resolution without sectioning, thereby has the potential to sample entire tissue specimen and avoid sampling artifacts.

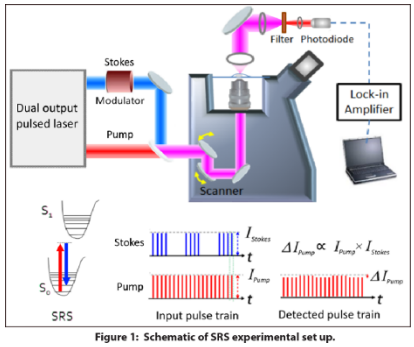

Figure 1: Schematic of SRS experimental set up.

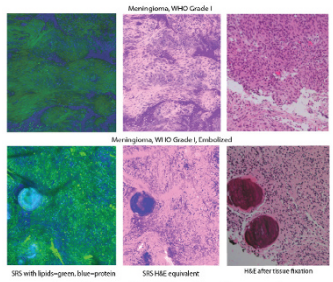

Figure 2: Comparison of SRS with histopathology of the same case tissue

Conclusions: Our preliminary data demonstrated the feasibility of using a stain-free SRS tissue scanner for tumor detection. The potential advantages of SRS imaging over traditional frozen section analysis are speed, cost, and accuracy. Additionally, the technology has proved capable of obtaining information in multiple image planes, paving the way to 3D imaging. This data is enabling us to move in a new direction for pathological diagnosis with direct application to intraoperative decision-making.

2286 Raman Spectroscopy for Detection and Analysis of Central Nervous System Tumors

Kseniya S Shin[1], *Natasha A Hippler*[2], *Laligam N Sekhar*[3], *Gordana Juric-Sekhar*[4]. [1]University of Washington, School of Medicine, Seattle, WA, [2]MarqMetrix, Inc., Seattle, WA, [3]University of Washington, [4]University of Washington, Seattle, WA

Background: Raman Spectroscopy (RS) is a technique used to interrogate vibrational and rotational frequency states in a system of interest, in our case neoplastic and uninvolved tissue. Utilizing inelastic scattering of light by tissue, we can discriminate the neoplastic from uninvolved tissue. Additionally, we can study chemical qualities of neoplastic processes as Raman shifts are unique for chemical information provided by molecules in cells. The aim of our study is to provide a proof-of-concept for RS use in surgically removed central nervous system tumors.

Design: The tumor specimens were obtained from 20 patients undergoing neurosurgical craniotomies. The cases included meningiomas and glial tumors. Tissue spectra were collected using a fully integrated Class I laser Raman spectroscopy system with touch probe from MarqMetrix, Inc. The Raman scattered energy was detected over the spectral interval of 200 – 2750 cm^{-1} with a spectral resolution of 7 cm^{-1}. Each tissue sample yielded at least 5 spectra and probe interrogation site was marked with a tissue dye to correlate RS measurements with neuropathological analysis.

Results: The spectra showed differences between glial tumors and meningiomas. Glial tumors had more prominent peaks at 1004 cm^{-1} (collagen assignment), 1450 cm^{-1} (CH_2 bending for proteins), and 1658 cm^{-1} (amide I). Moreover, for glial tumors, the 1250-1350 cm^{-1} region was unique for each sample corresponding to modes indicating differences in collagen count and nucleic acid content in tissues (Fig. 1). All meningiomas shared Raman characteristics at 746 cm^{-1} (thymine DNA/RNA base), 1002 cm^{-1} (phenylalanine), 1202 and 1233 cm^{-1} (amide III), 1447 and 1450 cm^{-1} (protein) and 1660 cm^{-1} (amide I). Raman peak at 957 cm^{-1} (hydroxyapatite) histologically corresponded to psammoma bodies (Fig. 2).

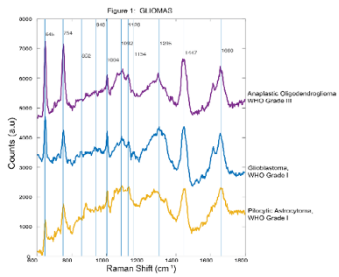

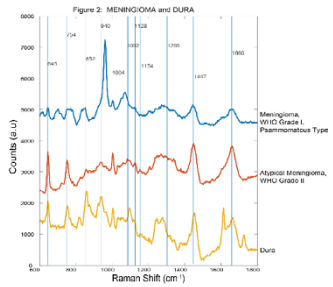

Conclusions: The results of this pilot study demonstrated that chemical composition variation elucidated by RS correlates to histopathology. Additionally, the information provided by RS is complementary and diagnostically relevant for future application in intraoperative consultations. As a future development, an extensive database of Raman spectra can be utilized as an effective tool for the analysis and discrimination of various central nervous system tumors in near real-time. Further investigations are necessary to confirm accuracy and precision of RS.

2287 Read Phase Related Error Could Cause Strand Bias in NGS Sequencing

Wen Shuai[1], *Richard Wu*[2]. [1]University of Miami / Jackson Memorial Hospital, Miami, FL, [2]U Health Pathology, Miami, FL

Background: Strand bias means the DNA sequences inferred from NGS of positive and negative strands on same targets are different. These differences were called as strand bias. While it was possible that the strand bias was caused by strand asymmetries during DNA evolution, the sequecing errors could play role in the strand bias reported from NGS, especially when the allelic frequency of the strand biased variants were lower. Here, we reported that the strand biased variants present in 16 cases were caused by read phase related errores.

Design: The illumina NGS platform was used to sequence 16 cases in two runs. The reason of unusual high numbers of variants with labeled sb (strand bias) was investigated, which was caused by read phase related error.

These cases were analyzed with different pipeline.

The runs were repeated after correcting the error. The variants identified with sb labels were disappeared after the read phase related error have been corrected.

Results: All 214 variants with labeled sb within 16 cases were present in two recent runs. After investigation, the high rate errores were present in forward reads and limited to each tile, which was confirmed in IGV (integrated genomics viewers) manually.

These variants were consistantly present in two different analyzing pipelines. Therefore, strand biased variants were not caused by alignment artifacts.

After switching the new reagent and new flow cells, the variants with sb label from same samples were disappeared in new runs. There were no high error reads that limited in one read phase or one tile in those new runs.

Conclusions: While it is possible that strand bias could be due to the differences existed in positive and negative strands of DNA, especially in bacteria, the strand biased variants reported by NGS with lower allelic frequency were caused by sequencing errores. Therefore, SB label is flag for further investigation of the sequencing QC and the variants with SB labels needed to be evaluated carefully before reporting the mutants out.

2288 Diagnostic Utility of SATB2 for The Origin of Neuroendocrine Tumors

Amal Shukri[1], *Arun Gopinath*[1], *Ahmad Alkhasawneh*[2]. [1]University of Florida College of Medicine, [2]Jacksonville, FL

Background: SATB2 protein is selectively expressed in glandular cells from the lower gastrointestinal tract, and it has been shown to be a sensitive diagnostic marker for colorectal carcinoma. However, very few studies have evaluated the expression of SATB2 in neuroendocrine tumors (NET). In this study we investigated the staining of SATB2 in NET from various sites and compared it is utility to CDX2.

Design: Tissue microarray was constructed using 3 mm core tissue (3 cores per case), and it consisted of all well differentiated neuroendocrine tumor cases diagnosed at our institution (2006-2016). Immunohistochemical staining for SATB2 and CDX2 were performed. Only nuclear staining was considered positive, and was scored as negative (-), weak/focal (w) and positive (+).

Results: 150 cases were included (70 males, 80 female) with a mean age of 59 years. SATB2 was positive in 86% of colorectal NET, while CDX2 was positive in 16% of colorectal tumors. None of the pancreatic cases was positive for SATB2 and only lung tumor was positive. Detailed comparison of SATB2 to CDX2 are summarized in Table 1.

Tumor site	SATB2 (+)	CDX2 (+)
Stomach (n=12)	4	2
Duodenum (n=16)	5	8
Terminal ileum (n=17)	5	13
Appendix (n=12)	12	12
Colon (n=50)	43	8
Pancreas (n=16)	0	5 (weak)
Lung (n=23)	1	1

Conclusions: Our results indicate that SATB2 is a sensitive marker for hindgut well-differentiated neuroendocrine tumors though it is not entirely specific. CDX2 is less often positive in hindgut neuroendocrine tumors, and it is frequently expressed in small bowel and pancreatic NET. Since SATB2 is rarely expressed in pancreatic and pulmonary NET, it can be used as adjunct in evaluating metastatic NET of unknown origin to exclude lung or pancreatic origin.

2289 High Sensitivity Detection of IDH1/2 Mutations for Assessment of Minimal Residual Disease

Parwiz Siaghani[1], *Lixin Yang*[2], *Leo Zhao*[3], *Milhan Telatar*[2], *Maria Cuellar*[4], *Evan Himchak*[5], *Holly H Yin*[6], *Dennis D Weisenburger*, *Patricia Aoun*[6], *Michelle Afkhami*[5], *Raju K Pillai*[1]. [1]City of Hope Medical Center, Duarte, CA, [2]City of Hope Medical Center, [3]Emory University, [4]City of Hope National Medical Center, [5]City of Hope, Duarte, CA, [6]City of Hope National Medical Center, Duarte, CA

Background: The presence of minimal residual disease (MRD) is one of the most important predictive factors for outcome in acute myeloid leukemia (AML). Flow cytometric methods of MRD detection, though effective in most cases, require large antibody panels and significant expertise for identification of rare leukemic cell populations. The RainDrop droplet digital polymerase chain reaction system (ddPCR) is an ultra-sensitive platform for nucleic acid detection in which the PCR reaction is carried out in up to 10 million droplets, each containing a single fragment of DNA. ddPCR measures the absolute target molecule number through the enumeration of "positive" droplets.

Design: This study describes the analytic and clinical validation of this assay for detection of IDH1 R132H mutations, frequently seen in AML.

Results: The maximum DNA input was first determined as 3 µg in a 50 µl reaction. The limit of blank, measured with maximum wild type (wt) DNA input, was 1.1 copies (N=20). The limit of detection was determined as 6.5 copies (N=20). The sensitivity of the assay, determined at LoD and maximal DNA loading, is 0.0024%. Fig 1 illustrates a scatter plot of 8 serial dilutions of IDH1 R132H mutant DNA from 0.64 pg to 2000 pg diluted in 200ng wtDNA. ddPCR was then used to compare IDH1 R132H levels in 13 bone marrow samples from 7 AML patients. These results were compared to variant allele frequencies determined by next generation sequencing (NGS) and MRD levels determined by flow cytometry. We found that 4/6 samples tested by NGS were positive for R132H, whereas all 6 samples were positive by ddPCR. We also found that 9/13 samples tested by flow cytometry were positive for abnormal blasts whereas ddPCR identified 8/13 positive samples including 2 that were MRD negative by flow cytometry. Additional validation of a larger cohort is currently ongoing.

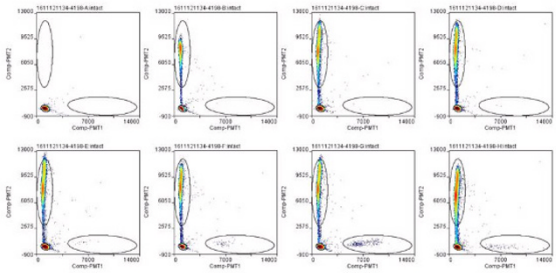

Conclusions: These data indicate that ddPCR is a highly sensitive technique for minimal residual disease evaluation in AML.

2290 Diagnostic Utility of Dual 5-hmC/Melan-A Red Immunohistochemistry in Differentiating Nodal Nevus from Metastatic Melanoma: An Effective First-Line Test for the Work Up of Sentinel Lymph Node Specimens

Andrew Siref[1], *Carissa Huynh*[2], *Bonnie Balzer*[1], *Richard Essner*[3], *Wonwoo Shon*[4]. [1]Cedars-Sinai Medical Center, Los Angeles, CA, [2]Cedars-Sinai Medical Center, Palmdale, CA, [3]Cedars-Sinai Medical Center, [4]Cedars-Sinai Medical Center, Studio City, CA

Background: The diagnosis of small melanocytic deposits in sentinel lymph nodes is one of the major diagnostic challenges in dermatopathology. Although currently available panmelanocytic markers (i.e., S-100, SOX-10, Melan-A, and MiTF) are sensitive, these markers cannot distinguish a nodal melanocytic nevus from metastatic melanoma. Moreover, HMB-45 expression has also been documented in benign nodal nevomelanocytes and macrophages. Prior studies have reported a loss of the epigenetic marker 5-Hydroxymethylcytosine (5-hmC) expression by immunohistochemistry in malignant melanomas and borderline melanocytic neoplasms. Prompted by these observations, the aim of this study is to evaluate the diagnostic utility of 5-hmC and Melan-A Red in distinguishing between nodal nevus and metastatic melanoma using a dual-color immunohistochemistry assay.

Design: Formalin-fixed, paraffin-embedded whole and tissue microarray sections from 20 metastatic melanomas and 12 nodal nevi were retrieved from our surgical pathology archive. Representative hematoxylin and eosin-stained slides were re-reviewed for each case to confirm the diagnosis. Nuclear 5-hmC (brown chromogen) and cytoplasmic Melan-A Red (red chromogen) double immunohistochemical staining was performed.

Results: Total or near-total loss of nuclear expression of 5-hmC was noted in all metastatic melanomas; these tumor cells were strongly positive for Melan-A Red, except one case of desmoplastic/spindle melanoma. All cases of nodal melanocytic nevi showed uniformly retained nuclear expression of 5-hmC accompanied by strong Melan-A Red cytoplasmic staining. In two cases with lymph node sections containing both metastatic melanoma and a nodal nevus, all melanocytes were positive for Melan-A Red, but nuclear expression of 5-hmC was selectively absent only in the melanoma tumor cells.

Conclusions: Dual 5-hmC/Melan-A Red immunohistochemistry is highly specific in distinguishing nodal nevi from metastatic melanoma. Our protocol for brown and red chromogens used in this study provides excellent color contrast and is easy to interpret. Furthermore, this dual staining method allows for the preservation of limited tumor tissue, which could be used for potential molecular studies. It is conceivable that this simple assay could be used as a cost-effective, first-line test in the workup of sentinel lymph node specimens.

2291 Comparison of Variant Detection by RNA–based and DNA–based Next Generation Sequencing Assay in Lung Adenocarcinoma

Aaron Stence[1], *Natalya Guseva*[1], *Krishnaveni Sompallae*[2], *Ramakrishna Sompallae*[2], *Aaron Bossler*[3], *Deqin Ma*[4]. [1]Univerisity of Iowa, [2]Univerisity of Iowa Hospitals and Clinics, [3]Iowa City, IA, [4]University of Iowa Hospitals and Clinics, Iowa City, IA

Background: Molecular testing for *EGFR* mutation and *ALK* and *ROS1* fusion is routinely performed in patients with stage IV lung adenocarcinoma to assess the eligibility for targeted therapy. Traditionally, separate assays are required for detection of DNA variants and gene fusions. Specimens tend to be limited, so detection of both gene rearrangements and DNA variants in one assay would be advantageous. We compare here the detection of point mutations (SNV) and small insertion/deletions (indel) from RNA with that from the DNA counterpart from an RNA–based NGS method that we previously validated for identifying fusion transcripts in lung adenocarcinoma (LAD).

Design: Total nucleic acids from 106 patients were extracted from formalin-fixed, paraffin embedded tissue or cytology smears, analyzed by an RNA-based (Archer FusionPlex CTL kit, ArcherDx) and DNA-based (Ion AmpliSeq Cancer Hotspot Panel, ThermoFisher or a laboratory-developed) targeted NGS assay in parallel, and sequenced on the Illumina MiSeq or Ion S5. Data was analyzed using Archer Analysis software or a laboratory-developed pipeline for RNA–based and DNA–based NGS, respectively. Variant filtering parameters were optimized to eliminate single nucleotide polymorphism and reduce false positives calls. The limit of detection was determined by serial dilution of RNA from a mutation-positive cell line with RNA from a negative cell line with comparable expression, and was determined to be 1% for SNV in transcripts with sufficient number of reads.

Results: Mutations in common oncogenes were detected by the CTL assay in 45 of the 106 cases including *EGFR* (7), *BRAF* (4), *KRAS* (30), *NRAS* (1), *HRAS* (1), *ERBB2* (1), and *MET* (1) (Table 1). The results from DNA-based assays were the same. Unlike allele frequency (%DNA) obtained from DNA-based testing, the RNA-based CTL assay represents the fraction of variant to wildtype transcript reads as a %RNA. Of the mutation positive cases, 32 had a %RNA>%DNA, 11 had %RNA<%DNA, 1 was equal between the two, and 1 had no %DNA data.

Table 1. Variants detected by the RNA-based NGS assay

Genes	Variant Detected	Number of Cases
EGFR	p.L858R	2
	p.E746_A750del	2
	p.L747_A750delinsP	1
	p.H773_V774delinsLM	1
	p.P772_H773insSNP	1
BRAF	p.V600E	1
	p.N581S	1
	p.G596R	1
	p.G469V	1
KRAS	p.G12A	1
	p.G12C	13
	p.G12D	1
	p.G12F	1
	p.G12V	10
	p.G13C	3
	p.G13D	1
NRAS	p.Q61R	1
HRAS	p.A18V	1
ERRB2	p.Y772_A775dup	1
MET	p.N394S	1

Conclusions: RNA-based testing to detect gene fusion transcripts in lung cancer can also be used to reliably detect SNV and small indels with no extra cost and minimal additional analyses. The assay works equally well on RNA form FFPE and FNA specimens. The ability to simultaneously detect multiple types of genomic variants from limited specimen is beneficial to the laboratory and for patient management.

2292 Strategies of Uniplex and Multiplex IHC Staining in Limited Tissue Biopsies

David Tacha[1], *Sara L Figueroa*[2], *Philip T Cagle*[3]. [1]Biocare Medical, Pacheco, CA, [2]Biocare Medical, Pacheco, CA, [3]Houston Methodist Hospital, Houston, TX

Background: A paradigm shift occurred in the past decade in the treatment of lung cancer with the use of targeted agents which improved significantly the survival of patients. With the introduction of targeted therapies based on selection for testing by cell type, the importance of accurate classification of squamous cell carcinoma (SCC) versus adenocarcinoma (ADC) has emerged with the utmost importance. Non-keratinizing SCC (NSCC) cannot be differentiated from solid ADC (SADC) based on H&E histology. The limitations of small sample size and the need to conserve tissue for additional molecular testing may necessitate the use of sensitive and specific markers on a single slide. A uniplex cocktail of mouse monoclonal (MM) antibodies desmoglein 3 (DSG3) and p40 has been shown to be a sensitive and specific marker for IHC in lung SCC. TTF-1 [SPT24] antibody has also been shown to be a sensitive marker when compared to clone [8G7G3/1] for lung ADC. In this study, we will attempt to develop an IHC uniplex/multiplex method using three MM antibodies on a single slide.

Design: TTF-1 single stains will be compared to TTF-1 staining after the elution step to ensure that the elution step does not degrade TTF-1 staining (n=43). In previously diagnosed archival lung cancers (n=32), 19 cases of SADC and 13 cases of NSCC were randomly selected. These cases were stained as follows: a MM cocktail of DSG3 + p40 (uniplex) was incubated for 30 min, followed by a universal HRP detection system and visualized with DAB. A sequential stain then continued with the application of an acid elution for 10 min. TTF-1 [SPT24] was then incubated for 30 min, followed by a mouse polymer AP detection system and visualized with fast red chromogen (multiplex). All tissues were stained on an automated IHC platform.

Results: In 43 cases of lung ADC, TTF-1 demonstrated equal staining sensitivity before and after the elusion step. Among the archival SADC cases, 18/19 (94.7%) stained with TTF-1. Clone SPT24 stained positive in one case which had previously been negative for TTF-1. Within the NSCC cases, 11/12 (91.7%) stained with either DSG3 (cytoplasmic/membrane) or p40 (nuclear). In one case of lung NSCC, DSG3 and p40 were both negative and TTF-1 was strongly stained; thus the case was reclassified as lung SADC.

Conclusions: A uniplex IHC cocktail incorporated into a sequential multiplex application which affords the use of three MM antibodies on a single slide may prove to be a valuable technique in aiding to preserve tissues biopsies.

2293 Comparative Mutational Profiling Differentiates Metastasis versus New Primary Cancers and Predicts Survival

Aditya Talwar[1], *Jan F Silverman*[2], *Christina Narick*[3], *Sydney Finkelstein*[4]. [1]Allegheny General Hospital, Pittsburgh, PA, [2]Allegheny General Hospital, Allegheny Health Network, [3]Interpace Diagnostics, Pittsburgh, PA, [4]Interpace Diagnostics

Background: Differentiating metastatic carcinoma from a new primary malignancy can be challenging, but the clinical management implications can be critical in patients with either synchronous or metachronous two separate malignancies. Comparative mutational profiling, based on the unique stepwise accumulation of mutations for each paired malignancy, was evaluated and its predictive power assessed in patients that were indeterminate after routine microscopic evaluation, including immunohistochemistry (IHC).

Design: 110 cases were analyzed, with most having a 5 year follow up outcome. The most common paired malignancies include two separate lung carcinomas; lung and head and neck carcinomas; followed by lung carcinoma with breast, pancreas, gastrointestinal or cutaneous malignancies. The two paired malignancies had either synchronous or metachronous presentation. Follow up survival was also available for each patient. Unstained FFPE sections and/or stained cytology slides were microdissected to provide control negative and enriched tumor samples. Molecular and cellular heterogeneity was addressed by securing multiple targets of each neoplasm. Molecular analysis consisted of oncogene point mutational sequencing and tumor suppressor gene loss of heterozygosity analysis using a panel of 24 markers linked to 10 tumor suppressor genes (1p, 3p, 5q, 9p, 10q, 17p, 17q, 19q, 21q, 22q).

Results: Molecularly related tumors (30/36; 83.3%) representing metastatic malignancies had a survival time of ≤2 years, including latency intervals for recurrence as long as 8 years after the primary cancer was diagnosed. 3/36 (8.3%) cases had a survival of 3 years, 1/36 (2.8%) survived 4 years and 2/36 (5.5%) survived over 5 years. In contrast, 61/74 (82.4%) of the two independent new primary malignancies had a greater than 5 year survival. 7/74 (9.5%) had a ≤2 year survival, 4/74 (5.4%) had a 3 year survival, and the remaining 2/74 cases were diagnosed less than 5 years ago. Predicted outcome was highly significant (p, 0.0001) for molecular distinction.

Conclusions: Mutational profiling involving both common oncogenes and tumor suppressor genes can define the relatedness of separate malignancies when the microscopic evaluation including IHC is indeterminate. Using this molecular profiling technique, cancer recurrence (metastasis) can be shown to occur even after long latency interval. Molecular profiling can be an effective predictive technique to optimize individual patient management by separating metastatic malignancies from two

2294 Comparison of In Situ Hybridization with Immunohistochemistry for Assessment of Programmed cell Death Ligand 1 (PD-L1) Expression

Robert Teachenor[1], *Sandra Rost*[2], *Shari Lau*[1], *Jeff Eastham-Anderson*[1], *Hartmut Koeppen*[3], *Scot D Liu*[4]. [1]Genentech, [2]South San Francisco, CA, [3]Genentech, Inc., South San Francisco, CA, [4]Genentech, South San Francisco, CA

Background: Immune checkpoint blockade therapies are promising tools for the treatment of malignancies, including drugs targeting the PD-1/PD-L1 axis. Multiple assays are approved as companion or complementary diagnostics to determine PD-L1 expression by immunohistochemistry (IHC). However, discordance between the different diagnostic assays has been demonstrated. Chromogenic in-situ hybridization (CISH) has not been utilized for the detection of PD-L1. We have developed a PD-L1-specific CISH assay and compared its performance to three approved IHC assays on a cohort of non-small cell lung cancer (NSCLC) samples.

Design: Serial sections of 31 NSCLC samples were cut and stained for PD-L1 with the 22C3 (DAKO), SP142 and SP263 (both Ventana) IHC assays using the protocols specified by the manufacturer. IHC assays were scored by a trained pathologist according to each assay's specific scoring algorithm. An additional section was assessed for PD-L1 mRNA expression using a CISH assay validated on PD-L1 expressing and non-expressing cell lines with PD-L1 specific riboprobes. Hybridization with a sense control probe showed no signal, while hybridization for a housekeeping gene showed adequate signal. The ISH assay was scored as a percentage of tumor cells positive for PD-L1 by pathologist and by imaging software (MatLab) trained to recognize PD-L1 positive cells. Results of both ISH scoring methods were compared to the tumor cell score for each IHC assay.

Results: Manual and digital CISH scores showed a strong positive correlation (ρ_s=0.7753) for tumor cell expression of PD-L1. Comparison between manual CISH and IHC scores by SP142, SP263, and 22C3 showed weak correlations (ρ_s=0.2784, 0.3286, and 0.2299, respectively). Digital CISH scores showed no correlation with IHC scores by SP142, SP263 or 22C3 (ρ_s=-0.1565, -0.06852, and -0.128, respectively).

Pearson correlation coefficient (ρ_s) between pathologist or automated ISH score and SP142, SP263, or 22C3 IHC scores.

	SP142 IHC	SP263 IHC	22C3 IHC
Pathologist ISH	0.2784	0.3286	0.2299
Automated software ISH	-0.1565	-0.06852	-0.128

Conclusions: Independent clinical studies have shown that each of the three IHC assays can enrich for patients likely to receive benefit from PD-1/PD-L1 targeted therapy despite discordant IHC scores when tested on the same samples. An orthogonal methodology to further address these discrepancies would be beneficial. However, our findings suggest that PD-L1 CISH is currently not capable to reconcile the scoring disparities between the different IHC assays.

2295 Microscopy with UV Surface Excitation (MUSE): Rapid, Simple, Non-Destructive Slide-Free Histology Consistent with Downstream Molecular Testing

Austin Todd[1], *Farzad Fereidouni*[2], *Croix Griffin*[3], *Alexander Borowsky*[4], *Mirna Lechpammer*[5], *Michael G Crump*[6], *John McPherson*[6], *John Bishop*[5], *Richard Levenson*[7]. [1]UC Davis, Sacramento, CA, [2]UC Davis, [3]School of Veterinary Medicine, UC Davis, Davis, CA, [4]Davis, CA, [5]University of California Davis, Sacramento, CA, [6]UC Davis Health, [7]Sacramento, CA

Disclosures:
Richard Levenson: *Ownership Interest,* MUSE Microscopy Inc.

Background: MUSE microscopy is a rapid approach for obtaining high-resolution, potentially diagnostic-quality histological images from unsectioned thick tissue specimens, either fresh or fixed. Although conventional transmission light microscopy requires the preparation of microns-thick tissue sections generated by multistep histological processing, these can be omitted if optically sectioned images are acquired directly. We have developed and tested MUSE instrumentation and staining procedures for suitability in clinical tissue diagnostics and for compatibility with precision medicine requirements.

Design: 280-nm UV excitation provided by off-axis light-emitting diodes (LEDs) are used to generate high-quality, diffraction-limited fluorescence images from the cut surfaces of arbitrarily thick specimens. The samples are briefly (seconds) exposed to common fluorescent stains, and visible-band fluorescence signals are captured using conventional lenses and standard color cameras. The resulting multicolor images have novel and useful contrast but can also be converted in real-time to resemble conventional H&E-staining. The images can also convey additional information arising from shape, shading and color cues that reveal surface profiles important in understanding the three-dimensional organization of complex specimens. MUSE images and corresponding H&E histology were compared across a variety of diagnostic categories using a blinded assessment design. Separately, MUSE-stained samples were submitted to subsequent molecular-based assays to look for evidence of possible interference.

Results: MUSE images proved to be of diagnostic quality using both fresh and fixed specimens, with blinded diagnoses from MUSE and matching FFPE H&E-stained slides agreeing in about 90% of cases. The slightly greater depth of optical sectioning and additional shape information, along with some challenges in handling soft fresh tissues increased difficulty in interpretation of some specimens. The method proved compatible with subsequent FFPE processes (if desired) as well as downstream molecular testing including FISH, IHC and RNA seq.

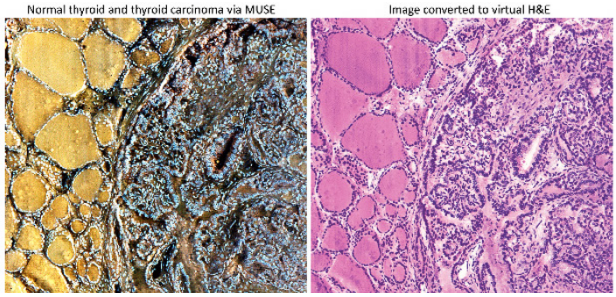

Conclusions: MUSE is a simple, rapid, efficient, and informative microscopy technique that can eliminate the need for prior slide preparation. It should find application in such tasks as frozen-section replacement, biopsy adequacy evaluation and intra-operative surgical guidance, and potentially could be used for primary diagnoses in both high- and low-resource settings.

2296 Comparison of PD-L1 (Clone 22C3) Expression Between Biopsy and Matched Cytology Samples: The Effect of Cytology Fixative

Jaylou Velez Torres[1], *Claudia Rojas*[2], *M Nadji*[3]. [1]University of Miami / Jackson Memorial Hospital, Miami, FL, [2]Hialeah, FL, [3]University of Miami, Miami, FL

Background: Testing for the expression of PD-L1 is now required for all cases of non-small cell lung cancer to evaluate patient candidacy for treatment with Pembrolizumab (Keytruda). The test is ordinarily performed on bronchial or core biopsies. In a considerable number of patients with lung cancer however, cytologic samples may be the only available diagnostic material and hence, PD-L1 testing is expected to be performed on such samples. It is therefore imperative to validate the adequacy of cytologic specimens for PD-L1 testing, including the potential effects of pre-analytical factors. Our aim in this study was to compare the results of PD-L1 testing on paired cytologic and histologic samples of the same patients.

Design: Thirty-eight matched histology and cytology samples of adenocarcinoma of the lung that met minimal tumor cell proportion (at least 100 tumor cells) were included in this study. Cytologic samples were received either fresh (21) or in CytoLyt (17). Cell blocks were prepared from all cytology specimens. Immunochemistry for PD-L1 (Clone 22C3) was performed on paraffin sections of tissue biopsies and cell blocks. The proportion tumor scores (TPS) were graded following the current recommendations as high (>50% of tumor cells), low (1-49%) and negative (<1%). The positive reaction of alveolar macrophages served as internal positive control in all cases.

Results: All of the tissue biopsies with low TPS (10) or negative TPS (20) matched the scores of corresponding cytologies. Of the 8 tissue biopsies with high TPS, the matched cytology samples showed low TPS in 4 cases; these were all cytology specimens received in CytoLyt.

Conclusions: This study shows that the concordance of TPS between paired cytology and histology samples is close to 90%. The discordant scores are all due to lower sensitivity of PD-L1 staining of cytologic samples fixed in CytoLyt. The lower sensitivity of this reagent has already been documented for other cellular biomarkers *(Gruchy JR, et al. Appl Immunohistchem Mol Morphol 2015; 23:297)*. When histology samples are not available, cytologic specimens are valid alternatives for PD-L1 testing as long as the effect of fixative is taken into consideration.

2297 Implementation of a Fluorescence In Situ Hybridization Technique for Detection of Integrated and non-Integrated Genomes of Human Herpesvirus 6 in Formalin-Fixed Paraffin-Embedded Tissues

Luis Veloza[1], *Cristina Teixidó*[2], *Maria Ángeles Marcos*[3], *Rocio Aguado*[4], *Isabel Machuca*[5], *Marta Marginet*[3], *Teresa Ribalta*[6], *Antonio Martinez*[3]. [1]University of Barcelona, Barcelona, [2]Hospital Clinic of Barcelona, Spain, [3]Hospital Clinic, [4]Instituto Maimónides de Investigación Biomédica de Córdoba, [5]Clinical Unit of Infectious Diseases, Instituto Maimónides de Investigación Biomédica de Córdoba (IMIBIC), Reina Sofía University Hospital/University of Cordoba, Cordoba, Spain, [6]Sant Joan de Deu Barcelona Children's Hospital, Esplugues de Llobregat, Barcelona

Background: Seroprevalence of Human herpesvirus 6 (HHV6) is estimated around 90% in the adult population. HHV6 is unique among all herpesviruses, as the virus can integrate into human chromosomes achieving latency. After integration HHV6 is able to replicate, infect new cells and in immunocompromised individuals may cause clinical infections. Integration into the gametes results in transmission to offspring, with 1% of the population with inherited chromosomally integrated HHV6 (ciHHV6). ciHHV6 determination is usually done by HHV6 DNA PCR in hair follicles or whole blood samples and also by Fluorescent in situ hybridization (FISH) on peripheral blood cells. Nevertheless, HHV6 DNA in situ detection technique which could help differentiate between ciHHV6 vs non-integrated HHV6 form in formalin-fixed, paraffin-embedded (FFPE) tissues has not been implemented so far.

Design: FISH study was performed on a HHV6 PCR positive FFPE brain and pulmonary tissues obtained from a 22-weeks fetus who was sent for necropsy after spontaneous abortion. ciHHV6 was previosly demonstrated in the mother's fetus by HHV6 PCR on patient's hair follicle. H&E stainigs of FFPE tissues were done for histopathologic evaluation and to select areas of better quality for FISH studies. Immunohistochemistry (IHC) evaluation for HHV6 (F59G) was performed to detect viral proteins. HHV6 detection in FFPE tissues was done using oligonucleotide-based FISH HHV6 customized specific probe which targets the sequence NC_001664.2. Briefly, 4-µm thick FFPE sections were deparaffinized, pre-treated and digested with pepsin at 37°C. After slides were denaturated at 80°C 10 min, hybridized at 45°C 120 min, dehydrated and counterstained with DAPI. Analysis were performed using a fluorescence microscope at 100X.

Results: H&E stainings did not show any histopathological finding and HHV6 expression was negative (–) by IHC in the fetus tissues (brain and lung). Fetus HHV6 FISH tests resulted positive and HHV6 signals were observed in around 90% of cells in both tissues. Both single signals (corresponding to ciHHV6) and several signals (representing non-HHV6 integration) were observed in both scenarios. No hybridization was detected in the HHV6 FISH– control (HHV6 PCR– sample).

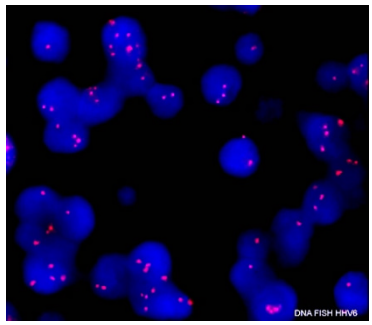

Conclusions: HHV6 has been successfully detected in FFPE tissues by interphase DNA FISH and allowed to distinguish between ciHHV6 vs non-ciHHV6. Others herpesvirus family members could be also studied with this methodology which may have diagnostic and therapeutic implications.

2298 The Core Needle Biopsy Wash as a Bridge to the Long Read Sequencing Roadblock

DIPING WANG[1], *Donald Yergeau*[2], *Weiguo Liu*[1], *W. D. Mojica*[3]. [1]University at Buffalo, Buffalo, NY, [2]University at Buffalo, [3]University at Buffalo, Williamsville, NY

Background: Sequencing technologies are slowly evolving and migrating from short to long reads. The latter approach is ideally suited to resolve the complexities associated with structural and copy number variations, in addition to providing details at the single nucleotide polymorphism level. However, the ability to perform long read sequencing (LRS) requires the input of high-quality, extended segments of intact DNA, something not associated with tissue specimens subjected to formalin-fixation, paraffin embedding (FFPE). The use of a simple wash step prior to fixation for tissue specimens, in particular core needle biopsies (CNBs) could address problems that currently present as potential roadblocks for the clinical integration of LRS technologies on these types of biospecimens. Theoretically, high molecular weight DNA, required as the input substrate for LRS platforms, can be recovered from the washed cells. This study was undertaken to determine the suitability of the DNA from these CNBw cells as substrates for LRS, using the 10X Genomics system as the model platform.

Design: Two separate tumors (1 Clear Cell Renal Cell Carcinoma and 1 urothelial tumor) were obtained unfixed, and two CNBs performed on each specimen. The tissue cores were washed in buffer and then removed. The cells in the washing buffer were subsequently spun down and DNA from each specimen extracted. Recovered DNA was electrophoresed for determination of molecular weight.

Results: Sufficient numbers of cells and DNA (average = 1464 ng/case) were recovered for downstream analysis. Intact segments of DNA, as determined by gel electrophoresis to have a molecular weight >> 23 kilobases (kb) were recovered from both samples. This equates to a level 3 in the 10X Genomics quality level metric, indicating a suitable size for DNA library preparation on their LRS platform.

Conclusions: The potential roadblock for incorporation of LRS technologies into the evaluation of clinical samples is the requisite need for intact segments of DNA in the kb range, something usually not associated with FFPE material. Cells obtained from clinical tissue specimens before they are fixed can serve as the substrate for these particular sequencers, allowing eventual integration of these LRS capabilities to genomic analysis. The inclusion of a pre-wash step of CNB's demonstrates one mechanism of circumventing the issues associated between FFPE tissues and LRS platforms.

2299 Feasibility of an RNAseq Assay for Mutational Analysis, Translocation Detection and Cell of Origin Determination in Aggressive B-Cell Lymphoma

Xiaoqiong Wang[1], *Brian Kudlow*[2], *Laura Johnson*[3], *Yuying Wang*[2], *Katelyn Trifilo*[2], *James Cook*[1]. [1]Cleveland Clinic, Cleveland, OH, [2]ArcherDx, [3]ArcherDx, Boulder, CO

Disclosures:
Brian Kudlow: *Employee*, ArcherDX
Laura Johnson: *Employee*, ArcherDx

Background: Several types of molecular abnormalities influence the classification and prognostic assessment of diffuse aggressive lymphomas, including mutations, translocations, and cell of origin (COO) profile (i.e., germinal center (GC) vs. activated B-cell (ABC) genotype). RNA based next generation sequencing (RNAseq) assays offer the potential to detect each of these types of abnormalities, although identification of lymphoma-associated translocations may be challenging as many do not produce fusion transcripts. We investigated the feasibility of an RNAseq assay for detection of recurrent mutations, translocations and COO profile in 20 cases of well characterized aggressive lymphomas.

Design: Formalin fixed paraffin embedded (FFPE) tissue from 20 malignant lymphomas (16 DLBCL, 3 double/triple hit lymphomas, 1 high grade B-cell lymphoma, NOS) were analyzed by RNAseq using the Archer FusionPlex Lymphoma assay (ArcherDx, Boulder, CO), targeting 125 genes. Libraries were sequenced on an Illumina NextSeq and normalized to a depth of 1.4 M reads each for analysis. Each case was previously characterized for COO using immunohistochemistry (IHC) via the Hans algorithm, and *MYC*, *BCL2* and *BCL6* translocation status was determined by FISH in all cases expressing MYC by IHC.

Results: Overall, 7.25 mutations were identified per case (range 2-12), with similar results in GC and non-GC phenotypes. Genes mutated in 5 or more samples included *KMT2A* (n=8), *CCND3* (n=7), PIM1 (n=7), *SERPINA9* (n=7), *TCF3* (n=7), *CDC50* (n=6), *DENND3* (n=6), *BCR* (n=5), *FOXP1* (n=5), *NOTCH1* (n=5) and *RAB7L1* (n=5). RNAseq detected 1/3 *MYC*, 1/4 *BCL2* and 2/3 *BCL6* translocations identified by FISH. Additionally, RNAseq detected 1 *MYC* and 1 *BCL6* translocation that were not detected by FISH. 7/10 cases with GC phenotype by IHC showed a GC or likely GC expression profile by RNAseq, while 9/10 cases with non-GCB phenotype by IHC showed an ABC or likely ABC expression profile.

Conclusions: RNAseq from FFPE is a promising technology for the identification of disease-associated abnormalities in aggressive B-cell lymphoma. NGS results complement, but do not replace, FISH for the detection of lymphoma-associated translocations. This method is capable of identifying recurrent mutations in targeted genes, and expression profiling allows for COO classification which correlates well with standard IHC testing. Additional revisions to COO algorithms are underway to further improve genotypic profile classification.

2300 Reproducible PD-L1 Immunohistochemistry Interpretation Across Various Types of Genitourinary and Head/ Neck Carcinomas, Antibody Clones, and Tissue Preparations

Chiyun Wang[1], *Elan Hahn*[2], *Bin Xu*[3], *Michelle Downes*[4]. [1]University of Toronto, Toronto, ON, [2]University of Toronto, Toronto, ON, Sunnybrook Health Sciences Centre, Toronto, ON, [3]Sunnybrook Health Sciences Centre - University of Toronto, Toronto, ON, [4]Sunnybrook Health Sciences Centre, Toronto, ON

Background: Programmed death-ligand 1 (PD-L1) expression by tumor cells is a mechanism for downregulation of antitumor T cell responses and is a target for immunotherapy in various cancers especially those with high rates of somatic mutations. PD-L1 status as a predictor of treatment response has led to the development of multiple biomarkers with different reference cutoffs. We aimed to (1) assess concordance of PD-L1 interpretation using two antibodies from both tissue microarrays (TMA) and whole sections (WS) of bladder (UC) and hypopharyngeal squamous cell carcinoma (SCC) and (2) examine PD-L1 expression in high grade salivary gland (HGSGC) and prostate carcinoma (PC).

Design: The study encompassed 129 cases of genitourinary and head/ neck carcinomas, including 59 UC, 21 PC, 27 SCC, and 22 HGSGC. PD-L1 staining was performed using SP263 and SP142 clones, with positivity determined using published cutoffs for UC (25% SP263, 5% SP142). PD-L1 status was evaluated blindly by three practicing/ training pathologists in UC and SCC for interobserver agreement. PD-L1 concordance between TMA and WS was compared in 27 SCC and 26 UC. Fleiss' kappa test was performed. PD-L1 staining was peformed in cases of PC and HGSGC.

Results: There was substantial interobserver agreement in determining overall PD-L1 positivity in UC and SCC using SP263 (κ=0.702, 95% confidence interval CI 0.579–0.824, p<0.001) and SP142 antibodies (κ=0.757, 95% CI 0.633–0.881, p<0.001). Subgroup analysis for both antibodies showed excellent agreement in UC (SP263: κ=0.812, 95% CI 0.663–0.960, p<0.001; SP142: κ=0.827, 95% CI 0.675–0.978, p<0.001), and moderate agreement in SCC (SP263: κ=0.469, 95% CI 0.251–0.687, p<0.001; SP142: κ=0.591, 95% CI 0.373–0.809, p<0.001).

Moderate to substantial agreement between TMA and WS was achieved using SP263 (overall: κ=0.573, 95% CI 0.304–0.842, p<0.001; UC: κ=0.424, 95% CI 0.039–0.808, p=0.031; SCC: κ=0.667, 95% CI 0.289–1.044, p=0.001), and SP142 (UC: κ=0.493, 95% CI 0.116–0.871, p=0.010).

No PC (0/21) was PD-L1 positive, compared with 21% to 23% PD-L1 positivity in UC, SCC, and HGSGC.

Conclusions: (1) Moderate to substantial agreement in PD-L1 assessment was achieved among observers and between TMA and WS for both SP263 and SP142 antibodies, suggesting that PD-L1 scoring is reliable and reproducible in various types of carcinomas; (2) PC rarely shows PD-L1 positivity, which may be explained by its low mutation burden.

2301 Utility of Electron Microscopy in Liver Biopsies from Neonates and Infants: Experience of a Single Children's Hospital (1991-2017)

Mikako Warren[1], *Mai Shimura*[1], *Hiroyuki Shimada*[1]. [1]Children's Hospital of Los Angeles, Los Angeles, CA

Background: Electron microscopy (EM) is an excellent screening tool for various congenital conditions in the liver and other organs, and widely used in pediatric settings.

Design: EM was performed on 166 of 677 native liver biopsies from patients younger than 1 year old (353 males and 324 females), excluding mass lesions, during Jan. 1991-Aug. 2017. Data were obtained from the electronic medical charts and the pathology reporting system. EM images and light microscopic slides were reviewed.

Results: Main clinical indications for the procedures were; cholestasis (total biopsy#/EM# = 575/118), liver failure (34/13), hepatomegaly (25/14), elevated liver enzymes (14/6), hypoglycemia (7/6) and others/ unknown (22/9). Final diagnoses were; biliary atresia (204/19), nonspecific cholestatic injury (91/28), paucity of bile ducts (84/31), neonatal hepatitis (64/16), TPN-related injury (63/13), nonspecific acute hepatitic injury (48/16), nonspecific obstructive pattern (22/11), nonspecific steatotic pattern (18/2), choledochal cyst (18/0), idiopathic cirrhosis (16/11), Alagille syndrome (8/5), cystic fibrosis (8/1), glycogen storage disease (GSD, 5/5), veno-occlusive disease/Budd Chiari syndrome (3/0), mitochondrial disorder (MD, 2/2), tyrosinemia (2/0), neonatal hemochromatosis (2/0), Caroli disease (2/0), congenital hepatic fibrosis (2/0), ornithine transcarbamylase deficiency (2/0), hypereosinophilic syndrome (2/0), alpha-1 antitrypsin deficiency (A1AT, 1/1), Niemann-Pick disease (NPD, 1/1), infantile Refsum disease (IRD, 1/1), congenital disorder of glycosylation (CDG, 1/1), carbamoyl synthetase deficiency (1/1), maple syrup disease (1/1), Aicardi–Goutière syndrome (1/0), vascular malformation (1/0), hemophagocytic lymphohistiocytosis (1/0), sepsis (1/0) and HSV hepatitis (1/0). Among them, EM provided critical diagnostic findings in 11 cases (Figure 1) including GSD with marked accumulation of glycogen (5), MD with mitochondrial pleomorphism and crystalloid inclusions (2), A1AT with electron dense material within endoplasmic reticulum (1), NPD with myelinosomes in Kupffer cells and hepatocytes (1), IRD lacking peroxisomes (1) and CDG with myelinosomes in hapatocytes (1).

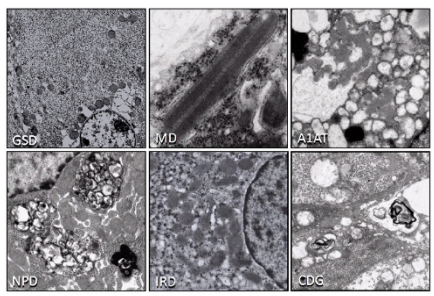

Conclusions: Trend of EM use in liver biopsies from patients younger than 1 year old is demonstrated. EM was widely used for the cases presenting cholestasis, hepatomegaly, liver dysfunction and hypoglycemia, whose etiology was unclear by clinical and microscopic features. We also present key EM "diagnostic" findings in 11 cases (6.6%).

2302 Ultrasensitive Detection of Genomic Chimerism by Single Molecule Molecular Inversion Probe Capture and High Throughput Sequencing of Copy Number Deletion Polymorphisms

David Wu[1], *Adam Waalkes*[1], *Kelsi M Penewit*[1], *Stephen Salipante*[1]. [1]University of Washington, Seattle, WA

Background: Accurate and sensitive methods for detecting minimal residual disease (MRD) are critical for improving the treatment

of aggressive hematologic neoplasms, including acute myeloid leukemia. In the post-allogeneic transplant state, early detection of minimal residual disease correlates with impending disease relapse. Genomic copy number variation (CNV) is an intrinsic source of genomic diversity. A unique sub-class of CNV includes regions of the genome that are absent in some individuals, and are so-called, "copy number deletion polymorphisms." By targeting these loci with single molecule molecular inversion probes (smMIPS), we hypothesized that we could discern between donor and host in the post-allogeneic transplantation setting at greater sensitivity than possible by short tandem repeat analysis or FISH chimerism testing. Accordingly, evidence of increasing host chimerism (loss of donor engraftment) may serve as a surrogate for recurrent disease.

Design: We designed a 160 smMIP probe capture panel spanning 40 deletion copy number loci and 2 sex-linked control loci, and an analytic framework for identifying informative probes. We evaluated performance using synthetic mixtures of defined DNA samples, as well as residual clinical samples for post-transplant clinical MRD detection as compared to standard of care (flow cytometry).

Results: Using synthetic mixtures of DNA from normal HapMap reference human trios, chimeric subpopulations below 1 in 10,000 relative abundance could be detected with quantitation over at least 3 orders of magnitude and a false positive rate of < 1 in 85,000 events examined. We identify regions of polymorphism within our larger targeted genomic regions, and show that genotypes of chimeric populations can be imputed without independently typing patient and donor specimens. We also demonstrate the ability to quantitate complex mixtures of DNA derived from multiple donors, such as which may occur during clinical treatment. Lastly, we evaluated a subset of residual clinical samples, as proof-of-principle, and compared quantitation of chimerism by smMIPS versus flow cytometry.

Conclusions: We developed a novel approach using smMIPS for post-allogeneic transplant monitoring of MRD, capitalizing on inherent genomic copy number variation between donor and host. Our approach provides ultrasensitivity and may be useful for MRD monitoring in allogenic-transplanted patients with acute myeloid leukemia and other aggressive hematologic malignancies.

2303 A Proposal of Glass-less Pathology: Novel Thin Film-based Slide for Digital Image and Tissue Banking of Small Biopsy Specimens

Akira Yoshikawa[1], *Junya Fukuoka*[2]. [1]Nagasaki University Hospital, Nagasaki, [2]Nagasaki University Graduate School of Biomedical, Nagasaki

Background: The glass slide has been used widely in pathology, although it is easy to crack, heavy, and space-occupying. We recently established a method of film-based section as a possible substitute for the glass slide (Figure 1). This method enables to section whole tissue block to one ribbon of film, obtain digital image of all layers, reconstruct them to three-dimensional image, and preserve specimens in the form ready to use for molecular analysis. In the present study, this method was applied for small biopsy specimens of gastric lesions, and its practical utility and diagnostic feasibility were investigated.

Design: Five biopsy specimens of gastric lesions with different diagnosis were selected. One paraffin-embedded formalin-fixed block for each case was applied for the method. Film tape was stuck onto a block, and the block was sectioned by microtome for 5 μm and directly transferred to the film. The section was stained with hematoxylin and eosin, and mounted with media and another film. Whole slide image was digitally obtained by the scanning system of Panoptiq™.

Results: The weight of the film-based sections was about 0.3 g. Quality of the film-based sections, including transparency of the film, staining contrast, and visibility of cells, was good enough to render the diagnosis for all cases. Digital images were obtained successfully and feasible enough for the accurate diagnosis as well (Figure 2).

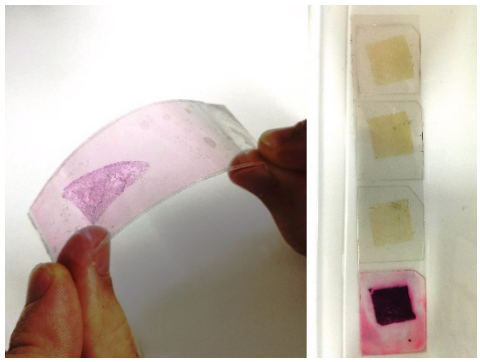

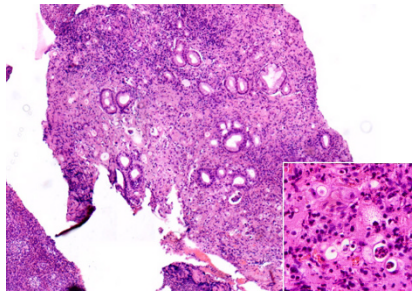

Conclusions: The film-based section combined with whole slide scanning has potential to substitute the glass slide and expand the opportunity to preserve whole tissue for further utility such as molecular analysis.

2304 Obviating Tissue Exhaustion on Core Needle Biopsies: Inclusion of a Simple Pre-Wash Step to Generate a Matched, Second Biospecimen for Molecular Studies

Haiying Zhan[1], *Antonios Papanicolau-Sengos*[2], *Jeffrey Conroy*[2], *W. D. Mojica*[3]. [1]The State University of New York at Buffalo, Williamsville, NY, [2]OmniSeq, Inc., [3]University at Buffalo, Williamsville, NY

Background: Preventing tissue exhaustion is a major challenge in the management of diminutive bio-specimens like core needle biopsies (CNB). Additional concerns center on the proportion of tumor representation and qualitative and quantitative metrics of the recovered DNA. The addition of a pre-wash step of the CNB has the potential to address these issues by generating a second bio-specimen, allowing the original tissue to be processed by traditional methods. In this manner, the CNB wash (CNBw) specimen can be dedicated for molecular studies while the fixed CNB tissue can be utilized for morphologic evaluation and interrogation by immunohistochemistry. The feasibility of this approach was tested on CNBw specimens and compared to matched formalin fixed and paraffin embedded (FFPE) tissues from those same tumors.

Design: Two CNB's were taken each from areas of excess tumor tissue in one case of Clear Cell Renal Cell Carcinoma (RCC) and the other from a case of an endometrial Carcinosarcoma (ECS). The CNB's were washed in buffer, the tissue fragments taken out, and the DNA extracted from the recovered, unfixed cells. The original tumor specimen itself, underwent routine FFPE for diagnostic microscopic examination. For comparative purposes, DNA was extracted from the FFPE tissue sections of each tumor. DNA libraries were generated from both (CNBw and FFPE) tumor samples, and then run on the OmniSeq Comprehensive™ 144-gene Next Generation Sequencing pan cancer panel.

Results: A total of 1107 ng of DNA was recovered from the RCC CNBw sample and 603 ng from the ECS CNBw sample. Qualitative metrics of mean depth were essentially similar (RCC case: 1133 (FFPE) vs 1005 (CNBw); case ECS: 1391 (FFPE) vs 1172 (CNBw)). There was high concordance between DNA sequenced from the CNBw and FFPE material in both cases. In the ECS case, the same mutations in the PIK3R1, PTEN and TP53 genes were found in the CNBw and FFPE specimens. In the RCC case, high concordance was also noted in the VHL gene for both the CNBw and FFPE specimen. Tissue separated from the CNBw pre-step and submitted for conventional processing by FFPE retained diagnostic morphology.

Conclusions: The addition of a simple pre-wash generates a second bio-specimen that can be dedicated for molecular analysis while preserving the original tissue component for traditional FFPE, morphologic examination and immunohistochemistry tests. Sufficient amounts of DNA from the CNBw can be recovered and utilized for generating libraries for genomic interrogation.

Distribution of N- and C-terminal Mutations in Informative Reads								
Patient No.*	Number of informative reads	Mutation 1	Mutation 2	Pattern 1 C-terminal mutation only Read count (%)	Pattern 2 n N-terminal mutation only Read count (%)	One mutation (1 or 2) Read count n (%)	Pattern 3 Both N-terminal and C-terminal mutation Read count (%)	Pattern 4 Wild- type reads Read count(%)
1	66	c.937_939dupAGA p. Lys313dup	c.334_346del p.Pro112fs	15 (22.7%)	8 (12.1%)	23 (35%)	2 (3%)	43 (65.2%)
2	297	c.937_939dupAGA p. Lys313dup	c.247delC p.Gln83fs.	59 (19.9%)	59 (19.99%)	118 (39.7%)	44 (14.8%)	180
3	86	c.915_920dupGCGCAA p.R306_N307insKR	c.230del p.F77fs	19 (22.1%)	13 (15.1%)	32 (37.2%)	8 (9.3%)	54 (62.8%)
4	269	c.910_939dupAAGCAGCGCAACGTGGAGACGCAGCAGAAG p.K304_K313dupKQRNVETQQK	c.232del p.L78fs	10 (3.7%)	40 (14.9%)	50 (18.6%)	8 (9.3%)	219 (81.4%)
5	440	c.937_939dupAAG p.K313dup	c.340_341del p.G114fs	71 (16.1%)	89 (20.2%)	160 (36.3%)	58 (13.2%)	280 (63.6%)
7	335	c.934_936dupCAG p.Q312dup	c.247del p.Q83fs	58 (17.3%)	58 (17.3%%)	116 (34.6%)	58 (17.3%)	194 (57.9%)
8	497	c.901_918dupGACAAGGCCAAGCAGCGC p.D301_R306dupDKAKQR	c.317_318insGGGCCCC p.F106fs	22 (4.4%)	31 (6.2%)	53 (10.7%)	6 (1.2%)	444 (89.3%)
12	298	c.895_933dupAGCCGCGACAAGGCCAAGCAGCGCAACGTGGAGACGCAG p.S299_Q311dupSRDKAKQRNVETQ	c.318dupT p.D107	21 (7%)	70 (23.5%)	91 (30.5%)	10 (3.4%)	207 (69.5%)
13	61	c.949_950insGTC p.E316_L317insR	c.177_178dupGA p.T60fs	16 (26.2%)	10 (16.4%)	26 (42.6%)	10 (16.4%)	35 (57.4%)

Informative reads were defined as the ones mapping both mutations, and therefore corresponded to amplicons with insert-sizes comprised in the range between the gap between both mutation +/- 250 base pairs. Four different patterns were described: 1) Amplicons with mutations in the C-terminal end (mutation 1), 2) Amplicons with mutations in the N-terminal end (mutation 2), 3) Amplicons with double mutations both in the C- and N-terminal ends and 4) Wild type amplicons. This information, was also bioinformatically retrieved by the cigar pattern in paired-reads.